PREDICTION AND MEASUREMENT OF THE UNWRAPPED PHASE FOR SPECKLE PROPAGATING IN TURBULENCE

Douglas C. Draper
MEng
Pennsylvania State University

A thesis submitted to the faculty
of the Oregon Graduate Institute of Science & Technology
in partial fulfillment of the
requirements for the degree
Doctor of Philosophy
in
Electrical Engineering

April 1992

The dissertation "Prediction and Measurement of the Unwrapped Phase for Speckle Propagating in Turbulence" by Douglas C. Draper has been examined and approved by the following Examination Committee:

J. Fred Holmes, Thesis Advisor
Professor

V.S. Rao Gudimetla
Assistant Professor

Rajendra Solanki
Associate Professor

Aslam Khalil
Professor

ACKNOWLEDGEMENTS

I would like to thank my thesis advisor, Dr. J. Fred Holmes, for his encouragement and guidance in directing my research and for his many innovative suggestions without which a large part of this thesis would not have been possible. I would also like to thank Dr. V.S. Rao Gudimetla for his support and help and for his insight in improving the organization of the thesis.

In addition I would like to thank John Hunt for his help in many aspects of experimental design and data collection. His expertise was of great value in solving many a problem that was encountered.

My appreciation also goes to John Peacock and Dr. Farzin Amzajerdian, with whom as a fellow student I shared many experiences, discussions and problems. John's thesis work is borrowed in various parts of this thesis and provides the justification for many of the conclusions. Farzin's many hours of perfecting the optical heterodyne system benefited me immensely, and I also gained much of my education in atmospheric optics from him.

I would like to thank Bev Kyler for her help and guidance in overcoming the many subtle problems encountered in preparing this and other manuscripts.

Finally I would also like to thank my wife and two daughters without whose patience this result would not have been possible and my parents who gave me values to live by which I appreciate more than any degree I may ever be awarded.

TABLE OF CONTENTS

LIST OF FIGURES AND TABLES

LIST OF FIGURES AND TABLES

ABSTRACT

Prediction and Measurement of the Unwrapped Phase for Speckle Propagating in Turbulence

Douglas Draper, Ph.D.
Oregon Graduate Institute of Science & Technology, 1992
Supervising Professor: J.F. Holmes

Intensity and wrapped phase characteristics of a signal from speckle propagating in a vacuum and from a point source propagating in air turbulence have been studied extensively. The intensity characteristics of a speckle signal propagating in turbulence have also been studied. Wrapped phase is phase data that is limited to the principal values of phase defined for a circle Additional information about the speckle and turbulence is contained in the unwrapped phase which is obtained by extending the wrapped phase beyond the principal values by mapping them onto an infinite line or by integrating the signal frequency.

Statistical models for the unwrapped phase of speckle produced by a laser illuminating a diffuse target and propagating through the atmosphere are proposed. It is shown that the unwrapped phase can be used to measure properties of a remote target or the atmosphere. Targets of different roughness can be distinguished at a distance of 1000 meters and target movement and wind activity are easily observable from the unwrapped phase data Measurements of unwrapped phase are also shown to be capable of sensing atmospheric turbulence levels from a remote location.

CHAPTER 1

INTRODUCTION

Intensity and wrapped phase characteristics of a signal from speckle propagating in a vacuum[1-7] and from a point source propagating in atmospheric turbulence[8-18] have been studied extensively. The intensity characteristics of a speckle signal propagating in turbulence have also been studied[17,18]. Additional information about the speckle and turbulence is contained in the unwrapped phase. The unwrapped phase is obtained from the wrapped phase by extending the phase values beyond their principal values, however, it is more readily obtained from the signal frequency.

A phase angle is uniquely defined on a circle for its principal value in the range $-\pi$ to π radians. On the other hand, frequency has no natural bound and since phase is the integral of frequency, when the phase is expressed as a function of time, it can also be defined over an unbounded domain as shown in figure 1.1. This unbounded representation of phase is referred to as unwrapped phase and bounded phase is called wrapped phase. Statistical models for the frequency and unwrapped phase of a speckle signal propagating in clear air turbulence along with the corresponding one and two point probability density functions will be presented.

The amplitude and phase effects of speckle and turbulence can be measured in an optical remote sensing system where a laser is used as a transmitter to illuminate a region of space and the back-scattered radiation from a remote object, called a target, or from particles in the atmosphere is

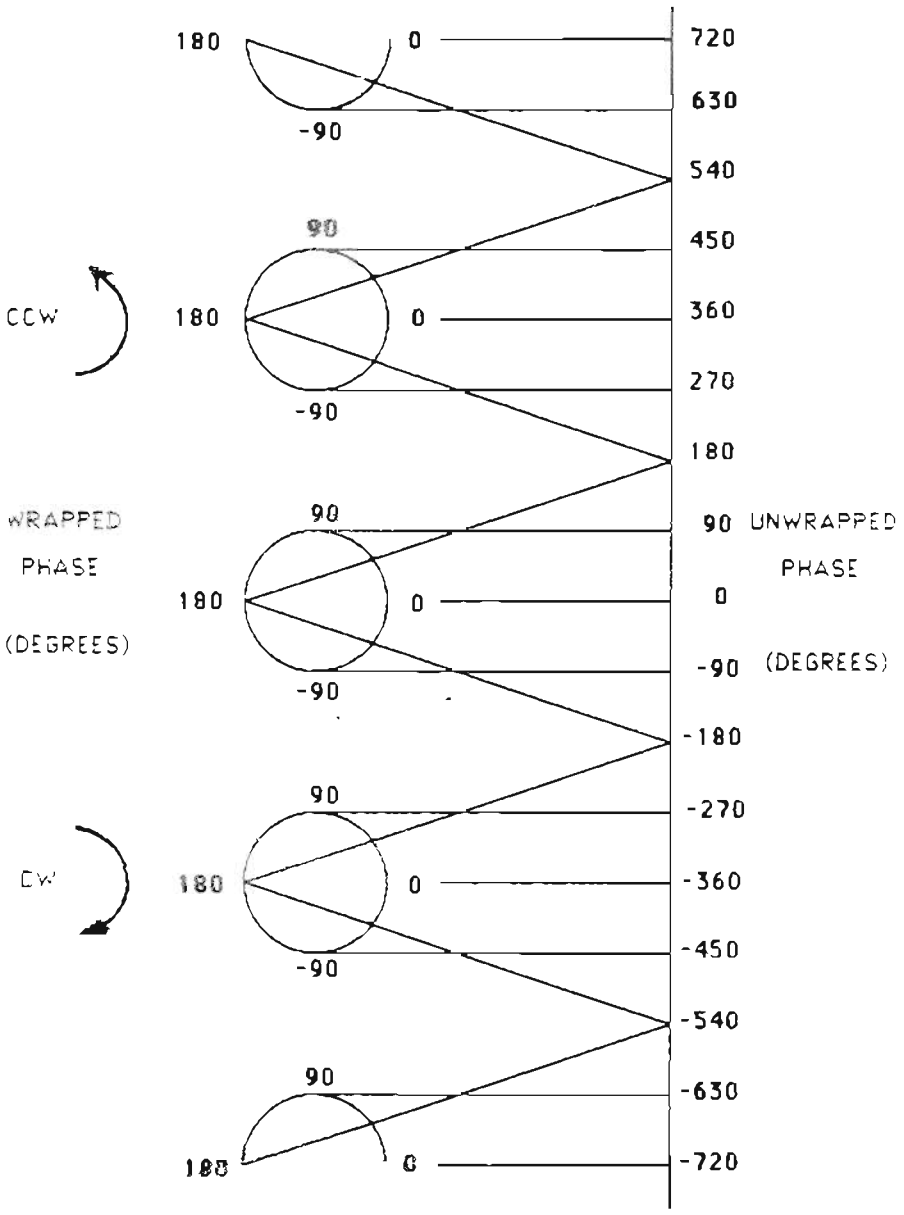

Figure 1.1 - Unwrapped Phase Compared to Wrapped Phase

received at the transmitter location. The back-scatter is processed in various ways to obtain information about the atmosphere or the target. If the target has a diffuse surface with random surface height variations on the order of the laser wavelength or larger, an interference pattern called speckle is produced that causes intensity and phase variations at the receiver.

Only a clear air atmosphere having no foreign particles is considered, and the only back-scatter that is expected is from the remote target. Nevertheless, the atmosphere will have an additional effect on the received signal intensity and phase due to air pressure and temperature changes and the wind that cause refractive index variations in the air and influence the speed and direction of the propagating light.

Speckle

Unlike ordinary light emission, the radiation from a laser is extremely coherent. Coherence is a property of a propagating wave where the phase of the wave is highly predictable over relatively long time intervals and distances. Speckle is caused by the combination of a large number of coherent waves with different phases. This typically occurs when a laser signal reflects off of a diffuse surface which scatters the laser radiation into separate waves which interfere with each other.

Variations in the surface height along the diffuse object introduce propagation path changes to the propagating waves causing the phases of the scattered waves to differ. At any receiver location, the scattered waves combine to produce an intensity that depends on the relative phases of the scatterers.

Figure 1.2 shows the appearance of a speckle pattern at some distance

Stationary Speckle Pattern

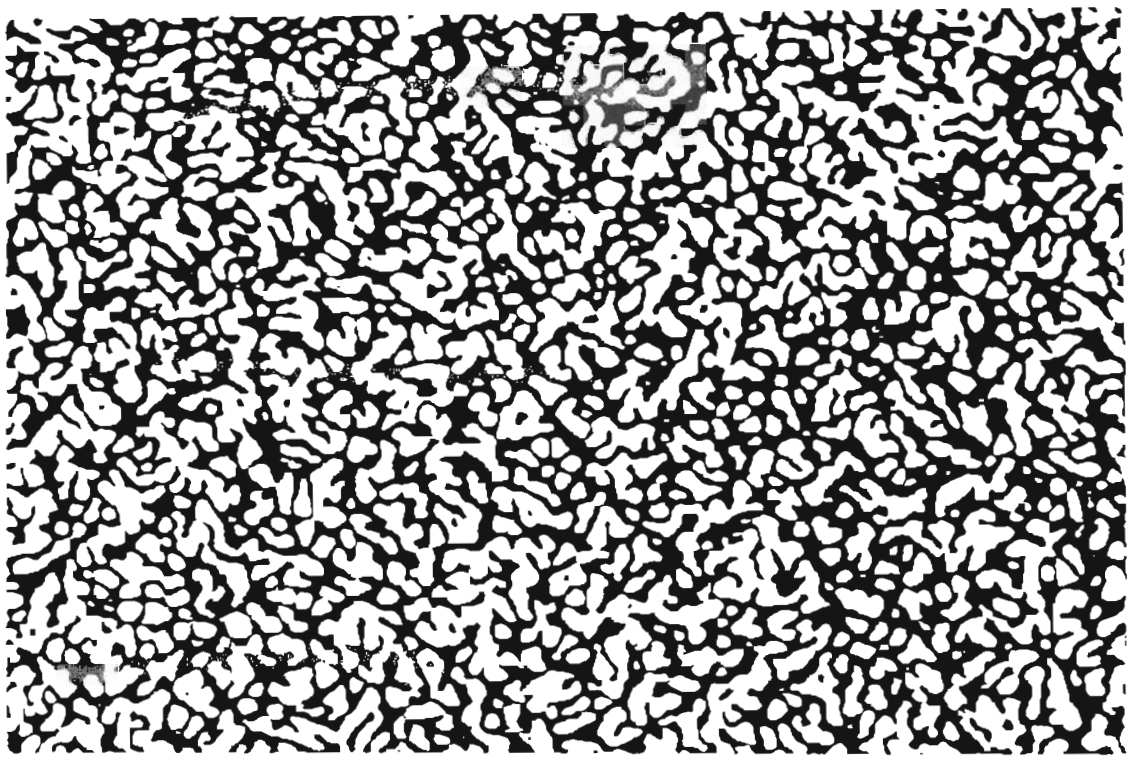

Figure 1.2 - Speckle Pattern

from a diffuse target. The laser source and the object are stationary in space and time and there is no air turbulence. The light spots represent areas where there is a high degree of constructive interference between the waves whereas the dark spots correspond to areas where the waves combine destructively. Areas of intermediate brightness occur for situations of partially constructive and destructive interference. The contrast of the speckle is given by the amount of intensity variation relative to the average intensity of the pattern. Surface height variations on the order of or greater than the laser wavelength produce high contrast speckle patterns.

Speckle is easily verified using a visible wavelength laser in a laboratory situation by reflecting a laser beam off of a diffuse object such as a sand-blasted aluminum plate and observing the reflection on a suitable surface such as a wall. Also, when the laser intensity is low enough so that reflections will not cause eye damage, speckle can be safely observed from laser energy reflected directly off of a wall.

Turbulence

In a typical remote sensing application, the speckle field produced by reflections from a diffuse target will not be stationary in time or space because either the transmitter or target will be moving or turbulence and wind in the atmosphere will cause the beam to wander across different regions of the target. In addition, refractive index variations due to the turbulence and wind will introduce random intensity and phase perturbations that will influence the speckle pattern.

When the turbulence is weak, the primary effect on the laser beam is

beam wander. In addition to beam wander, small phase variations will be added to the propagating wave. If the turbulence is distributed throughout a long path, even weak turbulence will cause appreciable phase changes at the receiver. When the turbulence is strong, the wave will scatter into separate waves which will eventually become incoherent over long propagation distances.

Consequently, the field observed at a given receiver location will have random intensity and phase variations produced by a combination of the target speckle and the turbulence.

Unwrapped Phase

There are various reasons for wanting to measure the unwrapped phase. The unwrapped phase represents optical path length variations due to the effects of turbulence or surface irregularities and movement of the target. Unwrapped phase changes greater than 2π radians are caused by even minor target movements. They can also be caused by large scale target roughness or long propagation paths through moderate to strong air turbulence. These large phase changes may represent valid data or unwanted interference. The wrapped phase represents a distortion of the phase data in either case. Interestingly, it also turns out that the statistics for unwrapped phase are considerably less complicated than those for the wrapped phase.

Phase detectors measure wrapped phase and the corresponding unwrapped phase must be obtained by processing the wrapped phase data. Phase unwrapping methods are simple in principle, however, when the phase changes rapidly and randomly as it does in a remote sensing environment, it

is very difficult to accurately unwrap the data and sophisticated techniques are needed. An alternative is to use a frequency detector to measure the frequency. The frequency data is then integrated to obtain the unwrapped phase.

Summary of Chapters

Chapter 2 presents background information on the one and two point statistics of wrapped phase for speckle propagating in a vacuum and for a point source propagating in turbulence. Gaussian unwrapped phase models are proposed, and using conventional methods for converting unwrapped phase to wrapped phase, the unwrapped phase probability density functions are compared with the wrapped phase probability density functions.

The one and two point probability density functions of the unwrapped phase and frequency for a speckle field propagating in air turbulence are presented in chapter 3. The statistics are based on a model used by Holmes and Gudimetla[17] to obtain the intensity distribution of high contrast speckle propagating in turbulence.

In chapter 4, each of two heterodyne systems that were used for remote sensing are explained and chapter 5 describes the detectors and special data processing algorithms that were used to obtain and process the experimental data.

Chapter 6 gives results from experiments at the atmospheric field site where sandblasted aluminum targets of various roughnesses were used. These results are compared to the models of chapters 2 and 3. Data on atmospheric conditions and target properties obtained independently from

calibrated instruments are used to test the results.

Also in chapter 6, potential applications for using the models and their statistics are mentioned. These applications range from determining features of a remote target to obtaining information about atmospheric conditions. The importance of measuring the unwrapped phase or the frequency is made clear since many features of the atmosphere or a remote target are indistinguishable from the wrapped phase but are evident from unwrapped phase or frequency measurements.

CHAPTER 2

MODELS FOR VACUUM SPECKLE AND A POINT SOURCE IN TURBULENCE

In this chapter, speckle and turbulence effects are treated separately, as existing literature on the statistics of speckle and turbulence is reviewed and expanded to include unwrapped phase. The statistics of the speckle field generated by a laser beam wandering over a diffuse target and its interaction with turbulence will be of primary concern in later chapters.

The one point statistics will be given followed by the two point statistics. The one point statistics give the statistics of a single receiver location. Additional information about the nature of the speckle and turbulence is contained in the two point statistics which give jointly statistical quantities for two different receiving locations.

The probability density functions for the phase will be given, and the wrapped and unwrapped phase distributions will be compared. It will be shown that the although the wrapped phase density functions may not be Gaussian, the unwrapped distributions are Gaussian for either a point source propagating in clear air turbulence, or when the target producing the speckle has a Gaussian surface height distribution, for a speckle field in free space The corresponding distributions for the amplitude of the received field will be given in Appendix A.

However, before the statistical distributions are presented, the models that are used to represent speckle and to characterize the diffuse targets will

be explained.

2.1 One Point Model for Speckle Phase

2.1.1 The Phasor Representation of Fields

The electromagnetic field that propagates from the laser source is assumed to be monochromatic and therefore a sinusoidal function of the wave position and of time. It can be described by,

$$E(\mathbf{s},t)=A(\mathbf{s})\cos[\mathbf{k}\cdot(\mathbf{s}+\mathbf{c}t)]=A(\mathbf{s})\cos\left((\mathbf{k}\cdot\mathbf{s}+\omega t)\right)$$

where $E(\mathbf{s},t)$ and $A(\mathbf{s})$ are vector functions and

$\mathbf{s}$ is the vector position of the wave in space

λ is the wavelength

$\mathbf{k}$ is the wave vector

$k=|\mathbf{k}|$ is the wave number $= 2\pi/\lambda$,

$\mathbf{c}$ is the (free space) velocity vector of the wave

$c=|\mathbf{c}| = 3\times10^8$ m/s

ν is the frequency of the source$=c/\lambda$

ω is the radian frequency $= 2\pi\nu$

$(...)\cdot(...)$ is the scalar product of vectors

and t=time.

In order to simplify various mathematical operations on the fields, they are represented as complex functions of the wave position and of time. This representation of a sinusoidal wave is commonly called a phasor and is based on Euler's identity,

$$e^{i\theta}=\cos\theta+i\sin\theta$$

The phasor representation of the sinusoidal field is then given as,

$$E(\mathbf{s},t)=A(\mathbf{s})\exp\left[i(\mathbf{k}\cdot\mathbf{s}+\omega t)\right]$$
$$=A(\mathbf{s})\left[\cos(\mathbf{k}\cdot\mathbf{s}+\omega t)+i\sin(\mathbf{k}\cdot\mathbf{s}+\omega t)\right]$$

where $i=\sqrt{-1}$.

The equation for the radiated field is the real part of the phasor expression. The amplitude of the wave is given by $A(\mathbf{s})$ and the phase by the angle $\mathbf{k}\cdot\mathbf{s}$.

2.1.2 The Formation of Speckle

The formation of speckle is illustrated in figures 2.1a and 2.1b. The total field at some point in space results from the sum of a large number of separate fields representing the reflections from different points on the target surface. The statistics of the speckle field depend on the model we choose for the diffuse target. Two slightly different models will be considered. The target model shown in figure 2.1a assumes that the reflections from the target are produced by a large number of point sources with a random height distribution. In addition the point sources are randomly located on the target surface. The reflected fields will therefore have random amplitudes and phases. This target will be referred to as a totally diffuse target.

A second target model is shown in figure 2.1b where there is a flat mirror like background surface at the mean surface height around which the random point reflectors are situated. Reflections from the flat surface produce a coherent term that is added to the random phase terms. This target will be called partially diffuse. Each of these models give a different set of

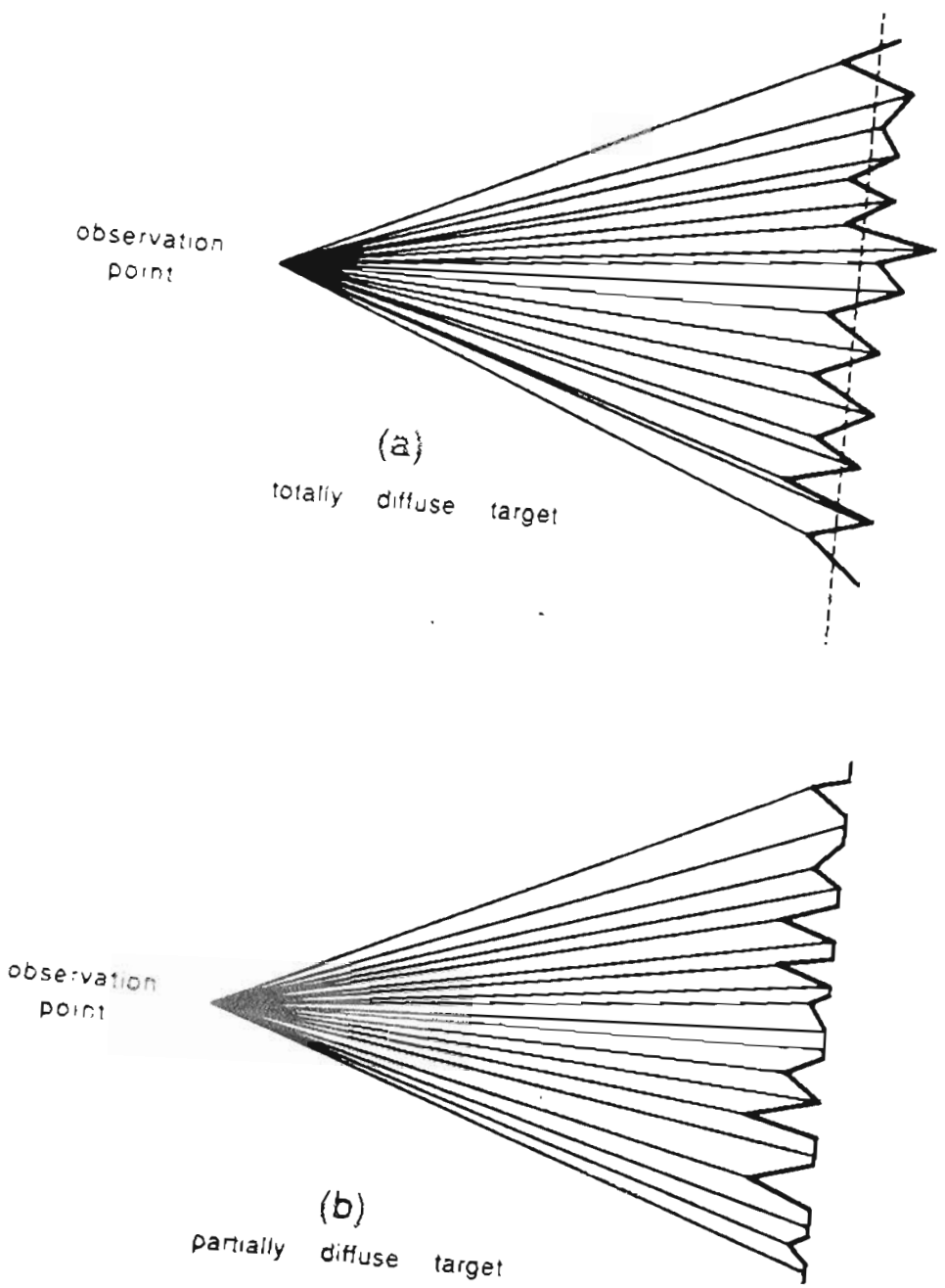

Figure 2.1 - Speckle Formation
(a) totally diffuse target (b) partially diffuse target

statistics, however, their differences are minor in many instances.

Referring to figure 2.1a and assuming the target has a linear reflection coefficient, each target scatterer will produce an electromagnetic field that can be represented by the phasor function,

$$E_j(\mathbf{s},t)=A_j(\mathbf{s})\exp\left[i(\mathbf{k}\cdot\mathbf{s}_j+\omega t)\right]$$

where j is an index number representing a reflected field.

At a given point in space, the vector $\mathbf{s}$ is fixed so that $A_j(\mathbf{s})$ can be replaced by the constant A_j and $\mathbf{k}\cdot\mathbf{s}$ by the constant ϕ_j. A_j represents the target amplitude and ϕ_j represents the target phase of the jth scattered field.

The electromagnetic field can then be written as,

$$E_j(t)=A_j e^{i(\omega t-\phi_j)}$$

The fields E_j are identical except for their amplitude and phase which are random. The field that results from N scatterers is given by,

$$E(t)=\sum_{j=1}^{N} E_j(t)=\sum_{j=1}^{N} A_j e^{i(\omega t-\phi_j)}$$

Each of the waves has the same frequency, therefore $e^{i\omega t}$ can be factored in the summation with the result,

$$E(t)=e^{i\omega t}\sum_{j=1}^{N} A_j e^{i\phi_j}$$

This represents the phasor equivalent of the total speckle field at some point in space. At a given instant of time this field is given by,

$$E(A,\theta)=Ae^{i\theta}=\sum_{j=1}^{N} A_j e^{i\phi_j} \qquad (2.1)$$

where the time value is taken as zero for convenience and A and θ are random variables.

Alternately (2.1) may be written in the rectangular form

$$E(A,\theta)=U+iV=\sum_{j=1}^{N} U_j+iV_j$$

where $U=A\cos\theta$ is the real and $V=A\sin\theta$ is the imaginary magnitude of the phasor field, $Ae^{i\theta}$.

The partially diffuse target produces a reflected field that can be described by,

$$E(A,\theta)=Be^{i\psi}+\sum_{j=1}^{N} A_j e^{i\phi_j}=(B\cos\psi+U)+i(B\sin\psi+V) \qquad (2.2)$$

B and ψ are the resultant amplitude and phase respectively that are contributed by the reflections from the coherent background surface.

The targets are assumed to have uniform reflectivity and to be a long distance from the observation point so that each scattered wave will propagate about the same distance to the receiver. Therefore, the received amplitude of each target reflection will be approximately the same, and A_j will be considered a constant in the summations of (2.1) and (2.2). However, path length variations will have a significant effect on the value of ϕ_j which is given by,

$$\phi_j=\frac{4\pi}{\lambda}L_j$$

where L_j represents the one way path length. L_j will depend on the surface height[2] and location of the jth point reflector. Through changes in ϕ_j, the path length variations will affect both the resultant amplitude, A, and phase, θ, in (2.1) and (2.2).

Random Walk Model for Speckle

The formation of speckle is often explained by a statistical random walk of phasors in the complex plane. The combined speckle field is given by the the sum of the separate phasors representing each target reflection.

In equation (2.1), let A_j be a constant equal to A/N and $\phi_j=\phi$ be a random variable with variance σ_ϕ^2 . U and V are random variables with mean values $<U>$ and $<V>$ and standard deviations σ_r and σ_i for the real and imaginary fields respectively. These quantities can be obtained from the characteristic function Φ defined by,

$$\Phi(\omega)=\Theta(\omega)+i\Psi(\omega)=<\exp(i\omega\phi)>=\int_{-\infty}^{\infty}\exp(i\omega\phi)P_\phi(\phi)d\phi$$

$P_\phi(\phi)$ is the probability density function of phase for the scattered fields at the target.

$$\Theta(\omega)=<\cos(\omega\phi)>$$
$$\Psi(\omega)=<\sin(\omega\phi)>$$

which for N random phase values gives[19],

$$<U>=A\Theta(1) \tag{2.3a}$$
$$<V>=A\Psi(1) \tag{2.3b}$$
$$\sigma_r^2=\frac{A^2}{2N}\left(1+\Theta(2)-2\Theta^2(1)\right) \tag{2.3c}$$
$$\sigma_i^2=\frac{A^2}{2N}\left(1-\Theta(2)-2\Psi^2(1)\right) \tag{2.3d}$$

$<.....>$ stands for the ensemble average.

For the case where ϕ has an even distribution around a mean value of zero, $\Psi(\omega)$ will be zero causing $<V>$ to be zero.

Two special cases of the speckle produced by a totally diffuse target will

now be considered. Figure 2.2a demonstrates a random walk in which the phase variance of the phasors is very small. This is characteristic of a relatively smooth target. When σ_ϕ is much smaller than a radian, ϕ will also be much less than one radian. and the small angle relationship,

$$\cos\theta \approx 1 - \frac{\theta^2}{2}$$

can be used. Consequently,

$$\Theta(1) \approx 1 - \frac{\sigma_\phi^2}{2}$$
$$\Theta(2) \approx 1 - 2\sigma_\phi^2$$

and

$$<U> \approx A$$
$$<V> \approx 0$$
$$\sigma_i \approx \frac{A}{\sqrt{N}}\sigma_\phi << 1$$
$$\sigma_r << \sigma_i$$

Each phasor has about the same direction and the phasor amplitudes add together. The amplitude and phase of the resultant phasor is not very random.

Figure 2.2b shows a random walk in which the phase variance of the phasors is very large, characteristic of a rough target. With σ_ϕ large compared to π radians, $\Theta(1)$ and $\Theta(2)$ will both be small relative to 1. The mean values $<U>$ and $<V>$ both approach zero and the standard deviations σ_r and σ_i approach the same value of $\frac{A}{\sqrt{2N}}$. The phasors wander in all directions and the resultant phasor is equally likely to take on any angle between $-\pi$ and π. The phasor amplitudes tend to cancel each other producing a

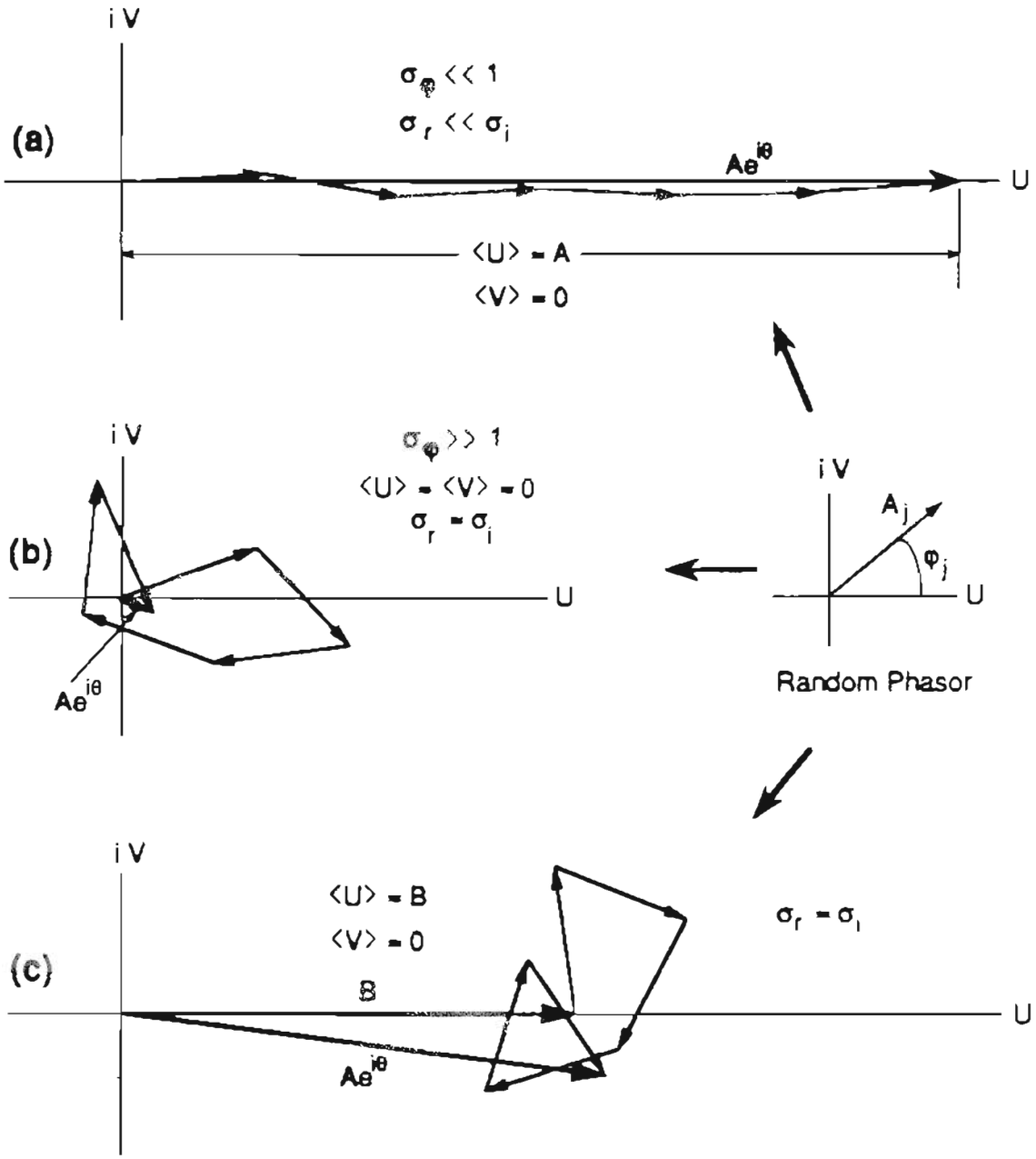

Figure 2.2 - Random Walk of Phasors in Complex Plane
(a) $\sigma_\phi << 1$ (b) $\sigma_\phi >> 1$ (c) partially diffuse target

resultant amplitude of the same order of magnitude as the separate phasor amplitudes.

In the figure, the average target phase is assumed zero. A non-zero value would cause a multiplication by a constant phase term, $<\exp(i\phi)>$, in (2.1), and a rotation by $<\phi>$ in the figure.

The partially diffuse target model can also be described by a random walk. In this case, (figure 2.2c), the random walk is offset by the constant phase term representing the reflections from the coherent background. Equal values of σ_r and σ_i are assumed for the random portion and ψ in (2.2) is considered to be zero.

Complex Field Distributions for Totally Diffuse Targets

All of the statistics for speckle are based on the random portion of the target having a large number of statistically independent scattering surfaces. Therefore, according to the central limit theorem of statistics, the random variables U and V will have a jointly Gaussian distribution with respect to each other. This will be true even if the target surface height distribution is not Gaussian. Therefore,

$$P(U,V)=\frac{1}{2\pi\sigma_r\sigma_i\sqrt{1-\rho^2}}\exp\left(-\frac{1}{2(1-\rho^2)}\left(\frac{\Delta U^2}{\sigma_r{}^2}-2\frac{\rho\Delta U\Delta V}{\sigma_r\sigma_i}+\frac{\Delta V^2}{\sigma_i{}^2}\right)\right) \quad (2.4)$$

where

$$\Delta U=U-<U>$$
$$\Delta V=V-<V>$$
$$\sigma_r{}^2=<\Delta U^2>$$
$$\sigma_i{}^2=<\Delta V^2>$$
$$\rho=\frac{<\Delta U\Delta V>}{\sigma_r\sigma_i}$$

In the equation, $<U>$ and $<V>$ are the mean values, and σ_r and σ_i are the standard deviations of the real and imaginary complex fields and ρ is the coefficient of correlation between them.

Using the change of variables, $I=A^2=U^2+V^2$ and $\theta=\tan^{-1}(V/U)$, this probability density function is used to obtain all of the intensity, amplitude and wrapped phase statistics for the speckle field.

In order to better understand the statistics of the complex field, Uozumi and Asakura[20] have introduced an equiprobability density ellipse that is defined for the joint probability density function of the complex field quantities U and V. An equiprobability density ellipse is shown in figure 2.3a for a typical joint probability density function of the complex fields. The ellipse is defined by the trajectory along which the joint probability density function of (2.4) equals $1/\sqrt{e}$ times the maximum density at the center.

The ellipse is completely defined by the five parameters of the probability density function of (2.4), ΔU, ΔV, σ_r, σ_i, and ρ. The inclination angle of the ellipse is given by.

$$\delta=\omega t=\frac{1}{2}\tan^{-1}\left(\frac{2\rho\sigma_r\sigma_i}{\sigma_r^2-\sigma_i^2}\right)=\frac{1}{2}\tan^{-1}\left(\frac{2<\Delta U\Delta V>}{\sigma_r^2-\sigma_i^2}\right)$$

The quantities U and V in addition to being random, are changing with time at a steady rate due to the term $e^{j\omega t}$ that was suppressed when time was arbitrarily set to zero. This means that the equiprobability density ellipse rotates at ω radians per second, and at times other than zero can be described by a coordinate transformation of U and V in figure 2.3a. At certain instants of time either $<U>$, $<V>$ or ρ become zero.

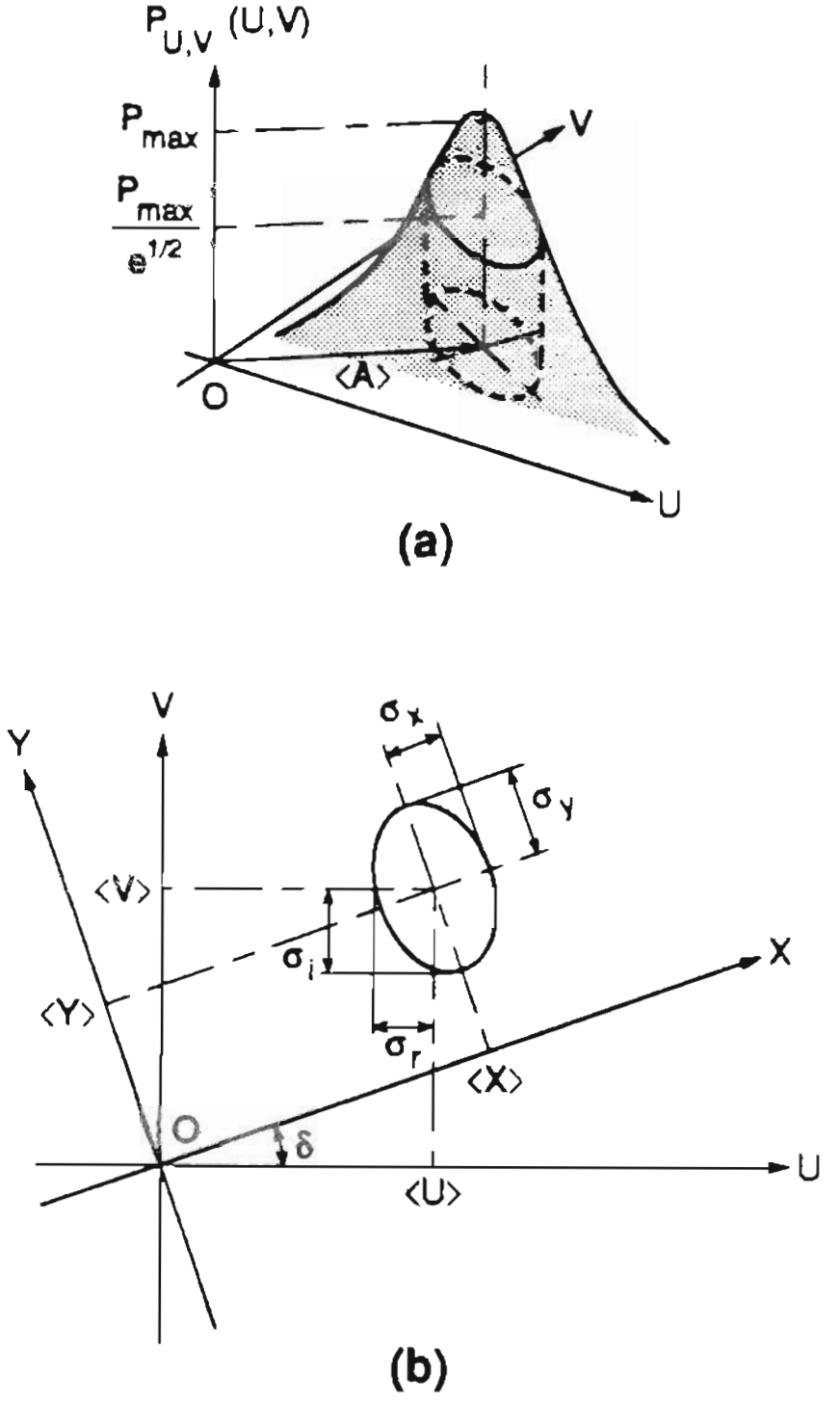

Figure 2.3 - (a) Equiprobability Density Ellipse and joint density function (b) with coordinate transformation to uncouple fields

Referring to figure 2.3b, a coordinate transformation equivalent to a rotation by the angle

$$\delta=\frac{1}{2}\tan^{-1}\left(\frac{2\rho\sigma_r\sigma_i}{\sigma_r^2-\sigma_i^2)}\right)$$

with

$$X=U\cos\delta+V\sin\delta$$
$$Y=V\cos\delta-U\sin\delta$$

is used to eliminate ρ in (2.4) and to obtain the uncoupled real and imaginary fields, X and Y. The coordinate transformation causes $<\Delta X\Delta Y>$ in the new coordinate system to be zero and X and Y are independent. The probability density function reduces to,

$$P(X,Y)=\left(\frac{1}{\sigma_x\sqrt{2\pi}}\exp\left(-\frac{\Delta X^2}{2\sigma_x^2}\right)\right)\left(\frac{1}{\sigma_y\sqrt{2\pi}}\exp\left(-\frac{\Delta Y^2}{2\sigma_y^2}\right)\right)$$
$$=\frac{1}{2\pi\sigma_x\sigma_y}\exp\left(-\left(\frac{\Delta X^2}{2\sigma_x^2}+\frac{\Delta Y^2}{2\sigma_y^2}\right)\right) \qquad (2.5)$$

where

$$\Delta X=X-<X>$$
$$\Delta Y=Y-<Y>$$
$$<X>=<U>\cos\delta+<V>\sin\delta$$
$$<Y>=<V>\cos\delta-<U>\sin\delta$$
$$\sigma_x^2=(\sigma_r^2\cos^2\delta-\sigma_i^2\sin^2\delta)/\cos(2\delta)$$
$$\sigma_y^2=(\sigma_i^2\cos^2\delta-\sigma_r^2\sin^2\delta)/\cos(2\delta)$$

Note that with the coordinate rotation, the ellipse axes are parallel to the coordinate axes and the ellipse is not tilted

The equiprobability density ellipse associated with (2.4) and (2.5) varies according to properties of the diffuse target and its location relative to the observation point. A thorough treatment of how the ellipse changes with

changes in the target phase standard deviation and the position of the receiver relative to the optical axis and the distance from the target is given in references 5,6 and 20. The standard deviation of target phases is related to the target surface roughness by[1,19],

$$\sigma_\phi = \frac{4\pi}{\lambda}\sigma_t \tag{2.6}$$

where σ_t is the r.m.s. target surface height variation.

Special Cases of Complex Field Distributions

The situations depicted in figures 2.2a and 2.2b represent special cases of (2.4). In both cases, δ and ρ are zero and (2.4) reduces to (2.5) with X=U and Y=V. In figure 2.2a, $\sigma_\phi << 1$, $<V>=0$, and $\sigma_r << \sigma_i$. The equiprobability density ellipse is shown in figure 2.4a where σ_r has been made zero so that the ellipse reduces to a straight-line. In reality, this condition requires that the receiver be in the far-field of the target and also on the optical axis defined by the laser source and the target. The real component of the complex field is no longer random and the probability density function of (2.4) simplifies to;

$$P(V) = \int_{-\infty}^{\infty} P(U,V)dV = \frac{1}{\sqrt{2\pi}\sigma_i} \exp\left(-\frac{V^2}{2\sigma_i^2}\right)$$

where $\sigma_i = \frac{A}{\sqrt{N}}\sigma_\phi$

In figure 2.2b, $\sigma_\phi >> 1$, $<U> = <V> = 0$, and $\sigma_r = \sigma_i$. The equiprobability density ellipse reduces to a circle centered at the origin as shown in figure 2.4b. This situation is referred to as fully developed speckle and the fields are said to have circularly Gaussian statistics. The probability

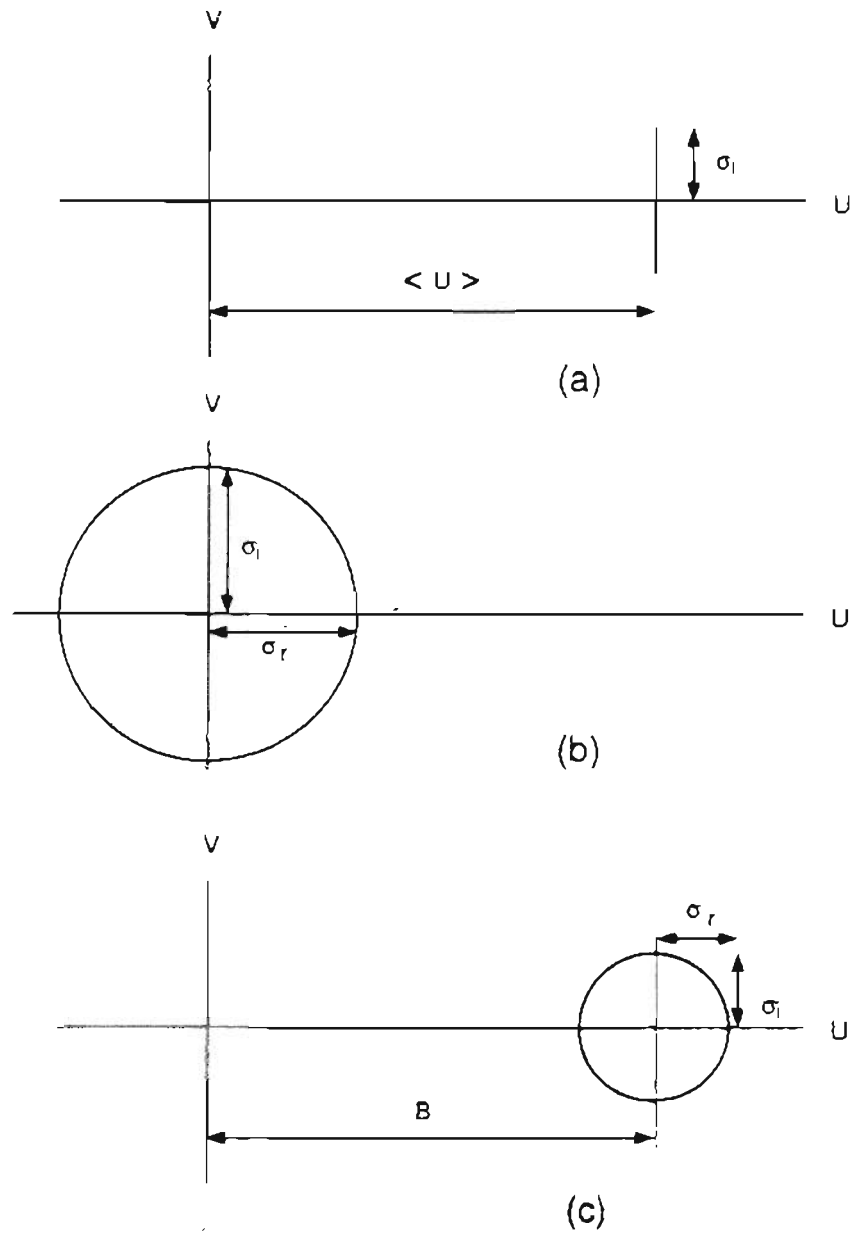

Figure 2.4 - Equiprobability Density Ellipse
(a) $\sigma_\phi << 1$ (b) $\sigma_\phi >> 1$ (c) partially diffuse target

density function of (2.4) becomes,

$$P(U,V)=\frac{1}{2\pi\sigma^2}\exp\left(-\frac{\Delta U^2+\Delta V^2}{2\sigma^2}\right)$$

where $\sigma = \sigma_r = \sigma_i = \frac{A}{\sqrt{2N}}$.

The fully developed speckle case is approached[3,5,6] as a limiting condition when either the target phase deviation, the distance from the receiver to the target or the receiver distance off the optical axis becomes large.

Figure 2.4c shows the equiprobability density ellipse for the partially diffuse target of figure 2.2c. As for fully developed speckle, it is also a circle but is offset by the non-random term, B.

2.1.3 Probability Density for Wrapped Phase

Totally Diffuse Target

The complex field quantities can be used to determine the statistics of the wrapped phase, but are not capable of predicting the unwrapped phase. Uozumi and Asakura[5] determined the one point probability density function of the wrapped phase from the joint probability density function of (2.5) and the substitutions,

$$I=EE^*=A^2=X^2+Y^2$$

and

$$\beta=\theta-\delta=\tan^{-1}(Y/X)$$

to be,

$$P_\theta(\theta)=\frac{\eta}{2\pi\tau}\left(1+\zeta\sqrt{\pi}\exp(\zeta^2)[1+\mathrm{erf}(\zeta)]\right)\exp\left(-\frac{\chi}{2\sigma_x^2}\right) \qquad (2.7)$$

where

$$-\pi<\theta<\pi$$
$$\eta=\sigma_x/\sigma_y$$
$$\tau=\cos^2\beta+\eta^2\sin^2\beta$$
$$\kappa=<X>\cos\beta+\eta^2<Y>\sin\beta$$
$$\zeta=\frac{\kappa}{\sigma_x\sqrt{2\tau}}$$
$$\chi=<X>^2+\eta^2<Y>^2$$

They evaluated the quantities in (2.7) for a laser focused on a totally diffuse target with a Gaussian distribution of target scatterers in terms of the standard deviation of target phases (σ_Φ), the correlation distance of the target scatterers (α), the laser beam waist radius on the target (w_o), the distance along the optical axis from the target to the receiver and the distance the receiver is off the optical axis.

Essentially the same result was obtained by Takai, Kadono and Asakura[8], but a more general approach was taken that also included the image field of the speckle phase. For both cases, when the receiver is on the optical axis in the far field of the diffraction, the quantities in (2.7) reduce to.

$$\delta=0$$
$$\beta=\theta$$
$$\chi=<U>^2$$
$$\kappa=<U>\cos\theta$$
$$<U>=<X>=Az^{-1}\exp(-\sigma_\Phi^2/2)$$
$$<V>=<Y>=0$$
$$\sigma_r^2=\sigma_x^2=\frac{A^2}{4Nz^2}\left(1+\exp(-2\sigma_\Phi^2)-2\exp(-\sigma_\Phi^2)\right)$$
$$\sigma_i^2=\sigma_y^2=\frac{A^2}{4Nz^2}\left(1-\exp(-2\sigma_\Phi^2)\right) \qquad (2.8)$$

The laser beam waist at the target is normal to the target surface. z is the distance from the target to the receiver normalized by the Rayleigh range $= \pi w_o^2/\lambda$, $N = (w_o/\alpha)^2$ is the number of scattered fields at the receiver, and $z >> 1$.

A similar situation was considered by Uozumi and Asakura[20] using a different approach. They found general relationships for the statistical quantities of (2.7) from the characteristic function of the random variable ϕ representing the phase of the scattered fields assuming N independent target scatterers. The receiver was assumed to be on the optical axis in the far-field or Fraunhoffer region of diffraction. They considered other target phase distributions, however, for a Gaussian distribution of target phases, they evaluated (2.3a)-(2.3d) as,

$$\begin{aligned} <U> &= A\exp(-\sigma_\phi^2/2) \\ \sigma_r^2 &= \frac{A^2}{2N}[1+\exp(-2\sigma_\phi^2)-2\exp(-\sigma_\phi^2)] \\ \sigma_i^2 &= \frac{A^2}{2N}[1-\exp(-2\sigma_\phi^2)] \end{aligned} \tag{2.9}$$

which except for a factor of $z\sqrt{2}$ in σ_r and σ_i and z in $<U>$, is the same as (2.8). The factor of z, representing the normalized receiver distance, cancels when evaluating (2.7), however, the $\sqrt{2}$ factor causes a slight difference in the two results.

When σ_ϕ is large with respect to π radians, σ_r and σ_i approach the same value of $A/\sqrt{2N}$ and $<U>$ approaches zero. This is the fully developed speckle case with circular Gaussian fields, and the wrapped phase is distributed uniformly between $-\pi$ and π with variance $\pi^2/3$.

In appendix B, it is shown that when $\sigma_\phi^2 << \sqrt{N}$, equation (2.7) asymptotically approaches a Gaussian distribution given by,

$$P_\theta(\theta)=\frac{1}{\sigma_s\sqrt{2\pi}}\exp\left\{\frac{-\theta^2}{2\sigma_s^2}\right\} \tag{2.10}$$

with $\sigma_s = \frac{\sigma_\phi}{\sqrt{N}}$ for (2.9) and $\sigma_s = \frac{\sigma_\phi}{\sqrt{2N}}$ for (2.8).

A quantity called the phase extent can be defined[6] for an equiprobability density ellipse to interpret the speckle phase deviations. Figure 2.5 shows an equiprobability density ellipse and the phase extent of the ellipse. The phase extent is defined as one half the angle formed by the two lines originating at the origin of the complex plane that are tangent to the ellipse. The phase extent is a measure of the speckle phase changes.

The phase extent is given as[6],

$$\theta_e=\frac{1}{2}\tan^{-1}\left\{2\frac{\sqrt{<X>^2\sigma_y^2+<Y>^2\sigma_x^2-(\sigma_x\sigma_y)^2}}{<X>^2+<Y>^2-\sigma_x^2-\sigma_y^2}\right\} \tag{2.11}$$

The phase extent is only defined when the argument in the square root of (2.11) is non-negative or when,

$$\frac{<X>^2}{\sigma_x^2}+\frac{<Y>^2}{\sigma_y^2}\geq 1$$

and the ellipse does not encircle the origin. This means that the phase extent is not defined for situations approaching fully developed speckle.

In the far-field of the diffracted radiation, $\rho = \delta = 0$, $<Y>=<V>$, $<X>=<U>$, $\sigma_x=\sigma_r$, $\sigma_y=\sigma_i$, and when $\sigma_\phi << 1$, $<V>=0$, $\sigma_r << \sigma_i$ and $<U>$ is much larger than either σ_r or σ_i. Therefore using (2.9) and

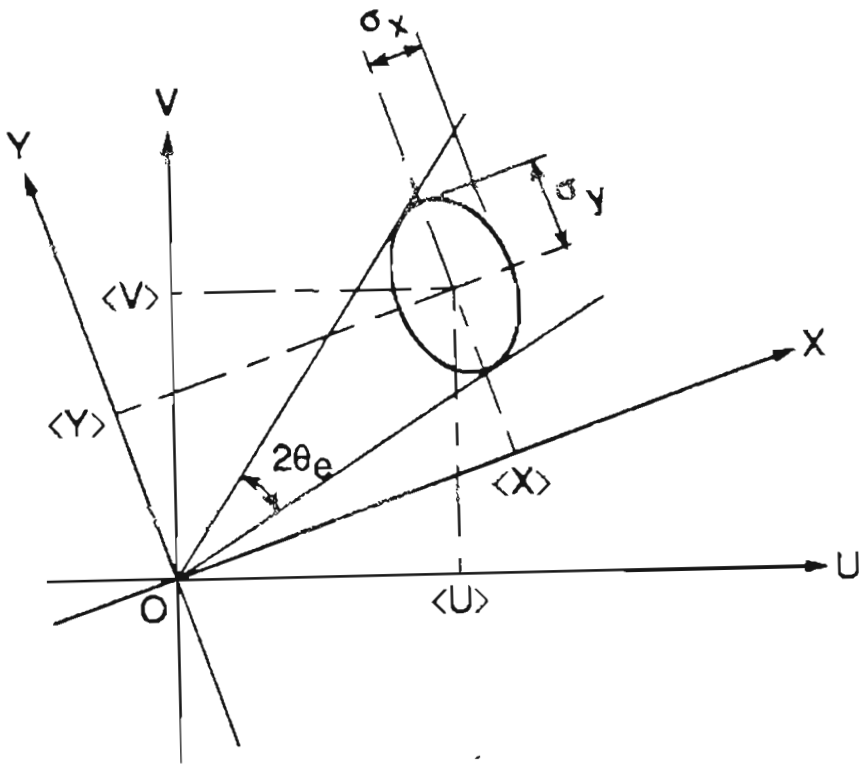

Figure 2.5 - Phase Extent of Equiprobability Density Ellipse

referring to figure 2.4a,

$$\tan(2\theta_e) \approx 2\frac{\sigma_i}{<U>} = \frac{\sqrt{(1-e^{-2\sigma_\phi^2})/N}}{e^{-\sigma_\phi^2/2}}$$

$$= \frac{\sqrt{e^{\sigma_\phi^2}(1-e^{-2\sigma_\phi^2})}}{\sqrt{N}} = \frac{\sqrt{e^{\sigma_\phi^2}-e^{-\sigma_\phi^2}}}{\sqrt{N}} = \sqrt{2\sinh\sigma_\phi^2/N}$$

Using a power series representation for e^x and the small angle formula for tan θ, for small values of σ_ϕ,

$$\theta_e \approx \frac{\sigma_\phi}{\sqrt{2N}} \tag{2.12a}$$

Using (2.9) the phase extent differs by a factor of $\sqrt{2}$ and,

$$\theta_e \approx \frac{\sigma_\phi}{\sqrt{N}} \tag{2.12b}$$

This result shows that when $\sigma_\phi^2 << \sqrt{N}$, the phase extent is equivalent to the standard deviation of wrapped phase.

Partially Diffuse Target

If the target is assumed to be partially diffuse with circular Gaussian statistics for the random part,

$$P(U,V) = \frac{1}{2\pi\sigma^2}\exp\left[-\frac{(U-B)^2+\Delta V^2}{2\sigma^2}\right] \tag{2.13}$$

where B is the constant field value and σ^2 is the total complex field variance $= \sigma_r^2 + \sigma_j^2$.

The probability density function for the wrapped phase is given by[1,21],

$$P_\theta(\theta) = \frac{e^{-r}}{2\pi} + \sqrt{r/\pi}\cos\theta\exp(-r\sin^2\theta)\Phi(\sqrt{2r}\cos\theta) \tag{2.14}$$

for $-\pi < \theta < \pi$ and zero otherwise and,

$$\Phi(b)=\frac{1}{\sqrt{2\pi}}\int_{-\infty}^{b} e^{\frac{-y^2}{2}}\,dy.$$

The parameter r is called the beam ratio parameter given by,

$$r=\frac{B^2}{\sigma^2} \tag{2.14a}$$

When r is small the random component dominates and the statistics approach circular. In this case (2.14) reduces to a uniform distribution equal to $\frac{1}{2\pi}$. On the other hand as r becomes large, the random part becomes small and it can be shown[1] that (2.14) approaches a Gaussian distribution equal to,

$$p_\theta(\theta)=\sqrt{r/\pi}\exp(-r\theta^2)=\frac{1}{\sigma_s\sqrt{2\pi}}\exp\left(-\frac{\theta^2}{2\sigma_s^2}\right) \tag{2.15}$$

where $\sigma_s^2 = \frac{1}{2r} = \frac{\sigma^2}{2B^2}$.

Therefore, for both the totally diffuse target and the partially diffuse target, the wrapped phase probability density functions vary from a Gaussian function when the target roughness is small to a uniform distribution when the surface roughness is large. To determine the character of the distribution for the partially diffuse target, the random term is compared to the magnitude of the coherent reflection, whereas for the totally diffuse target, the target roughness is compared to the number of independent scatterers.

The phase extent can also be defined for the partially diffuse target when $B > \sigma_r$. Referring to figure 2.4c,

$$\theta_e \approx \tan^{-1}\left(\frac{\sigma_i}{B}\right) = \tan^{-1}\left(\frac{\sigma}{B\sqrt{2}}\right)$$

and when $r >> 1$ is given by $\theta_e \approx \sigma/B\sqrt{2}$ Therefore for large values of r the phase extent is the same as the standard deviation of the wrapped phase in (2.15).

2.1.4 Probability Density for Unwrapped Phase

In what follows the wrapped probability density functions of (2.7) and (2.14) will be shown to compare favorably with a wrapped Gaussian distribution of the appropriate standard deviation.

An analytical method termed phase wrapping exists[22] for obtaining the probability density function of wrapped phase from the probability density of unwrapped phase. Figure 2.6 shows (2.7) plotted with N=10 for three values of target standard deviation. For comparison a Gaussian distribution is also plotted after it has been wrapped using the relationship[23],

$$P_\theta(\theta) = \frac{1}{\sigma_s\sqrt{2\pi}} \sum_{k=-\infty}^{\infty} \exp\left(\frac{-(\theta+2\pi k)^2}{2\sigma_s^2}\right) \qquad (2.16)$$

and $\phi = \theta + 2\pi k$ is the unwrapped phase. The unwrapped phase has a Gaussian distribution given by,

$$P_\phi(\phi) = \frac{1}{\sigma_s\sqrt{2\pi}} \exp\left(\frac{-\phi^2}{2\sigma_s^2}\right) \qquad (2.17)$$

The figure demonstrates how closely the wrapped Gaussian functions resemble the distributions of equation (2.7). The values of σ_s used for the wrapped Gaussian function were chosen so that the variances of the wrapped

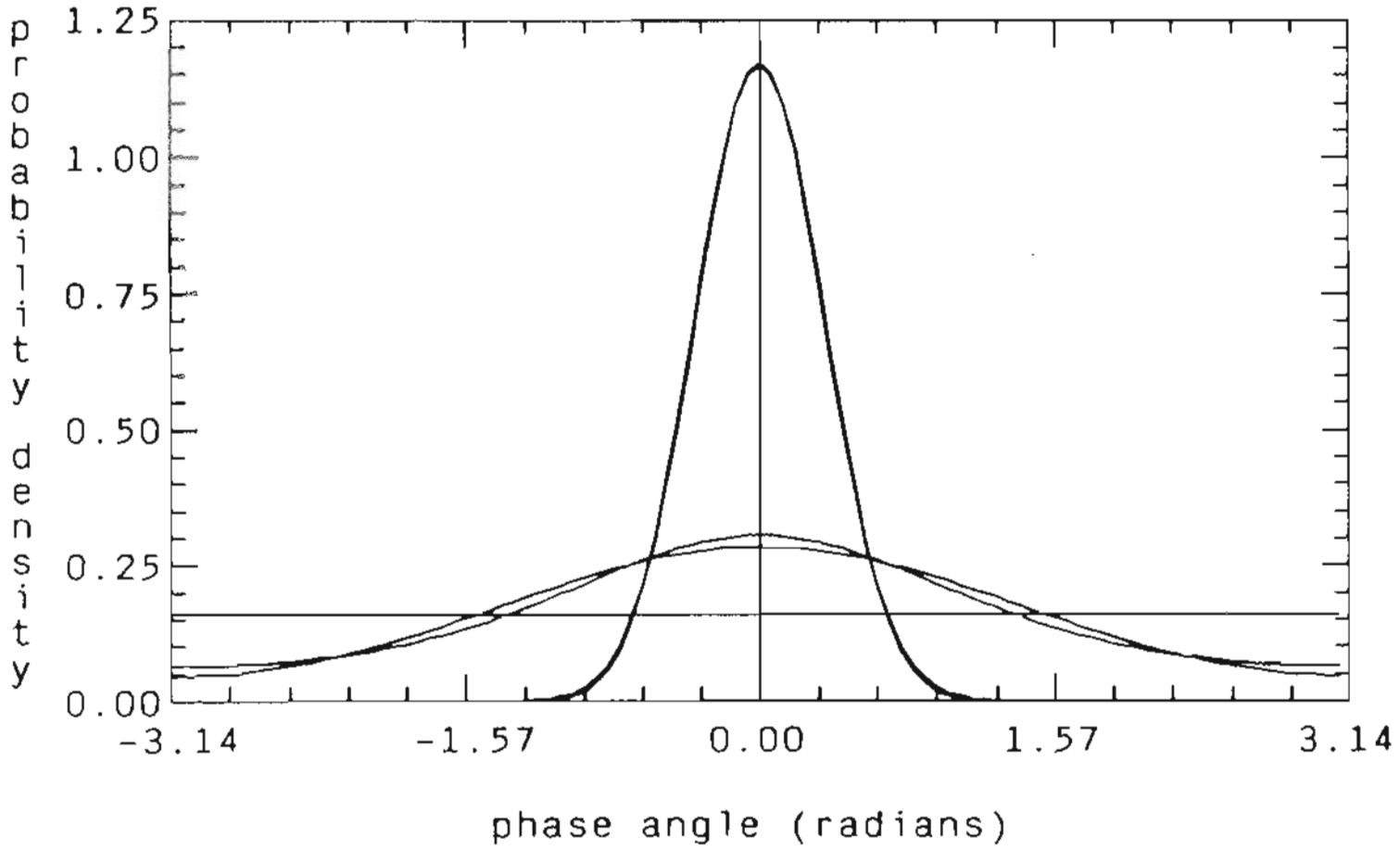

Figure 2.6 - Eqn 2.7 and Wrapped Gaussian N=10, σ_ϕ=1, 2, 5 , σ_s=0.34, 1.3, 5 radians

Gaussian distribution would be the same as the variance of (2.7).

Figure 2.7 plots values of σ_s that produce the wrapped variances of (2.7) vs. σ_ϕ for values of N = 5, 10 and 50 . For small and large values of σ_ϕ, σ_s is given by,

$$\sigma_s \approx \sigma_\phi / \sqrt{N}, \qquad \sigma_\phi^2 << \sqrt{N} \tag{2.18a}$$

$$\sigma_s \approx \sigma_\phi, \qquad \sigma_\phi^2 >> \sqrt{N} \tag{2.18b}$$

Barakat[23] has shown that the wrapped Gaussian distribution of (2.16) reduces to a Gaussian function for small σ_s and to a uniform distribution for large σ_s . It should be noted that the effects of wrapping are insignificant when σ_ϕ^2 is much smaller than $\sqrt{N}$.

Figure 2.8 shows (2.14) compared to a wrapped Gaussian function for three values of r. The figure shows that (2.14) is also approximately equivalent to the wrapped Gaussian functions. The values of σ_s used for the wrapped Gaussian function were chosen to match the variances of (2.14). As expected, σ_s reduces to $1/\sqrt{2r}$ as r becomes large. For small values of r, σ_s is given by the value of σ_r or σ_i of the complex field.

The wrapped phase probability density functions for speckle from a totally diffuse target, a partially diffuse target and a wrapped Gaussian function of the appropriate standard deviation have all been shown to be approximately the same. Therefore, Gaussian probability density functions for the unwrapped speckle phase will be used for either type of target.

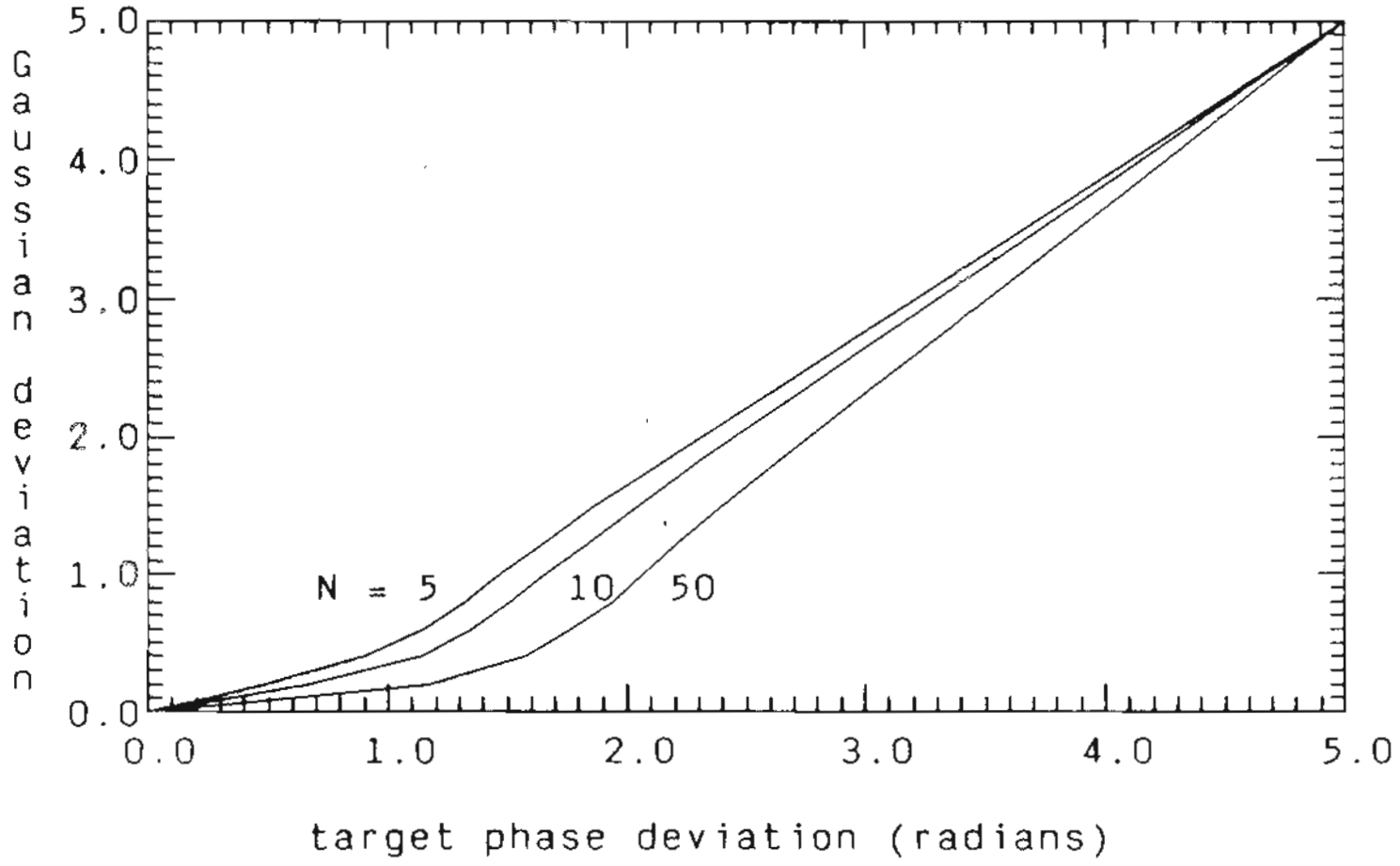

Figure 2.7 - Unwrapped Gaussian Standard Deviation vs. σ_ϕ

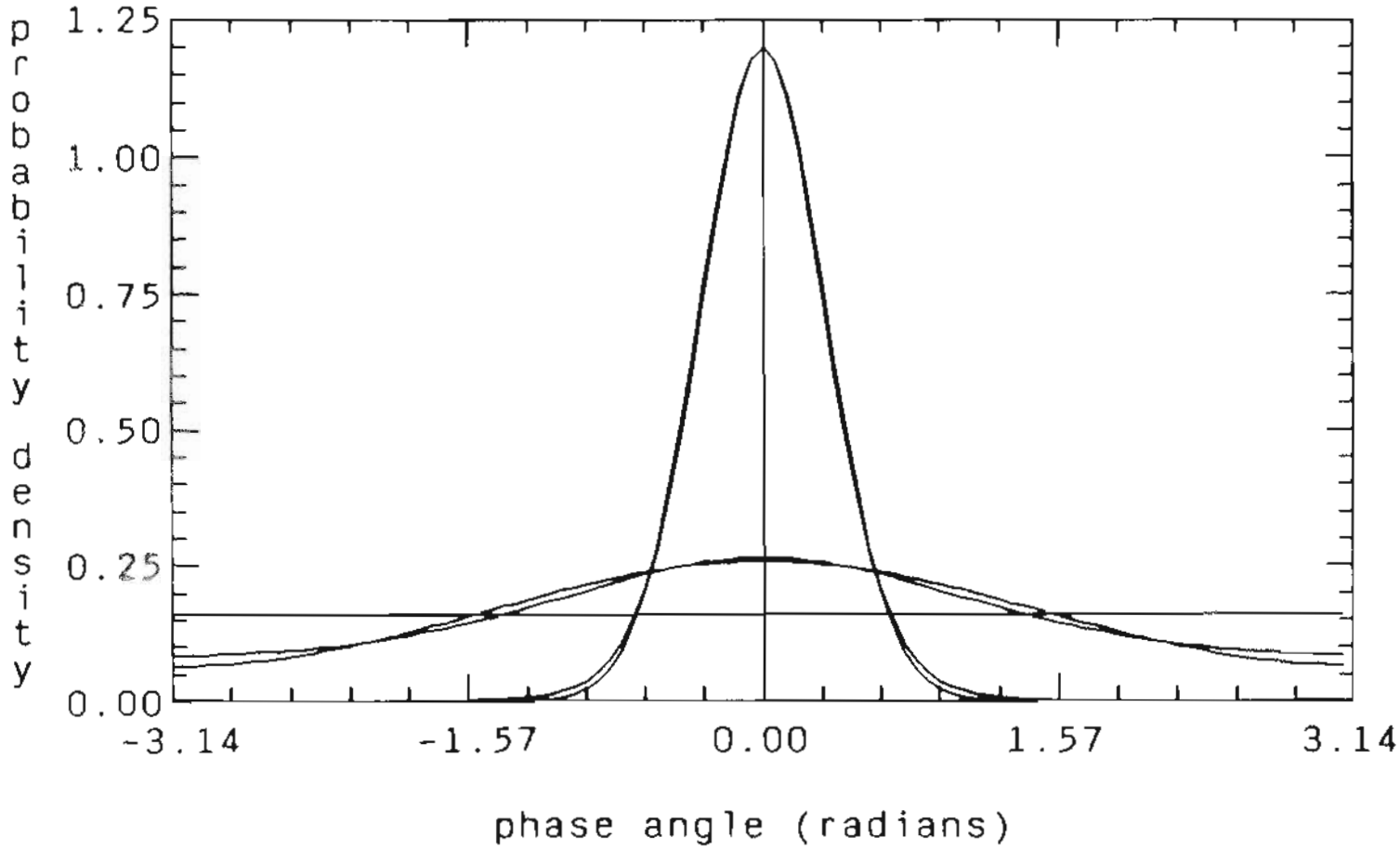

Figure 2.8 - Equation 2.14 and Wrapped Gaussian, r=4.5, 0.1, 0.0005, σ_s=0.33,1.5,3.0

2.2 One Point Models for Turbulence

2.2.1 Background

The atmosphere can have a pronounced effect on the transmission of an optical signal. This is evident when one considers the way in which clouds, rain, fog, dust and other disturbances in the atmosphere influence light transmission. Even what is classified as clean air, having no foreign particles or water vapor, can have a noticeable effect on light propagation.

The atmosphere contributes attenuation and phase shifts to the propagating light wave. These effects can be grouped into two categories, absorption and scattering. Both effects accumulate as the propagation distance increases so that the atmosphere may have a severe effect for long distance propagation, even when the atmospheric effects are weak.

Only a clear air atmosphere will be considered in this paper. This will greatly reduce the scattering and virtually eliminate absorption. Therefore, it will be assumed that the absorption is zero. The amount of scattering will be determined by random dielectric constant variations due to density changes, mixing and movement in the air caused by temperature, pressure and the wind. The scattering will introduce velocity and path direction changes to the propagating light which will affect both the amplitude and the phase of the propagating wave.

On a hot dry day it is easy to see these effects in the visible spectrum of wavelengths by the quivering of an image such as a highway road sign or telephone pole seen at a distance. The phase changes introduced by the atmospheric turbulence causes the light reflected from the object to deviate

in a random manner from its normal path.

These effects are best described by the refractive index variations rather than the dielectric constant changes in the air. The dependence of the refractive index on temperature, pressure and wavelength are well documented[12,24].

To help quantify the refractive effects, the clear atmosphere is modeled as randomly sized volumes of air called eddies. The eddies are approximately spherical in shape and have nearly uniform refractive index[12]. However, the refractive index of neighboring eddies varies randomly due to the density changes caused by pressure and temperature. These properties are characterized by the quantities C_n^2, l_o and L_o. The parameter C_n^2 is the refractive index structure constant, although it is not a constant but varies with space and time. It is a measure of the strength of the turbulence and gives the variation of the refractive index between the eddies[12,13]. L_o is called the outer scale of turbulence and l_o is the inner scale of turbulence. The outer scale represents the largest eddy radius that is expected and the inner scale the smallest radius. The size of any eddy is therefore a random variable that ranges between l_o and L_o.

Each eddy introduces a random amount of refraction and velocity change to the propagating wave. If the size of an eddy is larger than the laser beam diameter, the effect of the eddy will be to change the direction and focus or defocus the beam. Alternately, if the eddies are much smaller than the beam, they will produce a random phase delay to the wavefront reducing the coherence of the beam. It is expected that a combination of

both effects will occur as the propagating beam encounters eddies of all sizes from the outer scale to the inner scale.

Turbulence Models

To date, there is no single model that provides exact agreement with experiments in both weak and strong turbulence. Nevertheless, the unwrapped phase statistics seem to be well described by Gaussian functions in most cases.

Figure 2.9 is used to show the effects of single scattering where the turbulence is concentrated at a fixed distance from the observation point. The smaller eddies introduce a random phase shift to the propagating wave and the larger eddies randomly deviate the path of the wave. At the observation point, the received field will be composed of the sum of de-phased field components. If the phase shifts introduced by the turbulent eddies are large enough, an interference effect similar to speckle will be produced.

Single scattering applies to a limited number of situations since it requires that all of the turbulence be localized in one area. More realistically, the turbulence is distributed throughout the path from the source to the receiver. In this case random phase delays will be introduced continuously throughout the propagation path.

If the turbulence is very weak (C_n^2 is small or the path length is very short), the propagating wave remains coherent when it reaches the receiver. However, random phase shifts will nevertheless be introduced along the path that will, for each of the multiple paths taken by the wave, add a random phase. The statistics that describe this case should also be given by those of

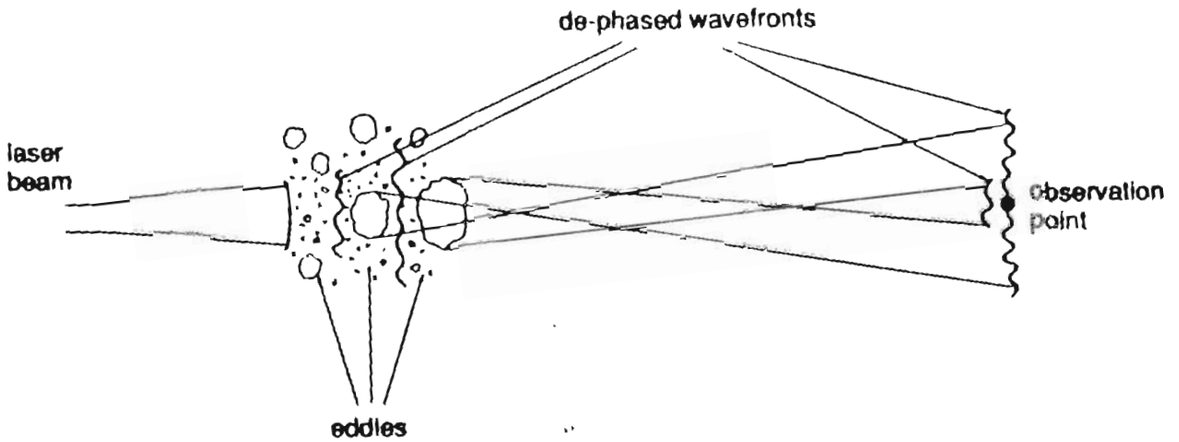

Figure 2.9 - Illustration of Turbulence (single scattering)

the single scattering model. However, if the turbulence is not weak, the wave will lose coherence and another model is needed.

Following Strohbehn[13], the propagation path is divided into a number of turbulence areas, and for convenience each area is considered to be larger than the outer scale in order to insure independence between the areas. Each turbulence area will introduce an attenuation and phase shift. The accumulated effect of the turbulence on a single wave is given by[13].

$$E_j = \prod_{m=1}^{n} e^{\chi_m + i\psi_m} \tag{2.19}$$

where E_j is a propagation factor representing the accumulated effects of the turbulence on one of the waves. The incident field phasor is multiplied by E_j to determine the phasor field received by the jth path.

χ_m represents the attenuation and ψ_m the phase introduced at each turbulence area. Since the multiplication of the exponentials results in the addition of exponents, the logarithms of the individual fields will add. This means that the logarithm of the combined field variations can be expressed by,

$$\ln(E_j) = \chi + i\psi = \sum_{m=1}^{n} \chi_m + i\psi_m$$

χ_m is the logarithm of the amplitude factor and ψ_m is the phase for the mth turbulence area. If the path is long compared to the outer scale so that the number of turbulence area is large, the probability density function of both χ and ψ will be Gaussian based upon the central limit theorem. ψ represents the unwrapped phase since the phase terms in (2.19) are additive.

This describes the turbulence effect on the wavefront of a single ray of light. Since the rays are being deflected randomly by the larger eddies, the

field received at any location is the sum of a large number of such randomly phased waves. For this reason, the phasor that represents the received field will be the sum of a large number of terms like (2.19) plus a constant term representing the unscattered part of the field. Therefore,

$$E=B+\sum_{j=1}^{N} E_j$$

This should produce a speckle type effect when the turbulence is weak and each wave is relatively coherent. Strong turbulence, however, should lessen the interference effects and the total received field will be an average of all of the received fields. For strong turbulence or long path lengths, a saturation effect for the intensity has been noticed experimentally[13]. At saturation the intensity variation at the receiver is a maximum and in fact may decrease slightly as the turbulence gets stronger[13]. This effect can be explained by the loss in coherence of the received fields and occurs when the variance of ψ is of the order of or greater than π^2.

A different approach has been taken by Andrews and Phillips[16]. They use a model that takes into account non-uniform statistical fluctuations that have been observed in intensity measurements for both localized and distributed turbulence. Their model simulates two different frequency scales that are observed in the data.

2.2.2 Probability Density for Turbulence Phase

Single Scattering

If the turbulence is weak or the turbulence is localized, the single scattering model can be used. The statistics for turbulence will be the same

as those for speckle from a partially diffuse target. Therefore, the complex field at the receiver will be composed of a constant term, assumed to be real, representing the portion of the wave that is unscattered and a zero mean random term due to the random refractive index variations of the turbulent eddies. If the random term is circularly Gaussian with variance σ^2, the probability density function of the wrapped phase is given by (2.14)[13],

$$P_\theta(\theta)=\frac{e^{-r}}{2\pi}+\sqrt{r/\pi}\cos\theta\exp(-r\sin^2\theta)\Phi(\sqrt{2r}\cos\theta) \qquad (2.14)$$

In this case the beam ratio parameter is given by,

$$r=\frac{I_s}{\sigma^2} \qquad (2.14b)$$

where I_s represents the intensity of the field in the absence of turbulence, and σ^2 is the total variance of the real or imaginary fields as determined by the strength of the turbulence.

The value σ^2 can be found from the variance of the intensity using[1].

$$\sigma_I^2=\sigma^4(1+2r)$$

or,

$$\sigma^2=\frac{\sigma_I}{\sqrt{(1+2r)}}$$

For weak turbulence r is large and (2.14) approaches a Gaussian distribution given by,

$$p_\theta(\theta)=\sqrt{r/\pi}\exp(-r\theta^2)$$

When the turbulence is strong, r is small and (2.14) approaches a uniform distribution. Of course, the single scattering model will most likely not be valid in this case.

Multiple Scattering

It is assumed that the probability density function for the unwrapped phase is Gaussian for both single or multiple scattering. Most of the evidence suggests that the unwrapped phase is Gaussian whether the received field is composed of the sum of coherent or partially coherent fields or results from the product of fields with a Gaussian distribution of the phase ψ_m. In fact, it has already been shown that the distributions of (2.7) and (2.14) are essentially wrapped Gaussian distributions. Therefore, the probability density function of unwrapped phase for a point source propagating through turbulence is given as,

$$P_\mu(\mu)=\frac{1}{\sigma_\mu\sqrt{2\pi}}\exp\left(-\frac{(\mu-\mu_0)^2}{2\sigma_\mu^2}\right) \tag{2.20}$$

where μ is the unwrapped phase and μ_0 is the mean phase.

To determine σ_μ, an equation for the covariance of phase at two receiver locations for a point source with two different wavelengths[10] is used. If only a single receiver location is considered, the covariance reduces to the variance and considering only a single wavelength, the equation reduces to

$$\sigma_\mu^2=0.132\pi^2k^2L\int_0^\infty KdK(K^2+L_o^{-2})^{-11/6}\exp(-K^2/K_m^2)$$
$$x\int_0^1 duC_n^2(u)\cos^2[u(1-u)K^2L/2k] \tag{2.21}$$

where

L = distance between the source and receiver

z = distance from source

u = z/L = normalized distance from source

$K_m = 5.92/l_o$

$k = 2\pi/\lambda$

K = spatial frequency variable

In (2.21) the von Karman turbulence spectrum is assumed.

For horizontal paths of only a few kilometers, and at a wavelength of 10.6 μm. C_n^2 does not change appreciably over the length of the path and a path averaged value can be used. If $L_o >> l_o$, $\exp(-K^2/K_m^2) \approx 1$ for all values of K that significantly affect the integral. Also if $\sqrt{L\lambda}$ is small compared to L_o then the second integral is approximately equal to one for all significant values of K. In this case the integration reduces to,

$$\sigma_\mu^2 \approx 0.132\pi^2 k^2 L C_n^2 \int_0^\infty K dK (K^2 + L_o^{-2})^{-11/6} \tag{2.22}$$

and

$$\sigma_\mu^2 \approx 0.0792\pi^2 k^2 L C_n^2 L_o^{5/3} \tag{2.23}$$

$$L_o >> l_o$$

$$\sqrt{L\lambda} << L_o$$

Equation (2.23) allows for the determination of phase variance for a point source propagating through turbulence from the values of outer scale of turbulence, path length, wavelength and C_n^2. The inner scale of turbulence is not needed if it is small compared to the outer scale. Typical values of L_o and l_o are 1 meter and 1 millimeter respectively. Considering a path length of 1 km and and CO_2 laser with $\lambda = 10.6$ micrometers, the above conditions for integration are met. When these conditions are not met, the integrals in (2.21) can be evaluated numerically. The equivalent of (2.22) and (2.23) was

also obtained by Flatte[25] using both the von Karman and Kolgomorov turbulence spectrums and by Fante[26] using the Kolgomorov spectrum.

2.3 Two Point Models for Speckle and Turbulence Phase

2.3.1 Probability Density for Speckle Phase

In this section two point models for the unwrapped phase of speckle and turbulence will be presented. In the first section, speckle propagating in a vacuum will be considered, and in the next section a point source propagating in turbulence will be covered.

The probability density function for the sum or difference of two Gaussian random variables is also Gaussian. Using the Gaussian models of unwrapped phase for the one point case, the probability distribution of phase differences for the unwrapped phase will be a Gaussian function of the phase difference between the two points.

Given that the density of phase ϕ_1 at point x_1 and ϕ_2 at point x_2 are

$$P_{\phi_1}(\phi_1)=\frac{1}{\sigma_{s_1}\sqrt{2\pi}}\exp\left[-\frac{(\phi_1-\mu_1)^2}{2\sigma_{s_1}^{\ 2}}\right] \tag{2.24}$$

and

$$P_{\phi_2}(\phi_2)=\frac{1}{\sigma_{s_2}\sqrt{2\pi}}\exp\left[-\frac{(\phi_2-\mu_2)^2}{2\sigma_{s_1}^{\ 2}}\right] \tag{2.25}$$

then the two point density function of phase differences will be[21]

$$P_{\Delta\phi}(\Delta\phi)=\frac{1}{\sigma_{\Delta s}\sqrt{2\pi}}\exp\left[-\frac{(\Delta\phi-\Delta\mu)^2}{2\sigma_{\Delta s}^2}\right] \tag{2.26}$$

where $\Delta\phi=\phi_2-\phi_1$ is the phase difference, $\Delta\mu=\mu_2-\mu_1$ is the mean phase

difference and $\sigma_{\Delta s}^2=\sigma_{s_1}{}^2+\sigma_{s_2}{}^2-2<(\phi_1-\mu_1)(\phi_2-\mu_2)>$.

If the receiver separation is small compared to the target distance from the receivers, the variables ϕ_1 and ϕ_2 can be assumed stationary in the wide sense and $\sigma_{s_1}{}^2=\sigma_{s_2}{}^2=\sigma_s^2$.

Therefore,

$$\sigma_{\Delta s}^2=2\sigma_s^2-2<(\phi_1-\mu_1)(\phi_2-\mu_2)>=2\sigma_s^2\left[1-\frac{<(\phi_1-\mu_1)(\phi_2-\mu_2)>}{\sigma_s^2}\right]$$

Assuming the correlation coefficient of phases defined as,

$$\rho_\phi^2=\frac{<(\phi_1-\mu_1)(\phi_2-\mu_2)>}{\sigma_s^2}$$

then $\sigma_{\Delta s}$ is given by,

$$\sigma_{\Delta s}=\sigma_s\sqrt{2(1-\rho_\phi^2)} \tag{2.27}$$

Considerable difficulty was experienced in obtaining an analytical expression for the correlation coefficient of speckle. A correlation function for the general case of partially developed speckle from a totally diffuse target was never obtained due to the complexity of the two point joint density function of the complex field amplitudes. Instead, the analysis of the two point phase statistics is divided into two parts.

The first part involves only fully developed speckle where the joint probability density function of the wrapped phases at two points has already been found[1,4,21] and depends on the mutual coherence function of the fields. The phase covariance and phase correlation coefficient functions are determined from the joint probability density function of wrapped phase, and the conditional probability density function for the phase at one point condi-

tioned on the phase at the second point will be compared to a wrapped Gaussian function.

Next, the work of Wang[7] is used to estimate the value of $\sigma_{\Delta s}$ in equation (2.26) from the phase extent of the complex fields when the receiver is in the far-field of diffraction and the target phase deviation is small. It is also shown that when the phase deviation is small, the square root of the correlation coefficient of phase differences is approximately equal to the correlation coefficient of the imaginary fields at the two receiver points. In determining the phase extent and correlation coefficient, the conditional probability density function of speckle phase at one point given the value of the intensity and phase at a second point is used.

Fully Developed Speckle

The joint probability density function of wrapped phase at two points for the special case of fully developed speckle, has been determined[1,21] from the fourth-order probability density function of the jointly Gaussian complex fields, $U_1V_1U_2V_2$. It is a function of the difference in the phases of the two points and the complex coherence factor and is given by,

$$P(\theta_1,\theta_2)=\frac{1-|\mu|^2}{4\pi^2}(1-\beta^2)^{-3/2}\left(\beta\sin^{-1}\beta+\frac{\pi\beta}{2}+\sqrt{1-\beta^2}\right) \tag{2.28}$$

where μ is the complex coherence factor defined by,

$$\mu=\frac{<E_1E_2^*>}{\sqrt{<I_1><I_2>}}\exp(-i\psi) \tag{2.28a}$$

$$<I_1>=<E_1E_1^*>$$

$$<I_2>=<E_2E_2^*>$$

$$\beta=|\mu|\cos(\Delta\theta-\psi)$$

$$\Delta\theta=\theta_2-\theta_1$$

E_1 and E_2 are the complex fields at points 1 and 2 respectively. Both θ_1 and θ_2 lie in the primary interval $-\pi$ to π.

The conditional probability density function of the phase θ_1 at point 1 given the phase θ_2 at point 2 is related to the probability density function of phase differences by,

$$P(\theta_2|_{\theta_1})=P(\theta_1,\theta_2)/P(\theta_1)$$

Both $P(\theta_1)$ and $P(\theta_2)$ are uniform and equal to $1/2\pi$ so the conditional distribution becomes,

$$P(\theta_2|_{\theta_1})=\frac{1-|\mu|^2}{2\pi}(1-\beta^2)^{-3/2}\left(\beta\sin^{-1}\beta+\frac{\pi\beta}{2}+\sqrt{1-\beta^2}\right) \qquad (2.29)$$

The parameter $|\mu|$ depends on the separation distance between the two receiver points[3] and can be determined after the parameters of the beam and the target are specified. When there is no separation, $|\mu|$ is one and (2.29) becomes the impulse function,

$$P(\theta_2|_{\theta_1})=\delta(\theta_2-\theta_1-\psi)$$

centered at ψ. As the separation becomes large, $|\mu|$ approaches zero, and (2.29) becomes a uniform distribution with a value of $1/2\pi$.

$P(\theta_2|_{\theta_1})$ depends on $\theta_2-\theta_1$ and not on θ_1 or θ_2. Therefore (2.29) will also represent the probability density function of the phase difference.

In order to use equation (2.27), an unwrapped phase correlation coefficient for the probability density function of unwrapped phase difference must be obtained. The correlation coefficient for the wrapped phase is defined as,

$$\rho_\theta = \frac{\sqrt{<\theta_1\theta_2>}}{\sigma_\theta} = \frac{\sqrt{<\theta_1\theta_2>}}{\pi/\sqrt{3}} \tag{2.30}$$

where $\pi/\sqrt{3}$ is the standard deviation of the one point wrapped phase, and the mean values of θ_1 and θ_2 are considered to be zero. The covariance of phase is defined by the integral,

$$<\theta_1\theta_2> = \int_{-\pi}^{\pi}\int_{-\pi}^{\pi} \theta_1\theta_2 P(\theta_1,\theta_2)d\theta_1 d\theta_2$$

which has been evaluated[21] as,

$$<\theta_1\theta_2> = \pi\sin^{-1}|\mu| - (\sin^{-1}|\mu|)^2 + \frac{1}{2}\sum_{n=1}^{\infty}\frac{|\mu|^{2n}}{n^2} \tag{2.31}$$

using the relationship,

$$<|\theta_2-\theta_1|^2> = 2(<\theta^2> - <\theta_2\theta_1>) = 2\left(\frac{\pi^2}{3} - <\theta_2\theta_1>\right)$$

where

$$\sigma^2_{\Delta\theta} = <|\theta_2-\theta_1|^2>$$
$$= 2\left(\frac{\pi^2}{3} - \pi\sin^{-1}|\mu| + (\sin^{-1}|\mu|)^2 - \frac{1}{2}\sum_{n=1}^{\infty}\frac{|\mu|^{2n}}{n^2}\right) \tag{2.31a}$$

was determined[21] from (2.28). Using (2.31), ρ_θ is plotted vs $|\mu|$ in figure 2.10.

Donati and Martini[4] use the same joint probability density function of wrapped phase given in (2.28) to obtain an expression for the conditional variance of θ_2 given the value of θ_1 as,

$$\sigma^2_{\theta_2|\theta_1} = \frac{\pi^2}{3} - \pi\sin^{-1}|\mu| + (\sin^{-1}|\mu|)^2 - \frac{1}{2}\sum_{n=1}^{\infty}\frac{|\mu|^{2n}}{n^2} \tag{2.31b}$$

which is exactly (2.31a) divided by two. They also determine the conditional variance of θ_2 conditioned on the intensity and the phase at receiver point one.

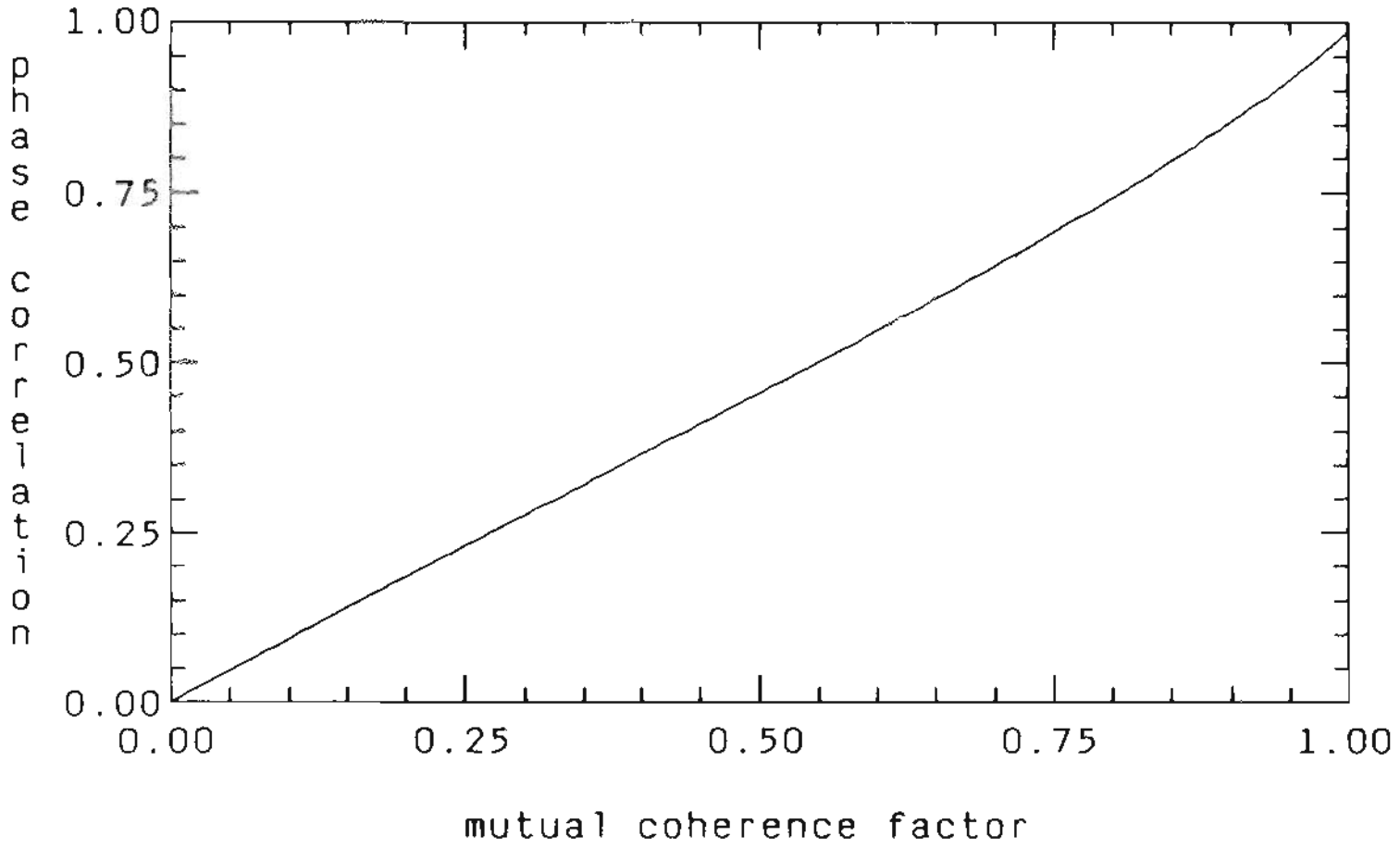

Figure 2.10 - Phase Correlation Coefficient vs. Coherence Factor (fully developed speckle)

It is difficult to relate the expressions for the wrapped correlation coefficient and wrapped variances to the case of unwrapped phase. The variance of unwrapped phase difference given in (2.27) requires both a value for the correlation coefficient and the unwrapped standard deviation of phase, the latter of which can be any value greater than about π radians for fully developed speckle. A comparison of (2.29) with a wrapped Gaussian distribution is shown in figure 2.11 for three different values of $|\mu|$. The values of the Gaussian standard deviation used for wrapping are shown in figure 2.12 and were chosen so that the wrapped Gaussian and (2.29) would have approximately the same shape and size. Also in figure 2.12 the square root of equations (2.13a) and (2.31b) are shown. The variance of phase was numerically calculated from (2.29) for several values of $|\mu|$ and is indistinguishable from equation (2.31b).

The probability density function of (2.29) does not match the wrapped Gaussian function well except where the distributions are both approximately uniform. Nevertheless, Gaussian functions of appropriate standard deviation can be found that agree reasonably well after phase wrapping. The major problem in order to use the Gaussian unwrapped probability density function to approximate (2.29) is to find the appropriate standard deviation of phase difference. As already mentioned, the standard deviation depends on both the value of unwrapped standard deviation and unwrapped correlation coefficient. This problem has not yet been solved.

Partially Developed Speckle

The phase extent of the equiprobability density ellipse for the condi-

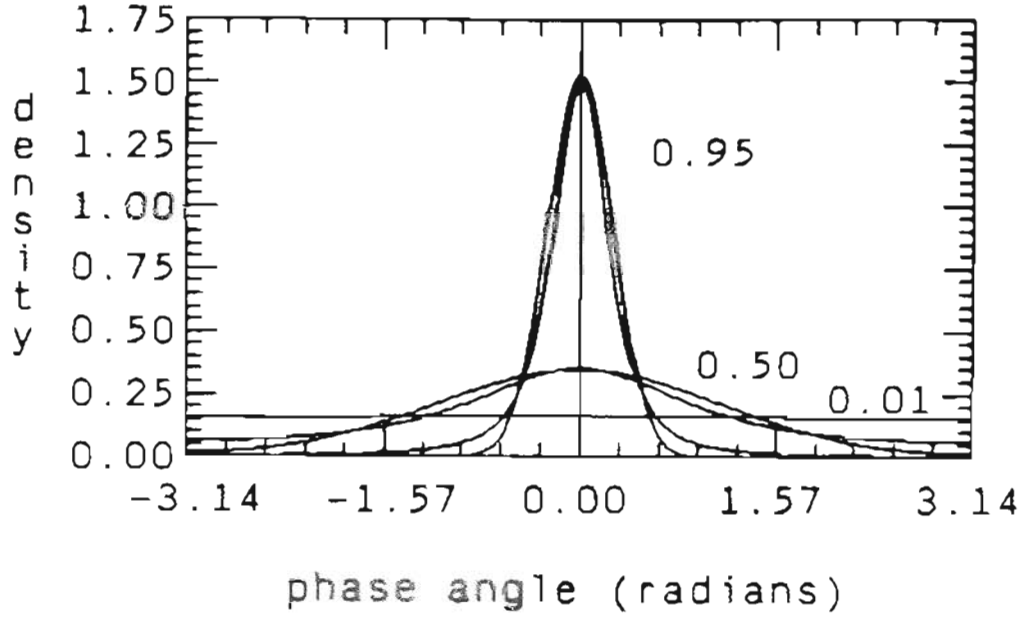

Figure 2.11 - Eqn. 2.29 and Wrapped Gaussian μ=.01, .5, .95

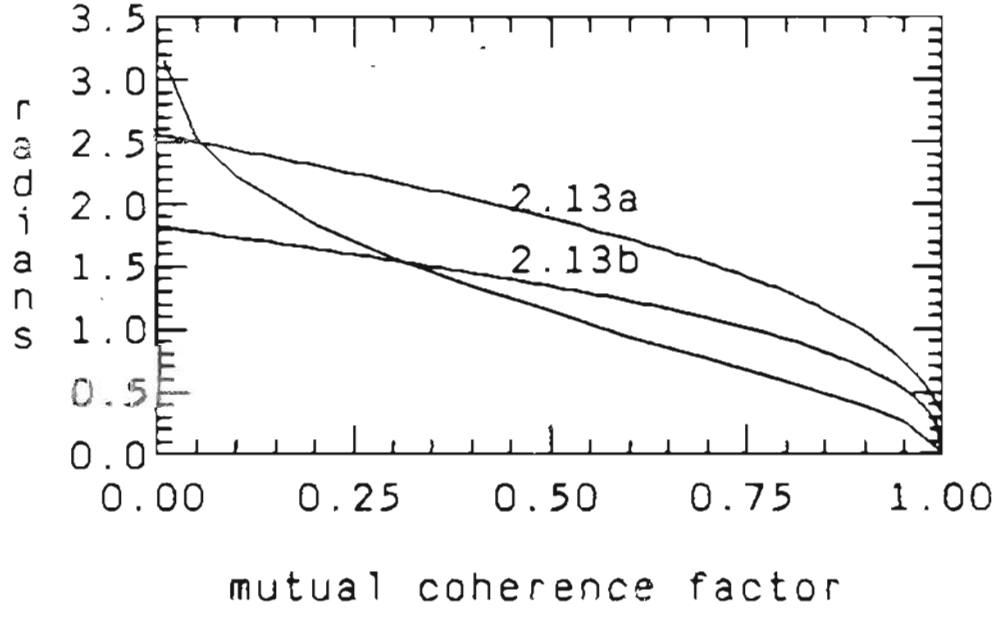

Figure 2.12 - Unwrapped Gaussian Deviation and eqns. 2.13a,b vs. μ

tional probability density function of the complex field quantities U_2,V_2 at one point given the complex field quantities U_1,V_1 at a second point can be used to estimate the variance of the phase difference between the points.

If a totally diffuse target is illuminated by a Gaussian beam at its waist and the observation points are in the far-field, the real and imaginary fields are uncorrelated, ρ in (2.4) is zero, and the one-point and two-point probability density functions have been shown by Wang[7] to be,

$$P(U_1,V_1)=\frac{1}{2\pi\sigma_{r_1}\sigma_{i_1}}\exp\left(-\frac{1}{2}\left(\frac{\Delta U_1^2}{\sigma_{r_1}^2}+\frac{\Delta V_1^2}{\sigma_{i_1}^2}\right)\right) \tag{2.33}$$

and

$$P(U_1,V_1,U_2,V_2)= \tag{2.34}$$

$$\frac{1}{2\pi\sigma_{r_1}\sigma_{r_2}\sqrt{(1-\gamma_r^2)}}\exp\left(-\frac{1}{2(1-\gamma_r^2)}\left(\frac{\Delta U_1^2}{\sigma_{r_1}^2}-2\frac{\gamma_r\Delta U_1\Delta U_2}{\sigma_{r_1}\sigma_{r_2}}+\frac{\Delta U_2^2}{\sigma_{r_2}^2}\right)\right)$$

$$\times\frac{1}{2\pi\sigma_{i_1}\sigma_{i_2}\sqrt{(1-\gamma_i^2)}}\exp\left(-\frac{1}{2(1-\gamma_i^2)}\left(\frac{\Delta V_1^2}{\sigma_{i_1}^2}-2\frac{\gamma_i\Delta V_1\Delta V_2}{\sigma_{i_1}\sigma_{i_2}}+\frac{\Delta V_2^2}{\sigma_{i_2}^2}\right)\right)$$

where

$$\Delta U_1=U_1-\langle U_1\rangle \quad \Delta U_2=U_2-\langle U_2\rangle \quad \Delta V_1=V_1-\langle V_1\rangle \quad \Delta V_2=V_2-\langle V_2\rangle$$

$$\sigma_{r_1}^2=\langle\Delta U_1^2\rangle \quad \sigma_{r_2}^2=\langle\Delta U_2^2\rangle \quad \sigma_{i_1}^2=\langle\Delta V_1^2\rangle \quad \sigma_{i_2}^2=\langle\Delta V_2^2\rangle$$

$$\gamma_r=\langle\Delta U_1\Delta U_2\rangle/(\sigma_{r_1}\sigma_{r_2})$$

$$\gamma_i=\langle\Delta V_1\Delta V_2\rangle/(\sigma_{i_1}\sigma_{i_2})$$

γ_r represents the correlation coefficient of the real components of the two fields and γ_i represents the same for the imaginary parts.

Dividing (2.34) by (2.33) gives the conditional probability density function of the fields at point 2 given the field at point 1 which simplifies[7] to,

$$P(U_2,V_2|_{U_1,V_1}) = \frac{1}{2\pi\sigma_r\sigma_i}\exp\left(-\frac{1}{2}\left(\frac{(U_2-<U>)^2}{\sigma_r^2}+\frac{(V_2-<V>)^2}{\sigma_i^2}\right)\right) \qquad (2.35)$$

where

$$<U> = <U_2> + \gamma_r\frac{\sigma_{r_2}}{\sigma_{r_1}}(\sqrt{I_1}\cos\theta_1 - <U_1>)$$

$$= <U_2> + \gamma_r\frac{\sigma_{r_2}}{\sigma_{r_1}}(U_1 - <U_1>)$$

$$<V> = \gamma_i\frac{\sigma_{i_2}}{\sigma_{i_1}}\sqrt{I_1}\sin\theta_1 = \gamma_i\frac{\sigma_{i_2}}{\sigma_{i_1}}V_1$$

$$\sigma_r = \sqrt{(1-\gamma_r^2)}\sigma_{r_2}$$

$$\sigma_i = \sqrt{(1-\gamma_i^2)}\sigma_{i_2}$$

are the conditional mean and standard deviations of the real and imaginary values of complex field at location 2 conditioned on the intensity and phase angle of the field at location 1 and,

$U_1 = \sqrt{I_1}\cos\theta_1$ and $V_1 = \sqrt{I_1}\sin\theta_1$ $U_2 = \sqrt{I_2}\cos\theta_2$ and $V_2 = \sqrt{I_2}\sin\theta_2$

The quantities in the above equations are evaluated[7] as,

$$\gamma_r = e^{-\frac{\Delta x^2}{2}}\left(\frac{h_+ - h_- e^{-2x_1x_2}}{\sqrt{(h_+ - h_- e^{-2x_1^2})(h_+ - h_- e^{-2x_2^2})}}\right)$$

$$\gamma_i = e^{-\frac{\Delta x^2}{2}}\left(\frac{h_+ + h_- e^{-2x_1x_2}}{\sqrt{(h_+ + h_- e^{-2x_1^2})(h_+ + h_- e^{-2x_2^2})}}\right)$$

$$\sigma_{r_2} = \frac{1}{2}\pi w_o\alpha e^{-\sigma_\delta^2/2}\sqrt{h_+ - h_- e^{-2x_2^2}}$$

$$\sigma_{i_2}=\frac{1}{2}\pi w_o\alpha e^{-\sigma_\phi^2/2}\sqrt{h_+ + h_- e^{-2x_2^2}}$$

$$\sigma_{r_1}=\frac{1}{2}\pi w_o\alpha e^{-\sigma_\phi^2/2}\sqrt{h_+ - h_- e^{-2x_1^2}}$$

$$\sigma_{i_1}=\frac{1}{2}\pi w_o\alpha e^{-\sigma_\phi^2/2}\sqrt{h_+ + h_- e^{-2x_1^2}}$$

$$<U_1>=\pi w_o^2 e^{-\sigma_\phi^2/2}e^{-x_1^2}$$

$$<U_2>=\pi w_o^2 e^{-\sigma_\phi^2/2}e^{-x_2^2}$$

$$<V_1>=<V_2>=0$$

where

$$h_+=\sum_{n=1}^{\infty}\frac{\sigma_\phi^{2n}}{n!n}$$

$$h_-=-\sum_{n=1}^{\infty}\frac{(-\sigma_\phi{}^2)^n}{n!n}$$

x_1 is the normalized distance in the receiver plane from the optic axis to receiver 1

x_2 is the normalized distance in the receiver plane from the optic axis to receiver 2

and $\Delta x=x_2-x_1$.

The normalizing distance is $\lambda L/\pi w_o$ and L is the distance from the target to receiver number 1.

$N=(w_o/\alpha)^2$ is the number of independent scatterers, where w_o is the beam waist of the laser on the target, σ_ϕ is the target phase deviation, α is the correlation length of the target scatterers defined by

$$\rho(\Delta\chi)=\exp\left(\frac{-|\chi_2-\chi_1|^2}{\alpha^2}\right)$$

and χ is the transverse distance along the target surface.

The phase extent for the conditional density function is given by (2.11) as,

$$\theta_e = \frac{1}{2}\tan^{-1}\left[2\frac{\sqrt{<U>^2\sigma_i^2+<V>^2\sigma_r^2-(\sigma_r\sigma_i)^2}}{<U>^2+<V>^2-\sigma_r^2-\sigma_i^2}\right] \qquad (2.11a)$$

In (2.11a), θ_e, $<U>$, $<V>$, σ_r and σ_i refer to the equiprobability density ellipse for the conditional probability density function of (2.35).

The above relationships for the conditional density functions are extremely involved, and are valid only for the special case of the far-field of observation. A general case for partially developed speckle has not been found. In order to simplify the equations further, assumptions consistent with the far-field of observation will be made.

In the far field, $<V_2> = <V_1> = 0$ in (2.35) and the probability density ellipses for either location 1 or 2 have a large offset along the real axis. They also have a larger imaginary than real width (see figure 2.4a). Consequently V_1 and V_2 will be small compared to U_1 and U_2 respectively, $\Delta U_1 <<< U_1>$ and $\Delta U_2 <<< U_2>$. Therefore, noting that γ_r and γ_i are both less than or equal to one and the ratios $\sigma_{r_2}/\sigma_{r_1}$ and $\sigma_{i_2}/\sigma_{i_1}$ will both be about one unless Δx is extremely large, $<V>$ can be considered zero and $<U>$ can be approximated by $<U_2>$. Equation (2.11a) will therefore reduce to,

$$\theta_e \approx \frac{1}{2}\tan^{-1}\left[2\frac{\sqrt{<U_2>^2\sigma_i^2-(\sigma_r\sigma_i)^2}}{<U_2>^2-\sigma_r^2-\sigma_i^2}\right]$$

If in addition σ_Φ is small compared to one, $\sigma_{r_2} << \sigma_{i_2}$ and $\sigma_{r_1} << \sigma_{i_1}$.

Therefore, σ_r and σ_i are both small compared to $<U_2>$ and,

$$\theta_e \approx \frac{1}{2}\tan^{-1}\left\{\frac{2\sigma_i}{<U_2>^2}\right\} \approx \frac{1}{2}\tan^{-1}\left\{2\frac{\sigma_{i_2}\sqrt{1-\gamma_i^2}}{<U_2>}\right\}$$

When $\sigma_\phi << 1$, $h^+ \approx h^- \approx \sigma_\phi^2$, and if $\Delta x << x_1$ or x_2,

$$\sigma_{i_2} \approx 1/2\pi w_o \alpha \sigma_\phi \sqrt{1+e^{-2x^2}}$$
$$<U_2> \approx \pi w_o^2 e^{-x^2}$$
$$\gamma_i \approx e^{-\Delta x^2/2}$$

where $x_1 \approx x_2 = x$.

When the approximation, $\tan\theta \approx \theta$ for small angles is used equation (2.11a) further reduces to,

$$\theta_e \approx \frac{\alpha\sigma_\phi\sqrt{(1+e^{-2x^2})(1-e^{-\Delta x^2})}}{2w_o e^{-x^2}}$$
$$\approx \frac{\sigma_\phi \Delta x}{2}\left\{\frac{e^{2x^2}+1}{N}\right\}^{1/2} \qquad (2.11b)$$

Figure 2.13 shows equation (2.11a) vs. Δx for x_1 equal to 0 and 1.0 and three values of σ_ϕ. In the figure, N=100 and the shaded areas represent values of U_1 and V_1 within the probability density ellipse of figure 2.4a. The approximation of equation (2.11b) is also shown in the figures. When $\sigma_\phi << 1$ the conditions of figure 2.4a apply and $\theta_e \approx \sigma_s$ for the one point probability density function. The wrapped and unwrapped density functions are approximately the same and $\sigma_{\Delta s}$ will given approximately by (2.11b).

In the next section the correlation coefficient of phase differences will be shown to be approximately equal to the square root of the correlation coefficient for the imaginary fields when the target phase deviation is small.

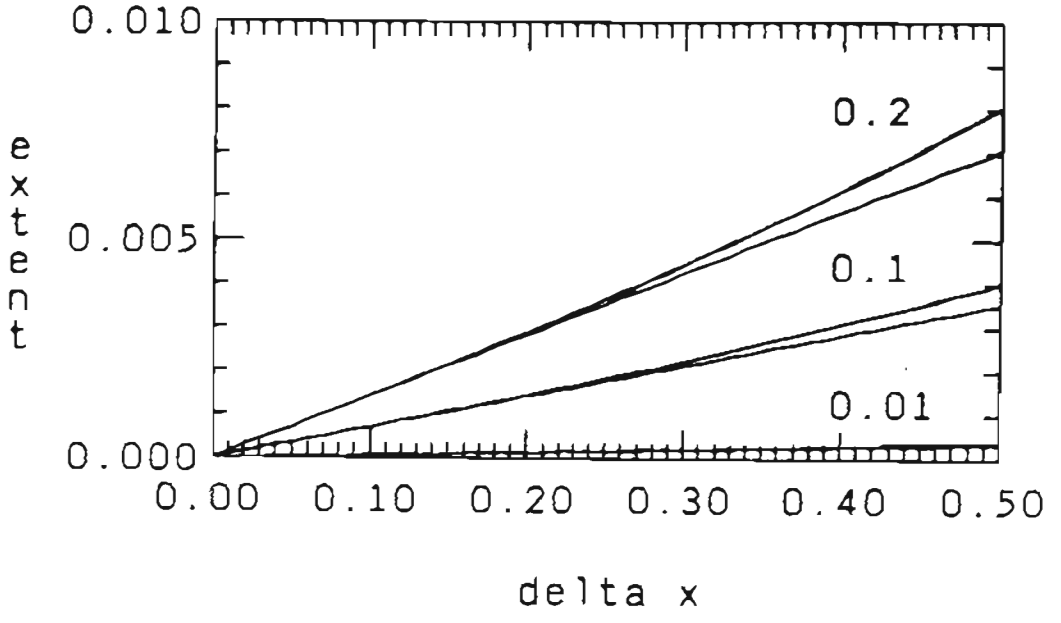

(a) x1=0

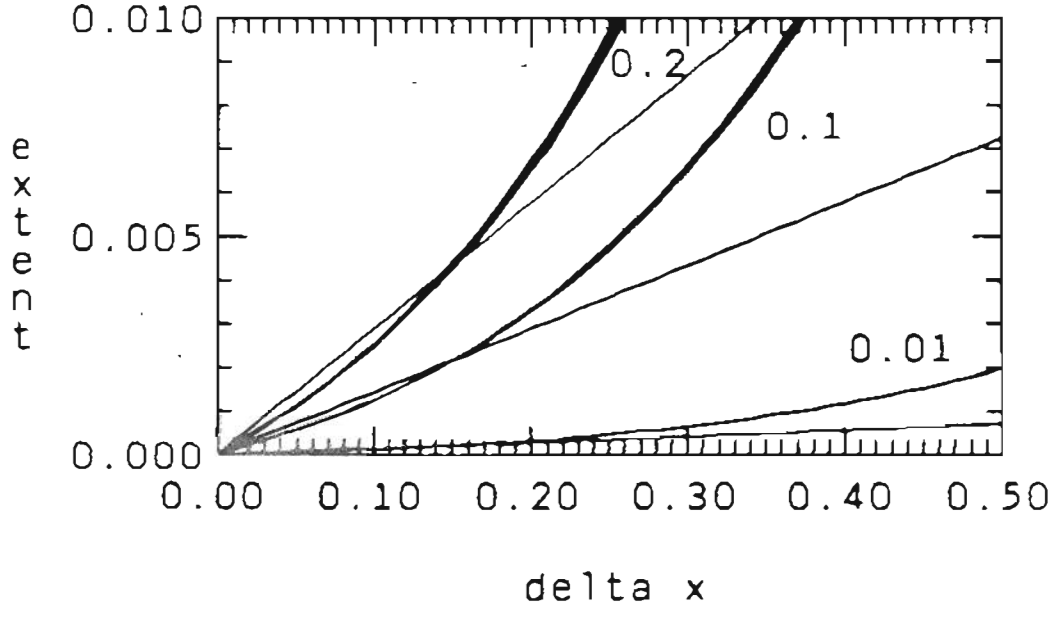

(b) x1=1.0

Figure 2.13 - θ_e and eqn. 2.11b vs. Δx,
σ_ϕ=0.01, 0.1, 0.2

The correlation coefficient of phase differences is found from the covariance of phases at the two receiver points. Therefore,

$$\rho_\phi^2 = \frac{<\phi_1\phi_2>}{\sigma_\phi^2}$$

where the mean phases are assumed zero and

$$<\phi_1\phi_2> = \int_{-\infty}^{\infty}\int_{-\infty}^{\infty} \phi_1\phi_2 P(\phi_1,\phi_2)d\phi_1 d\phi_2$$

When $\sigma_\phi << 1$, and in the far-field, the one point unwrapped and wrapped phase have been shown to be essentially the same (see figure 2.4a) and that $\tan\phi \approx \phi \approx V/U$. Therefore,

$$<\phi_1\phi_2> \approx < \frac{V_1}{U_1}\frac{V_2}{U_2} > = \int_{-\infty}^{\infty}\int_{-\infty}^{\infty}\int_{-\infty}^{\infty}\int_{-\infty}^{\infty} \frac{V_1}{U_1}\frac{V_2}{U_2} P(U_1,V_1,U_2,V_2)dU_1dV_1dU_2dV_2$$

The real and imaginary fields in (2.34) are not correlated, therefore,

$$<\phi_1\phi_2> \approx$$
$$\int_{-\infty}^{\infty}\int_{-\infty}^{\infty} V_1V_2P(V_1,V_2)dV_1dV_2 \int_{-\infty}^{\infty}\int_{-\infty}^{\infty} \frac{1}{U_1U_2} P(U_1,U_2)dU_1dU_2 \qquad (2.36)$$

As noted previously, when $\sigma_\phi << 1$, ΔU_1 and ΔU_2 are small compared to $<U_1>$ and $<U_2>$ respectively. Therefore the second integrals in (2.36) reduce to $1/<U_1><U_2>$. Consequently,

$$<\phi_1\phi_2> \approx \frac{1}{<U_1><U_2>} \int_{-\infty}^{\infty}\int_{-\infty}^{\infty} V_1V_2P(V_1,V_2)dV_1dV_2 = \frac{<V_1V_2>}{<U_1><U_2>}$$

Therefore,

$$\rho_\phi^2 = \frac{<\phi_1\phi_2>}{\sigma_\phi^2} \approx \frac{<V_1V_2>}{<U_1><U_2>\sigma_\phi^2} \qquad (2.37)$$

Since the correlation coefficient of the imaginary fields is given by,

$$\gamma_i = \frac{<V_1 V_2>}{\sigma_{i_1}\sigma_{i_2}}$$

and the random variables ϕ_1 and ϕ_2 are assumed zero mean and stationary in the wide sense. Therefore, $\sigma_\phi^2 = <\phi^2>$ which for small ϕ can be considered equal to $<\frac{V_1^2}{U_1^2}> \approx \frac{<V_1^2>}{<U_1>^2}$ since the real field values are considered to be constant. Therefore,

$$\sigma_\phi^2 \approx \frac{<V_1^2>}{<U_1^2>} = \frac{\sigma_{i_1}^{\ 2}}{<U_1^2>} \tag{2.38}$$

Substituting (2.38) in the denominator of (2.37) and letting $<U_2>=<U_1>$ and $\sigma_{i_2}=\sigma_{i_1}$,

$$\rho_\phi^2 \approx \gamma_i \tag{2.39}$$

Figure 2.14 shows γ_i vs. Δx when σ_ϕ is equal to or less than 0.1 for two values of x_1. This figure can be used to predict the correlation coefficient of unwrapped phases when the target phase standard deviation is small compared to one.

2.3.2 Probability Density for Turbulence Phase

The phase structure function for turbulence has been studied extensively[8–16] and is a measure of the strength of turbulence. One way to measure the structure function is to measure the variance of phase difference. As for the one point statistics of turbulence phase, the probability density function of the unwrapped phase difference for a point source propagating through clear air turbulence is assumed to be a Gaussian function and is given by,

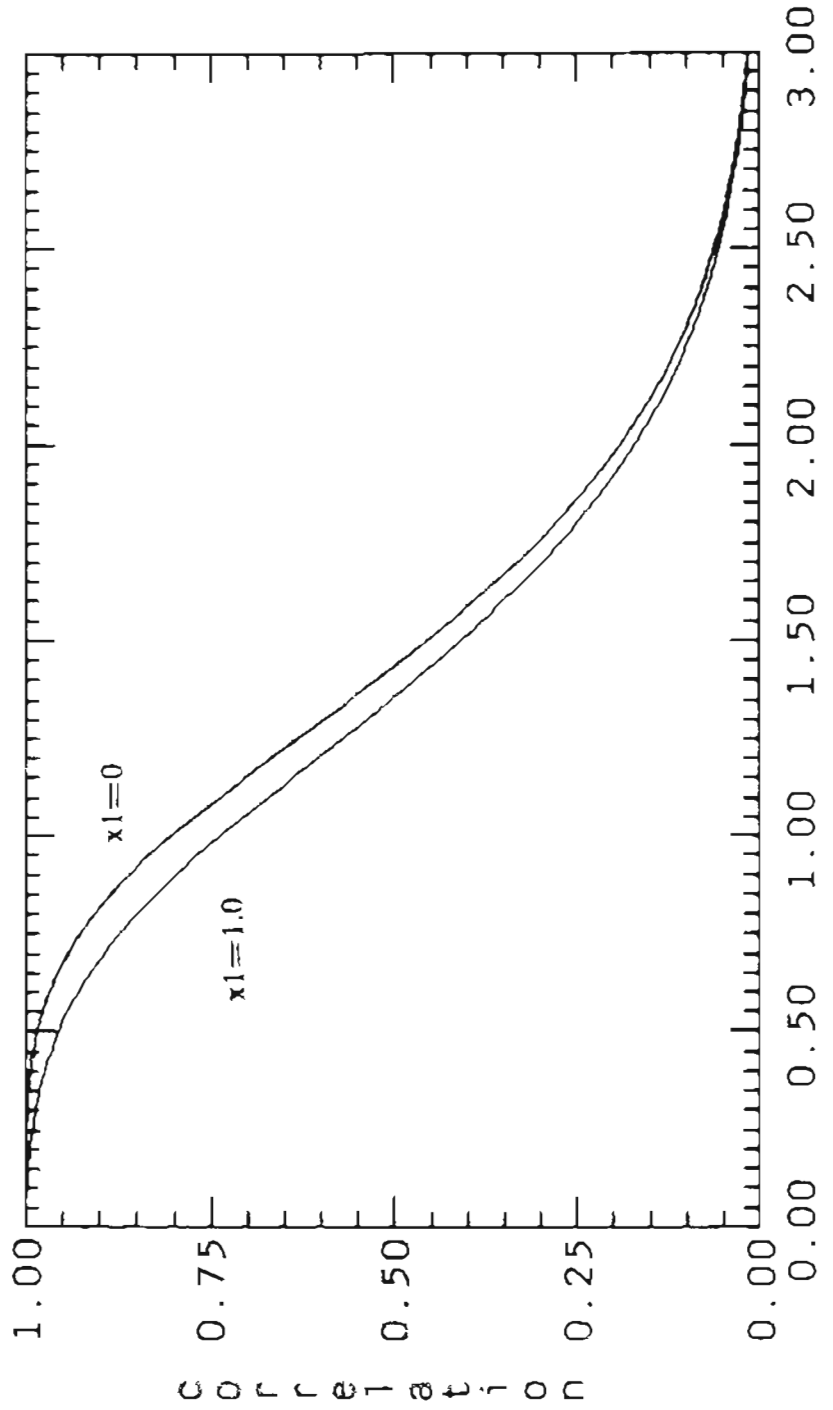

Figure 2.14 - γ_1 vs. Δx, $\sigma_\phi < 0.1$

$$P_{\mu}(\Delta\mu)=\frac{1}{\sigma_{\Delta\mu}\sqrt{2\pi}}\exp\left[-\frac{(\Delta\mu-\Delta\mu_0)^2}{2\sigma_{\Delta\mu}{}^2}\right] \tag{2.40}$$

where the variance[8] of phase difference is given by,

$$\sigma^2_{\Delta\mu}=2.92k^2LC_n^2\Delta x^{5/3} \tag{2.41}$$

$\Delta\mu_0$ is the mean turbulence phase difference and Δx is the receiver separation.

Using (2.41), the value of C_n^2 can be determined for a given path length of turbulence by measuring the variance of phase difference at a known receiver separation.

Some of the literature suggests that the probability density function of phase differences is not always Gaussian. Reference 14 compares histograms of phase difference measurements to Gaussian, exponential and one dimensional K distributions. The distributions tend toward bilateral exponential for small separations and Gaussian for large separations and higher moments of the measured distributions agree well with the moments of the K distribution for all separations. It is also suggested in the paper that the distributions tend toward Gaussian as the ratio of outer to inner scales of turbulence increases. These observations, however, are based on measurements in a restricted region of heated air rather than through a long path of natural turbulence.

CHAPTER 3

PROBABILITY DENSITY FUNCTIONS FOR UNWRAPPED PHASE AND FREQUENCY OF SPECKLE IN TURBULENCE

The speckle intensity pattern in the presence of turbulence and wind moves around in a random fashion due to temporal changes of the turbulent eddies which cause the beam to wander over the diffuse target. In addition, the wind and turbulence alter the speckle statistics and contribute an additional amplitude and phase modulation to the received field.

Following chapter 2, the unwrapped phase probability density functions for both speckle propagating in a vacuum and for a point source propagating in turbulence are assumed to be Gaussian. In order to account for the combined effect on the received phase of speckle propagating in turbulence, the turbulence is introduced into the speckle by allowing the mean value of the speckle phase to be modulated by the phase fluctuations of a point source propagating in turbulence.

The probability density function of the unwrapped phase is then found by integrating the marginal density function for the unwrapped speckle phase multiplied by the probability density function of unwrapped phase for a point source propagating through turbulence. This model is based on the model presented by Holmes and Gudimetla[17] for determining the probability density of the intensity for speckle propagating in turbulence (see appendix A).

In using the unwrapped phase with a Gaussian distribution, the results need not be limited to optically rough targets and will include all degrees of target roughness. In this way differences can be seen between the distributions produced by different targets in varying turbulence conditions even when the r.m.s. roughness of the target approaches or exceeds one wavelength or the strength of the turbulence approaches or exceeds the saturation value.

3.1 The Probability Density Function of Phase

Assume a laser beam incident upon a diffuse target and a receiver located at some distance away in a clear air turbulent medium. Each of the separate reflected fields produced by the diffuse target will be delayed or advanced according to refractive index variations caused by turbulence and wind. The variation in travel time about the mean travel time for any field component will depend on the refractive index variations along its path. Since the travel time is directly proportional to unwrapped phase, the mean value of the unwrapped speckle phase will also be proportional to the refractive index.

The model assumes that the mean value of the probability density function for speckle is modulated by the turbulence in the same manner as the phase from a point source would be modulated. Therefore the conditional probability density function of unwrapped phase given the mean value of speckle phase can be expressed as

$$P_{\phi}(\phi \mid \mu) = \frac{1}{\sigma_s \sqrt{2\pi}} \exp\left[-\frac{(\phi - \mu)^2}{2\sigma_s^2} \right] \tag{3.1}$$

where σ_s = the standard deviation of unwrapped phase at the receiver of a speckle field in free space, μ is the mean value of speckle phase, and ϕ is the combined phase due to speckle and turbulence.

The probability density function of unwrapped phase for a point source propagating through turbulence is given by,

$$P_\mu(\mu)=\frac{1}{\sigma_\mu\sqrt{2\pi}}\exp\left(\frac{-(\mu-\mu_o)^2}{2\sigma_\mu^2}\right) \tag{2.20}$$

where σ_μ = the standard deviation and μ_o = the mean value of phase at the receiver of a point source propagating through turbulence. Using equation (3.2) in (3.1), the unwrapped phase probability density function for speckle propagating through turbulence is given by,

$$P_\phi(\phi)=\int_{-\infty}^{\infty} P_\phi(\phi)\,|_\mu P_\mu(\mu)d\mu$$

$$=\frac{1}{2\pi\sigma_s\sigma_\mu}\int_{-\infty}^{\infty}d\mu\,\exp\left(\frac{-(\phi-\mu)^2}{2\sigma_s^2}-\frac{(\mu-\mu_o)^2}{2\sigma_\mu^2}\right) \tag{3.2}$$

which reduces to,

$$P_\phi(\phi)=\frac{1}{2\pi(\sigma_s^2+\sigma_\mu^2)^{1/2}}\exp\left(-\frac{(\phi-\mu_o)^2}{2(\sigma_s^2+\sigma_\mu^2)}\right)$$

or

$$P_\phi(\phi)=\frac{1}{\sigma\sqrt{2\pi}}\exp\left(-\frac{(\phi-\mu_o)^2}{2\sigma^2}\right) \tag{3.3}$$

where

$$\sigma=[\sigma_s^2+\sigma_\mu^2]^{1/2} \tag{3.4}$$

The model suggests that the combined unwrapped speckle/turbulence phase perturbations are Gaussian, additive and independent when the target characteristics and the turbulence effects are both Gaussian. The probability density function can then be found from the variance for target speckle and turbulence separately from the relationships given in chapter 2.

3.2 The Probability Density Function of Phase Difference

The probability density function of the sum or difference of two Gaussian random variables is also Gaussian. In chapter 2 the two point probability density function of unwrapped speckle phase was proposed as,

$$P_{\Delta\phi}(\Delta\phi)=\frac{1}{\sigma_{\Delta s}\sqrt{2\pi}}\exp\left[-\frac{(\Delta\phi-\Delta\mu)^2}{2\sigma_{\Delta s}^2}\right] \tag{2.26}$$

where $\Delta\phi = \phi_2-\phi_1$, $\Delta\mu = \mu_2-\mu_1$ and

(2.27)

is the standard deviation of phase difference

σ_s is the one point standard deviation of unwrapped speckle phase. The correlation coefficient is given by,

$$\rho_\phi^2=\frac{<(\phi_1-\mu_1)(\phi_2-\mu_2)>}{\sigma_s^2}$$

For a point source propagating in turbulence the distribution of phase differences is also Gaussian, and in chapter 2 was given as,

$$P_\mu(\Delta\mu)=\frac{1}{\sigma_{\Delta\mu}\sqrt{2\pi}}\exp\left[-\frac{(\Delta\mu-\Delta\mu_0)^2}{2\sigma_{\Delta\mu}{}^2}\right] \tag{2.40}$$

where

$$\sigma_{\Delta\mu}^2=2.92k^2LC_n^2\Delta x^{5/3} \tag{2.41}$$

is the variance of phase difference and Δx is the separation between the two points.

Using the same methods already used for treating speckle propagating in turbulence,

$$P_\phi(\Delta\phi \mid \Delta\mu)=\frac{1}{\sigma_{\Delta s}\sqrt{2\pi}}\exp\left[-\frac{(\Delta\phi-\Delta\mu)^2}{2\sigma_{\Delta s}^2}\right] \tag{3.5}$$

and the probability distribution for the two point unwrapped phase differences for a speckle field propagating in turbulence is,

$$P_\phi(\Delta\phi)=\int_{-\infty}^{\infty} P_\phi(\Delta\phi)\mid_{\Delta\mu} P_\mu(\Delta\mu)d\Delta\mu$$

Using equation (2.40) in (3.5)

$$P_\phi(\Delta\phi)=\frac{1}{\sigma_\Delta\sqrt{2\pi}}\exp\left[-\frac{(\Delta\phi-\Delta\mu_o)^2}{2\sigma_\Delta^2}\right] \tag{3.6}$$

where

$$\sigma_\Delta=[\sigma_{\Delta s}^2+\sigma_{\Delta\mu}^2]^{1/2}$$

and $\Delta\mu_0$ is the mean turbulence phase difference. In this case $\sigma_{\Delta s}$ refers to the standard deviation of phase differences for a speckle field in free space and $\sigma_{\Delta\mu}$ refers to the same for a point source propagating through turbulence.

3.3 The Probability Density Function of Frequency

If the frequency of the received field is a function of time, its statistics are closely related to the unwrapped phase statistics since the frequency is the derivative of the unwrapped phase. Based on the special property that linear operations on a Gaussian random variable produce statistics that

remain Gaussian, the probability density function of frequency will be a Gaussian random variable as long as the probability density of unwrapped phase is Gaussian. Therefore if the unwrapped probability density of phase is,

$$P_{\phi}(\phi)=\frac{1}{\sigma_{\phi}\sqrt{2\pi}}\exp\left(-\frac{\phi^2}{2\sigma_{\phi}^2}\right) \tag{3.7}$$

then the probability density function for the frequency is given by,

$$P_{\nu}(\nu)=\frac{1}{\sigma_{\nu}\sqrt{2\pi}}\exp\left(-\frac{\nu^2}{2\sigma_{\nu}}\right) \tag{3.8}$$

where ν is the frequency of the signal at the receiver and $\nu = \frac{d\phi/dt}{2\pi}$.

Both σ_{ϕ} and σ_{ν} can be found from their respective auto-covariance functions. The auto-covariance function of a variable x that is a random function of t, is itself a function of t and is given by the expected value of the product of x at one value of t with x at a different value of t. Therefore. $R_x(t,\tau) = <x(t)x(t+\tau)>$ and τ can take plus or minus values.

For the special case where x is a stationary random variable, the auto-correlation function is not a function of t and $R_x(t,\tau) = R_x(\tau)$.

The auto-covariance, $<x(t)x(t+\tau>$ reduces to the variance, $<x(t)^2>$ as τ approaches zero so,

$$\sigma_x^2=<x(t)^2>-<x(t)>^2$$

To obtain σ_{ν} from σ_{ϕ} the second derivative of the auto-covariance function[7] of ϕ is found using,

$$4\pi^2R_{\nu}(\tau)=-\frac{d^2R_{\phi}(\tau)}{d\tau^2} \tag{3.9}$$

and

$$R_{\phi}(\tau)=<\phi(t)\phi(t+\tau)>. \tag{3.10}$$

Then the limit of R_{ν} is evaluated for τ approaching zero.

This approach can be taken with the numerical data from the phase or frequency detectors used in the experiments. Using the unwrapped phase data a suitable averaging interval over time is used to obtain the autocorrelation function as a function of τ. Then the second derivative of the autocorrelation function is computed numerically. Finally the limit of the autocorrelation function is taken to arrive at the value of σ_{ν}. An inverse process can be used to obtain the phase variance from the frequency variance.

Another technique for relating the variances of the phase and the frequency is by use of the Fourier transform. The power spectral density is related to the autocorrelation function of a random variable by its Fourier transform,

$$S_{x}(\omega)=\frac{1}{2\pi}\int_{-\infty}^{\infty} R_{\phi}(\tau)e^{-i\omega\tau}d\tau \tag{3.11}$$

The Fourier transform of the derivative of a function is ω times the transform of the function, therefore since $\omega = d\phi/d\tau$,

$$S_{\nu}(\omega)=\frac{\omega^2 S_{\phi}(\phi)}{4\pi^2} \tag{3.12}$$

Using this relationship the variances of the frequency and phase are related by ω^2 and,

$$\sigma_{\phi}^2=2\pi\int_{-\infty}^{\infty}\frac{S_{\nu}(\omega)}{\omega^2}e^{i\omega\tau}d\omega \tag{3.13}$$

In the equations, ω represents the transformed variable τ.

Here again, using numerical methods, the autocorrelations can be found from the experimental data and from these the power spectrums are obtained.

These methods can be used for converting between the statistics of unwrapped phase and the statistics of frequency for both one and two point measurements.

CHAPTER 4

EXPERIMENTAL SYSTEM DESCRIPTION

Two different optical heterodyne systems were used to obtain the experimental data. The primary system made use of a single laser which provided both the transmitter and the local oscillator signals. Acousto-optic modulators produced the frequency shifts needed for the heterodyne frequency. In the other system the transmitter and local oscillator functions were provided by different lasers. Unfortunately it was not possible to obtain the necessary phase synchronization between the two lasers for phase or frequency measurements. Nevertheless both systems are reported here since the potential exists for improving the phase control of the two laser system. Each system has its own merits as to system cost, complexity and optical isolation between the transmitter and local oscillator beams.

Before each system is described in detail, the use of a heterodyne system to measure amplitude, phase and frequency information will be explained.

4.1 The Heterodyne System

Heterodyne systems have been used for electronic communication and measurement applications for many years. Some common examples are radio, television, radar and spectrum analyzers. From the early years of radio, with the advent of the superheterodyne receiver, heterodyne systems have provided a convenient method for channel selection and improved signal reception in the presence of background noise. Additionally, heterodyne sys-

tems allow coherent detection so that the instantaneous values of amplitude, phase and frequency of a signal can be received. More recently the invention of the laser has allowed heterodyne systems to operate at optical frequencies.

An optical heterodyne system is shown in figure 4.1. The local oscillator and transmitter provide optical signals with constant amplitude and frequency. The transmitter frequency is offset from the local oscillator frequency by a fixed amount, the heterodyne frequency. The received field has an amplitude, frequency and phase that vary according to the propagation path and the characteristics of a remote target. Using a beam splitter, the received field is combined with the local oscillator field at the optical detector to produce an output voltage or current that, within the frequency response limits of the detector, is proportional to the instantaneous value of the power contained in the combined fields.

The local oscillator field can be described by,

$$E_o = A_o \cos\theta_o \tag{4.1}$$

and the received field by,

$$E_r = A_r \cos\theta_r \tag{4.2}$$

A_o and θ_o represent the instantaneous amplitude and phase respectively of the local oscillator field and A_r and θ_r the corresponding quantities for the received field. Both fields are assumed to have the same polarization. Since the optical detector responds to the power of the total field, it's output is proportional to the square of the incident field. Neglecting a proportionality constant due to detector responsivity and mirror losses, the detector voltage is given by,

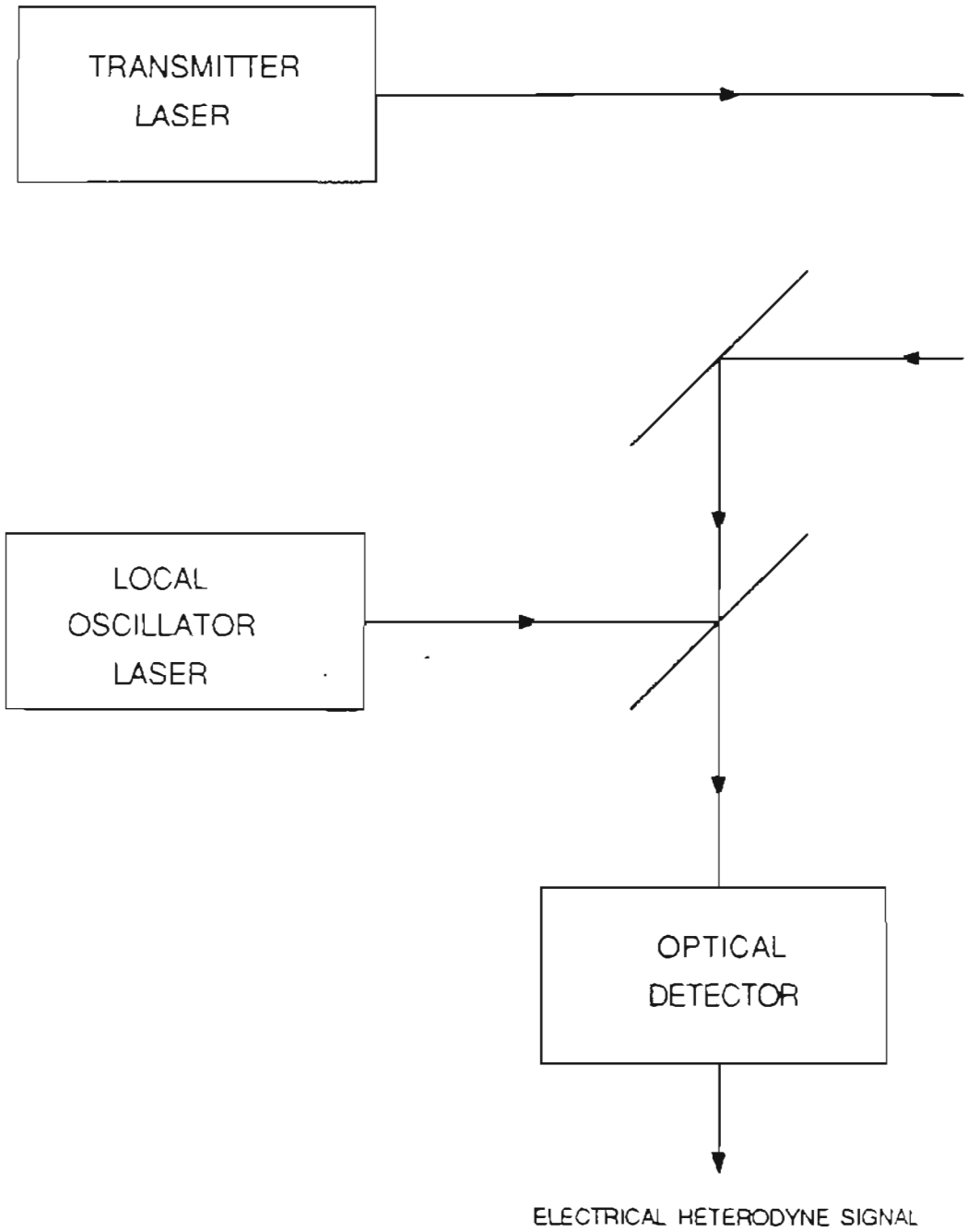

Figure 4.1 - Optical Heterodyne System

$$V_d = \left(A_o \cos\theta_o + A_r \cos\theta_r\right)^2 \tag{4.3}$$

which expands to

$$V_d = A_o^2 \cos^2\theta_o + A_r^2 \cos^2\theta_r + 2A_o A_r \cos\theta_o \cos\theta_r \tag{4.4}$$

The angle θ can be written in terms of the angular velocity of the wave. where $\omega = d\theta/dt$, $\omega = 2\pi\nu$, and ν is the instantaneous frequency of the signal. A_o and θ_o can be considered constants, and if for the moment the effects of the atmosphere and the remote target are neglected, θ_o and θ_r can be replaced by $\omega_o t$ ant $\omega_r t$ respectively.

Substituting the trigonometric identity $2\cos A \cos B = \cos(A+B) + \cos(A-B)$ in each of the terms of (4.4), the first two terms give a constant (d.c.) term and cosine terms at twice the frequency of the local oscillator and received frequencies. The third term in the equation produces a component at the sum of these two frequencies and another at the difference of the frequencies. The sum frequency and the double frequencies are optical frequencies well beyond the response capabilities of the detector as well as any electronic processing instrumentation and are not received. But the difference frequency is within the frequency limits of the system as long as the local oscillator and transmitter frequencies are adjusted appropriately. Therefore the d.c. and the difference frequency terms are the only components of the fields that are received. The d.c. component is removed by electronic filtering so that the received voltage is given by,

$$V_d = A_o A_r \cos(\theta_o - \theta_r) \tag{4.5}$$

The angle $\theta_o - \theta_r$ represents the instantaneous phase of the received field and $A_o A_r$ represents the instantaneous amplitude.

In practice a phase reference must be used for the phase detector. The phase detector measures the phase difference between the received phase and this reference. The phase reference is provided by the electronic oscillators that determine the transmitted and local oscillator frequencies and is equivalent to the phase angle $\theta_o-\theta_x=2\pi(\nu_o-\nu_x)t$ where ν_x is the transmitted frequency, ν_o the local oscillator frequency and both ν_o and ν_x are constant values. Subtracting this reference phase angle from the received phase in (4.5), the phase detector output voltage is proportional to $\theta_x-\theta_r$. This represents the instantaneous phase introduced by propagation of the optical signal from the transmitter to the receiver.

The phase received at a single location or the phase difference of two received signals at different locations can be measured. When the phase difference is measured, the reference phase for the phase detector is provided by one of the received signals. Each heterodyne signal has the same local oscillator and transmitter so that the phase measured by the detector is $\theta_{r_2}-\theta_{r_1}$ where the subscripts 1 and 2 refer to the two different receiver locations.

The phase was also measured indirectly by measuring the frequency ν. In this case the phase was obtained by integration of the frequency data since θ is given by $\int 2\pi\nu dt$. For one point measurements, $\nu=\nu_x-\nu_r$ and for two point measurements $\nu = \nu_{r_2}-\nu_{r_1}$. As will be explained in the next chapter, two point frequency measurements were not made due to limitations in the frequency detector.

4.2 The Single Laser System

Figure 4.2 shows a diagram of the single laser system[27]. A single CO_2 laser is used for both the transmitted output and the local oscillator. Acousto-optic modulators (AOM) driven by RF generators at 39.95 MHz and 40.05 MHz produced a heterodyne frequency of 100 kHz. Two modulators were used so that stray optical reflections from the transmitter beam would be at the wrong frequency to produce false signals at the detector. This method[28] produced a high degree of optical isolation between the transmitted and received signals. Beam splitters (B.S.) were used to reduce the power of the local oscillator signal for the sensitive liquid nitrogen cooled HgCdTe optical detectors.

A 3x beam expander was used to increase the radius and reduce the divergence of the laser beam. A half-wave plate was used to rotate the laser polarization from vertical to horizontal. The transmitter beam was further magnified by a ratio of 5x and a quarter wave plate was used to obtain a circularly polarized transmitted beam.

A two-inch mirror was used to direct the returning radiation through an a-focal telescope onto a pair of detectors. The telescope consisted of two lenses of focal lengths 25.4 and 6.2 cm giving a magnification of 4.1. The low magnification was needed to lessen angle of arrival fluctuations which in turn demanded large detector areas. The detectors were photoconductive detectors which have an advantage of large size and low cost. They were 2mm x 2mm in dimension placed side by side 0.1mm apart in a single dewar. This gave an effective spacing of 8.6mm between the detectors. The detectors were posi-

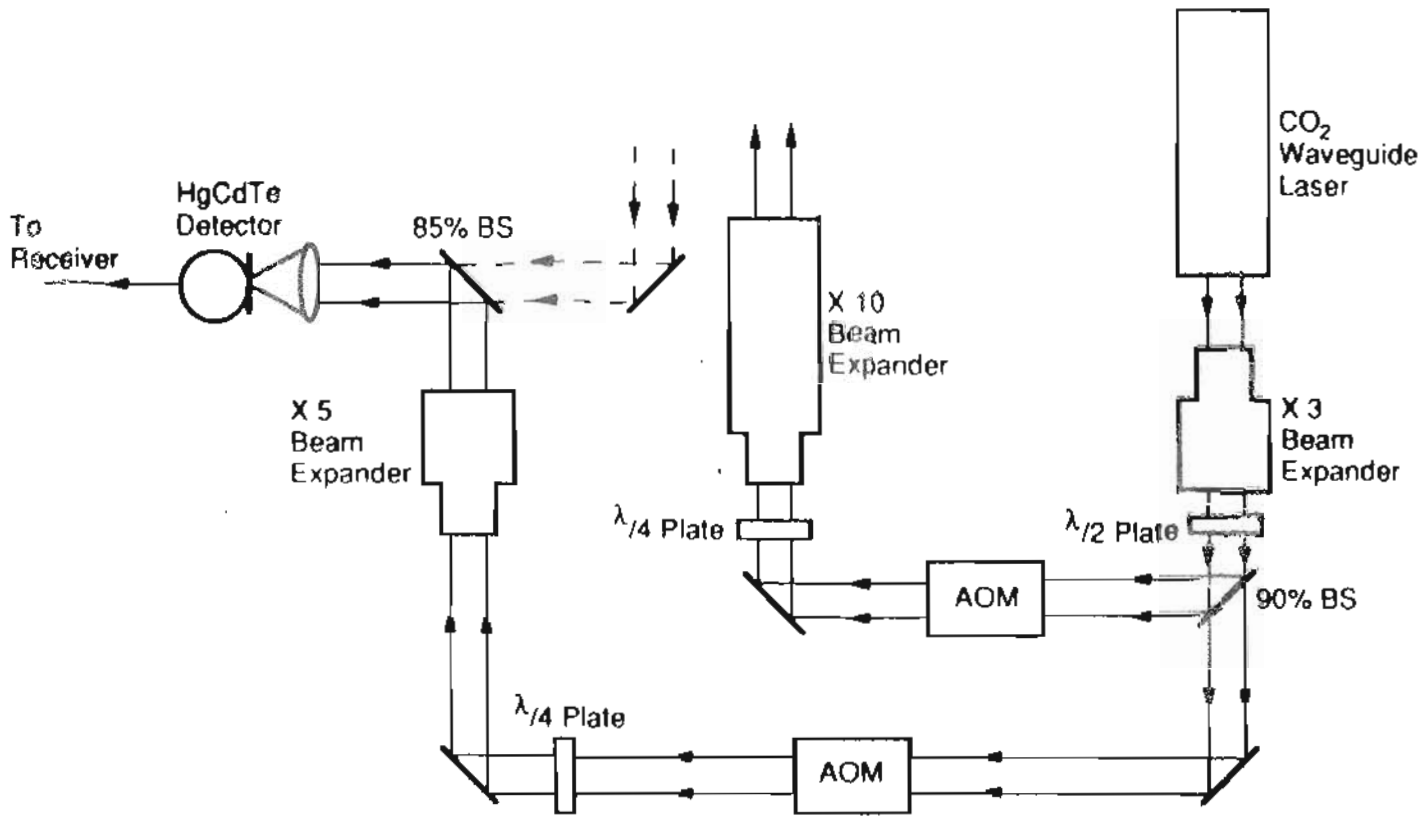

Figure 4.2 - Single Laser Heterodyne System

tioned close to the focal plane of the imaging lens where the image is least dependent on the incidence angle.

A pinhole placed at the common focus of the lenses in the telescope, limited the field of view of the detectors and also helped cancel spherical aberrations. The 5x beam expander on the LO path provided a collimated beam several times larger than the detector area, resembling a plane wave on the detector surfaces. Another quarter-wave plate was used on the LO beam so that it would also have circular polarization.

Details concerning the single laser optical heterodyne system can be found in the PhD dissertation of F. Amzajerdian[27].

4.3 The Two Laser System

A two laser optical heterodyne system has an inherent isolation between the transmitter and local local oscillator. Transmitter feed-through from optical reflections can theoretically be eliminated if the system locks onto the signal return from a remote target rather than part of the transmitted signal since the transmitter and local oscillator will have no common optical elements. Consequently, maximum optical isolation between the transmitter and local oscillator is provided. In addition, since the return signal rather than the transmitted signal is used for control, the system may be useful for long ranges where laser drift causes the transmitted and return frequencies to be radically different and beyond the frequency range of the receiver. In order to use the two laser system to make intensity measurements, a method was needed to synchronize the frequencies of the two lasers. Furthermore, if frequency or phase data was desired, the phases of the two lasers must be

locked.

A simple and inexpensive method for frequency synchronizing the two lasers was used[29]. The system could track frequency changes of several hundred megahertz that were caused primarily by frequency drift of the lasers. Phase synchronization could not be achieved so the two laser system was not able to provide phase or frequency measurements. The length transducer in the laser cavity was used for frequency control of the LO laser. The length transducer was intended for dither stabilization to prevent frequency drift away from the laser peak output level.

The two laser optical heterodyne system is shown in figure 4.3. The return signal from the remote target was combined with the local oscillator using a beam splitter and directed onto the optical detector. The signal from the optical detector represents both the signal input to the receiver and the control signal used for frequency synchronization of the local oscillator. A 5MHz heterodyne frequency was selected although other frequencies were also used.

The lasers used in the system were tunable by means of a diffraction grating which was adjusted with a micrometer dial. The cavity length transducer was a piezoelectric transducer on which the rear laser mirror was mounted. An electrical signal applied to the transducer varied the laser frequency in response to the changing cavity length. After the two lasers were brought to the same spectral emission line by manually adjusting the diffraction grating, the system maintained control by detecting any frequency change from the desired heterodyne frequency and applying a correcting vol-

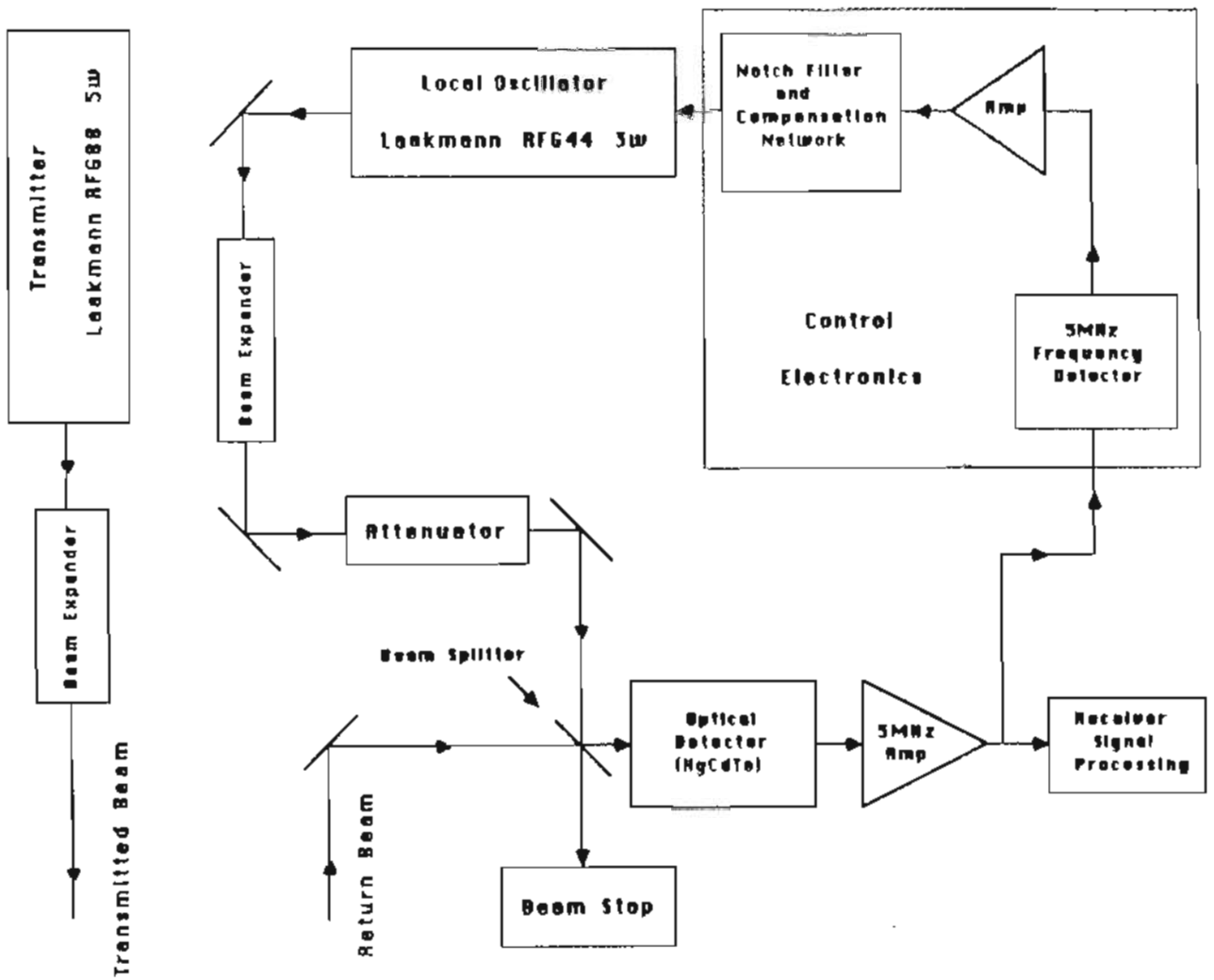

Figure 4.3 - Two Laser Heterodyne System

tage to the length transducer.

The signal from the optical detector was amplified and the frequency detected using a frequency demodulator. The detected signal represents an error signal proportional to the difference between the desired and actual receiver frequencies. The signal was amplified to provide a large amount of control loop gain in order to minimize the frequency drift and maintain small errors in the heterodyne frequency. Special electronic compensation was needed to achieve a stable system. The compensation problem was complicated by the resonant response of the piezoelectric length transducer. The transducer had a prominent resonant peak which severly limited the frequency response of the control system and made it difficult to achieve a large control loop gain. This problem was solved through a compensation method described below and stable control was achieved with a control loop gain of 120 dB.

The measured laser response to electrical control inputs as a function of control frequency is shown in figure 4.4 Of particular interest is the pronounced resonance at 3.4 kHz evidenced by the extreme increase in amplitude response and phase shift at this frequency. The response is that of a second order system with a damping ratio of about 0.025. Beyond the peak at 3.4kHz, the curve falls off rapidly and response is lost to higher frequencies. For this reason, even with stable control conditions, any disturbances in laser emission wavelength at rates higher than the resonant frequency were uncontrollable. The inability to control these high frequencies resulted in frequency modulation or FM noise added to the heterodyne signal. Therefore

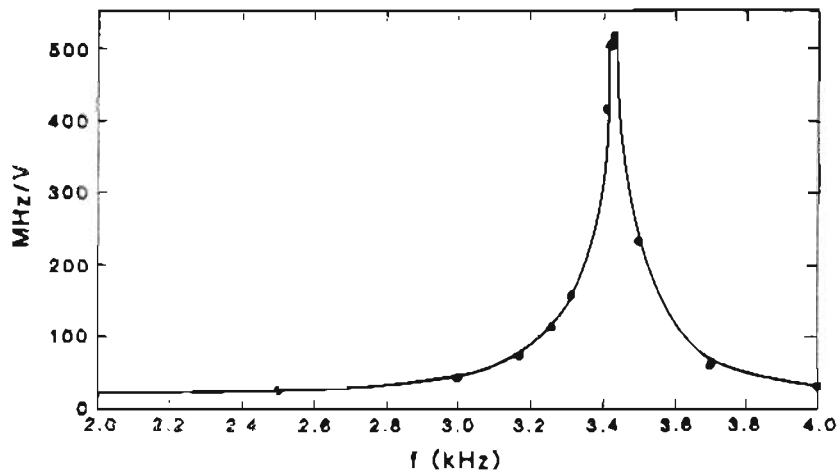

(a) amplitude

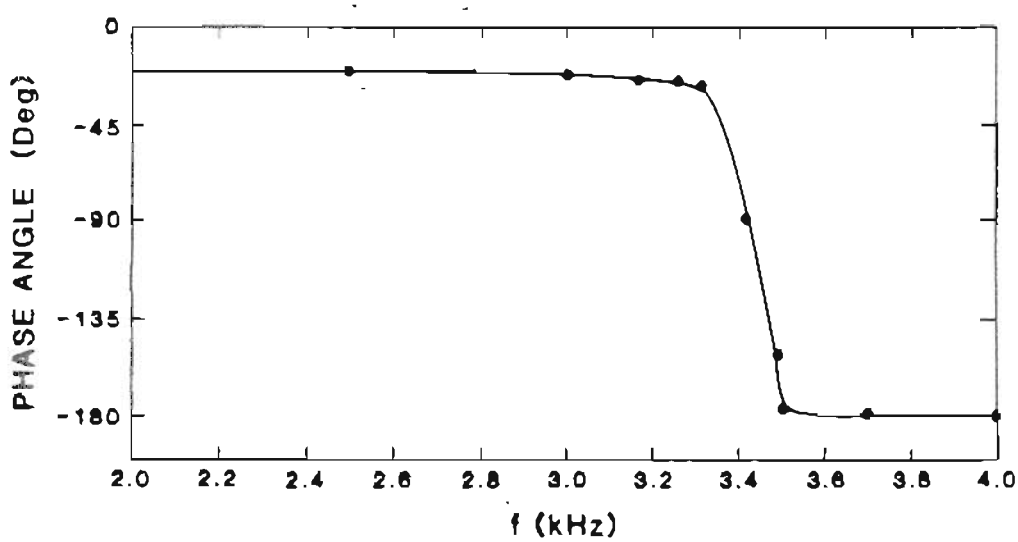

(b) phase

Figure 4.4 - Laser Response

FM noise caused by inherent laser instability or external disturbances such as vibrations could not be removed by the system if the FM rate was above the 3.4 kHz response of the length transducer.

The heterodyne signal was observed using an oscilloscope and a spectrum analyzer. The FM noise varied from 5 kHz to 50 kHz representing 0.1% to 1% of the 5 MHz heterodyne frequency. Reduction of the FM noise in this frequency range would require a control element having a frequency response extending beyond the 3.4kHz range of the internal length transducer.

A notch filter at 3.4 kHz was added to minimize the effects of the transducer resonance. In addition, a compensation network with a double pole at 4Hz and a zero at 100 Hz was also needed for stability. The maximum control loop gain that could be achieved with this compensation was 120 dB. With a loop gain of 120 dB, the theoretical steady state error to a unit input change of frequency is 10^{-6}. Laser frequency drift is mainly due to temperature variations. The lasers drift 900 MHz per degree C and were controlled to within plus or minus 0.1 degree C by water cooling. A 0.1 degree change in temperature represents a 90 MHz change in laser frequency. Frequency drift was measured over a period of three hours using a control loop gain of 60 dB. The 5 MHz heterodyne frequency drifted less than 50 kHz. With a loop gain of 120 dB the corresponding drift would be only about 50 Hz or less than one part per million of the expected laser frequency drift of 90 MHz. Assuming the electronic control system has the necessary dynamic range, the lasers can maintain control as long as they do not drift outside

their free spectral range of about 500MHz.

Using this method of control the heterodyne signal does not follow slow frequency shifts which might be needed for instance to determine target velocity. Nevertheless, the output of the frequency detector does provide information about the frequency of the return signal.

Attempts were made to phase lock the heterodyne frequency of the two lasers to a stable reference oscillator by controlling the frequency of one of the lasers, however, these attempts were unsuccessful. It is felt that a combination of the inability of the laser transducer to respond above 3.4 kHz and a practical limit to the lock in range of the control loop prevented phase locking. The large amount of FM noise produced phase errors beyond the 2π range of the phase detector used in the phase locked loop. The loop gain could be reduced to lessen the FM noise, however, this prevented sufficient loop gain for stable phase locking. Successful phase locking of two CO_2 lasers in a much more complicated heterodyne system has been reported[30].

Stable frequency control at a loop gain of 120 dB was demonstrated in a field environment using a diffuse target at 80 meters from the lasers. The target generated an almost fully developed speckle pattern at the receiver. The average speckle contrast ratio was measured to be 0.7, and the average received power level was about 10^{-12} watts.

The combined effect of speckle and atmospheric turbulence resulted in large fluctuations in the amplitude and phase of the received optical signal. These fluctuations caused the optical signal to go below the background noise level for short durations in the order of several milliseconds. Even with this

temporary loss of signal, the system maintained frequency control. Occasionally when the return signal was lost for longer periods, such as when an object interrupted the beam, reacquisition of control was required by adjusting the diffraction grating. It may be possible to alter the electronic frequency compensation to allow longer periods of signal loss, but for situations where the beams may be interrupted for lengthy periods, some system for automatic signal acquisition would be needed.

CHAPTER 5

PHASE AND FREQUENCY DETECTORS

In this chapter, the methods used to process the phase and frequency detector data are described. In order to obtain unwrapped phase information from the phase detector, a method was needed to place the measured phase data in the appropriate 2π segment of the infinite line that represents unwrapped phase. In theory there is no exact way to do this because a given point on a circle representing a wrapped phase value could be placed in any one of an infinite number of 2π segments of the line. The best that can be done is to predict where the phase should be from past, present or future data points.

If the range of the expected unwrapped phase variations is known ahead of time, unwrapped phase can be obtained directly from the phase detector data without unwrapping by using frequency dividers to divide the phase before it is measured so that it always stays within a range of 2π. Another alternative to unwrapping the phase is to measure the frequency instead of the phase and integrate the frequency data. The integral of frequency represents unwrapped rather than wrapped phase.

Figure 5.1 shows the instrumentation that was used to measure phase and frequency. The weak heterodyne signals received from the HgCdTe detectors were amplified with amplifiers tuned to 100 kHz. When the phase difference was measured, both received signals were applied to the phase detectors. This is shown for the switch in position 1 in the figure. As will be

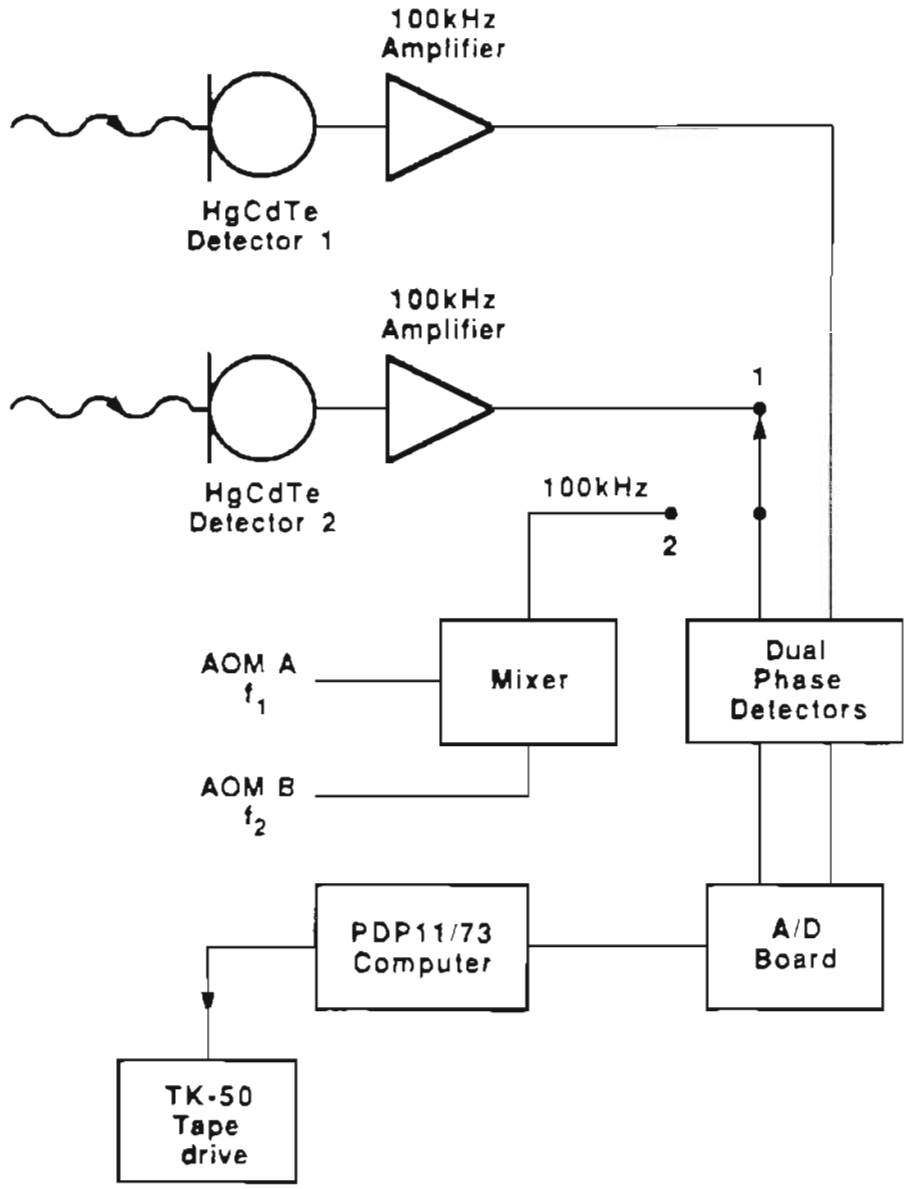

Figure 5.1 - Instrumentation Used to Measure Phase and Frequency

explained later, usually two separate phase detector outputs were recorded. When frequency dividers were used, they were placed before the phase detectors. When frequency detectors were used, they replaced the phase detectors.

With the switch in position 2, the phase at a single point was measured. A reference phase angle was generated using the electrical signals that supply the frequency shifts to the acousto-optic modulators (AOM) used to produce the heterodyne frequency. The electrical signals were applied to an electronic mixer to produce the 100 kHz heterodyne reference signal for measuring phase and only one amplifier output was used.

The detector outputs were digitized with analog to digital converters (A/D) and recorded on a magnetic tape drive (TK-50) using a PDP11/73 computer.

5.1 0-2π Phase Detector

A phase detector is limited by its dynamic range which is given by the range of phase values that it can measure. Typically the response is from 0 to 2π radians, although with added complexity, detectors that respond to 4π and beyond can be made. A simple 0 to 2π phase detector that was initially used to measure phase data is shown in Figure 5.2.

In order to remove amplitude fluctuations, the 100 kHz heterodyned signals were clipped by the phase locked loops (PLL) to produce square waves. A bistable multivibrator (MV) and low pass filter (LPF) averaging circuit were used to produce a phase detector response that was linear from 0 - 2π radians or 0 - 360 degrees.

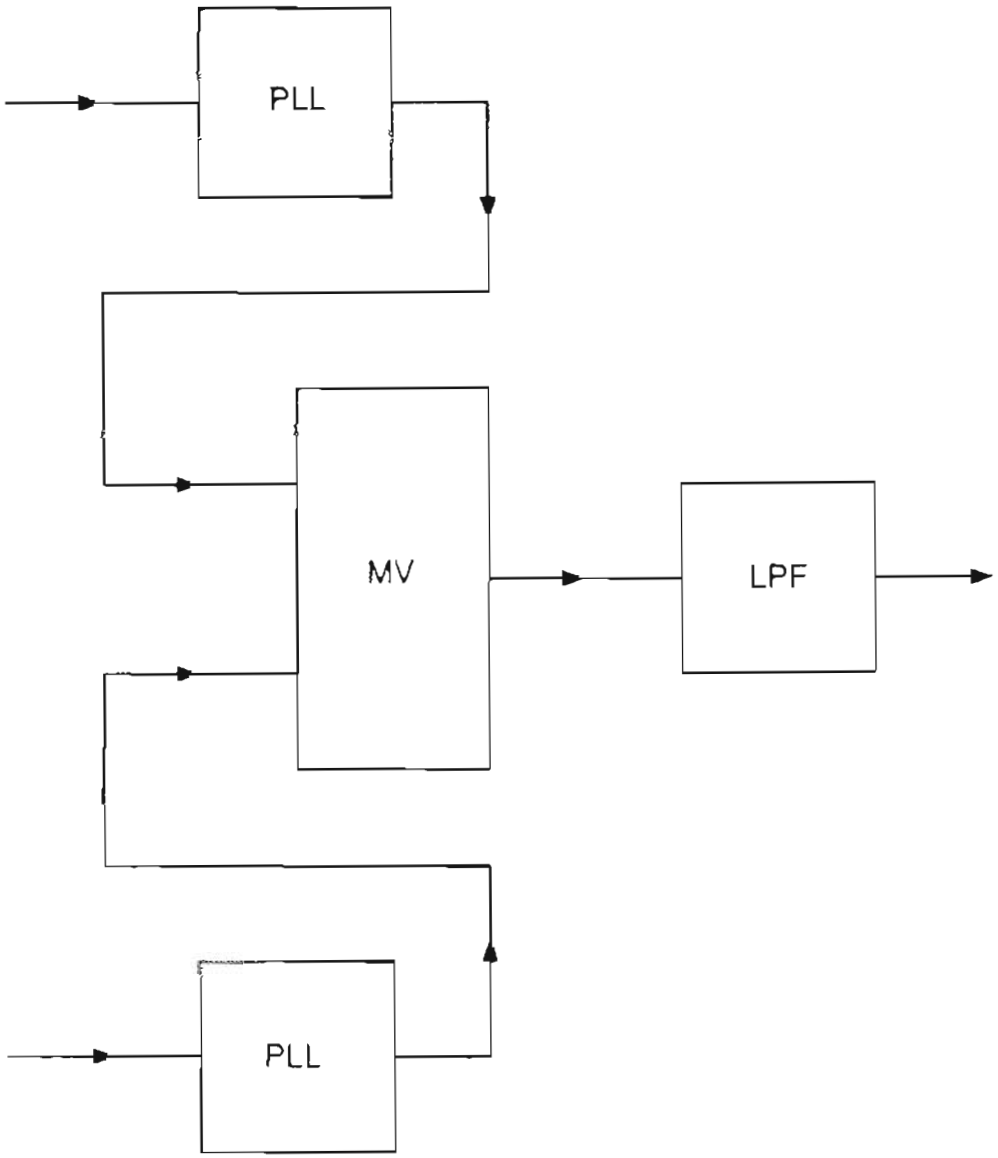

Figure 5.2 - 0-2π Phase Detector

The phase detector response is shown in figure 5.3. As with any 2π phase detector, there is a transition zone at the discontinuity in the response curve where 0 meets 360 degrees. The transition zone provides inaccurate output and complicates the task of unwrapping the phase data.

In order to unwrap the phase data, each time the phase detector makes a transition from 360 degrees back to 0 or from 0 to 360 degrees, a constant value representing 360 degrees must be added or subtracted depending on the direction of the transition. When the phase changes rapidly and randomly it is very difficult to determine when a transition is made. For example a phase change from 359 degrees to 1 degree could be interpreted as an increase of 361 - 359 = 2 degrees or a decrease of 359 - 1 degree = 358 degrees. In the first case , 360 degrees should be added to current and future phase data values, but in the second case there should be no correction. Based solely on these two data points, the logical choice is to select the smaller change (less than 180 degrees), in this case the 2 degree change.

The 0-2π phase detector was used to unwrap the phase by measuring the magnitude and direction of the change from one data value to the next, and as explained above, 2π was added or subtracted to the data when the change was greater than π radians. However, the width of the transition zone, which can be several degrees wide in a practical detector, caused erroneous outputs near the discontinuity and slowed the rate of transition through the discontinuity. This increased the number of unwrapping errors. Acceptable results were obtained by this method only when the wrapped phase was changing slowly. More involved phase unwrapping algorithms

have been proposed[31,32] that may improve the unwrapping process when a single phase detector is used, however, the methods that are described below using two detectors eventually led to acceptable results.

In order to lessen the unwrapping problems created by the transition zone, two separate phase detectors were used. The response of each detector, V_a and V_b, was shifted in phase by π radians with respect to the other as shown in figure 5.4. A threshold at $-V_m$ and $+V_m$, equivalent to a range of π radians, was set for each detector. When one of the detector outputs was within the threshold limits the other detector output would be outside the limits, and the transition zone could theoretically be avoided.

The algorithm used to unwrap the two phase detector outputs is described by the flow chart given in figure 5.5. The algorithm selected V_a when its value was between $-V_m$ and V_m and switched to V_b when outside these limits. In this way the discontinuity was avoided, and the number of unwrapping errors was reduced. In order to compensate for the switch from V_a to V_b, when V_a was greater than V_m, π radians was added, and when V_a was less than $-V_m$, π was subtracted. A similar correction was made for a switch from V_b to V_a. The algorithm kept track of the number of π corrections to add or subtract as the output switched back and forth between V_a and V_b. The rate at which the phase is sampled of course must be high enough that there is less than π radians of phase change between samples in order to accurately unwrap the phase.

Although this reduced the number of unwrapping errors, there were situations when both detector outputs were in their transition zone at the

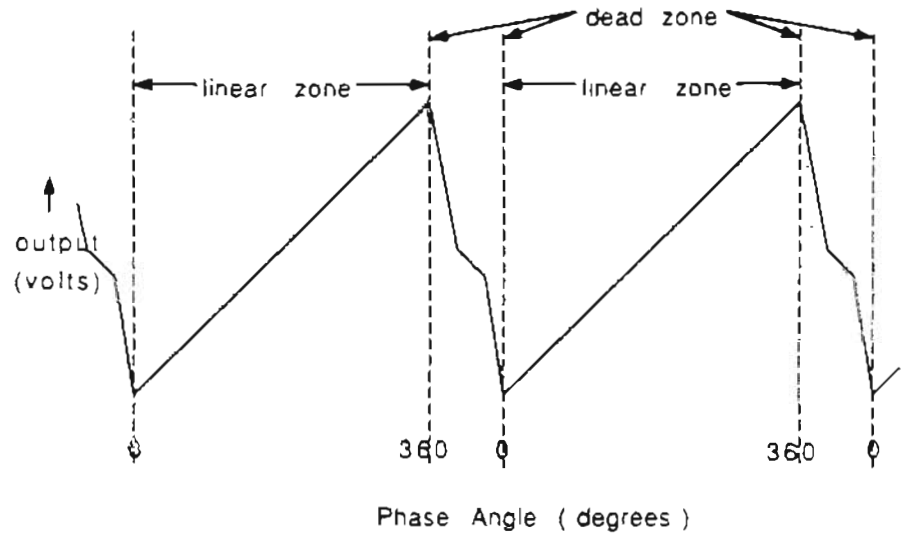

Figure 5.3 - 0-2π Phase Detector Response

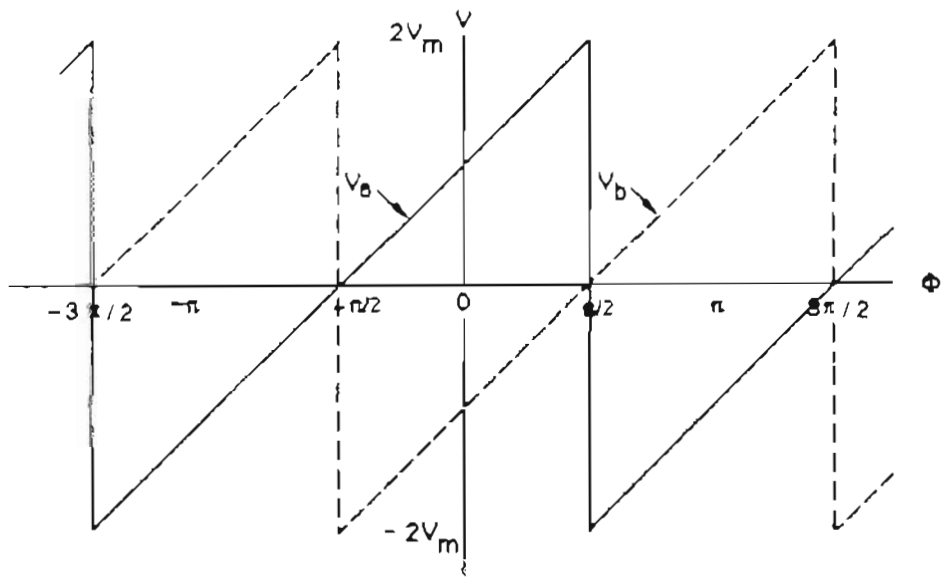

Figure 5.4 - 0-2π Responses Shifted by π Radians

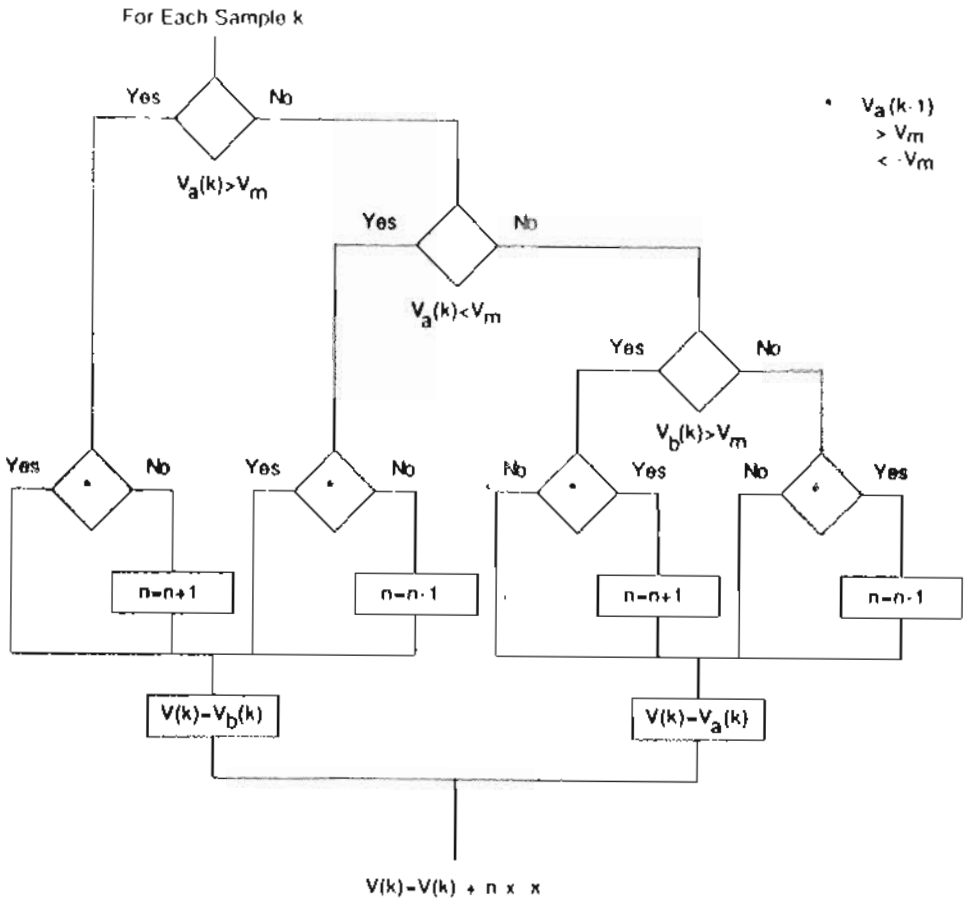

Figure 5.5 - Algorithm Used to Unwrap Detector Outputs of Figure 5.4

same time. This happened when the detectors were near the threshold limits. While one detector was within the threshold limits the other was slightly out of the limits. If the phase stayed near the threshold for several data samples, the detectors typically made several transitions through the threshold area causing occasional unwrapping errors.

5.2 0-π Phase Detector

Another type of phase detector that had a linear response for only π radians was used to avoid the transition zone problem. Two separate detectors were also required in order to unwrap the phase data, but in this case the responses were shifted by $\pi/2$ radians with respect to each other. As shown in figure 5.6, each detector was implemented with a logical AND gate and LPF averaging circuit. The inputs were amplified and clipped with PLL's to produce square waves. Each PLL was adjusted so that a 90 degree phase relationship would exist between the two phase detectors.

The phase detector response is is shown in figure 5.7. The phase detector response alternated between a positive slope and a negative slope every π radians. The desirable feature of this phase detector is that, unlike a zero to 2π phase detector, there are no discontinuities in the response. Phase data was measured and processed in two steps. First, two equivalent zero to 2π wrapped phase detector responses like the ones shown in figure 5.4 were calculated from the two zero to π phase detector outputs using the algorithm.

if $V_2>0$ or $V_2=0$ then

$V_a=V_1+V_m$

$V_b=V_1-V_m$

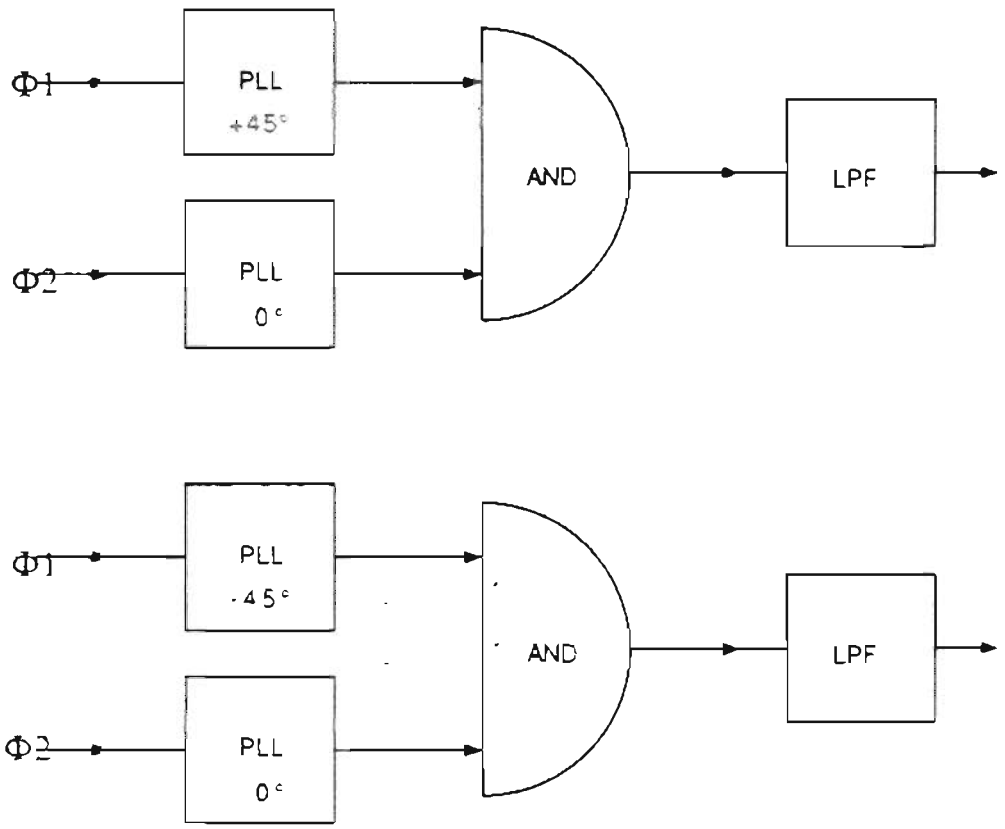

Figure 5.6 - 0-π Phase Detector

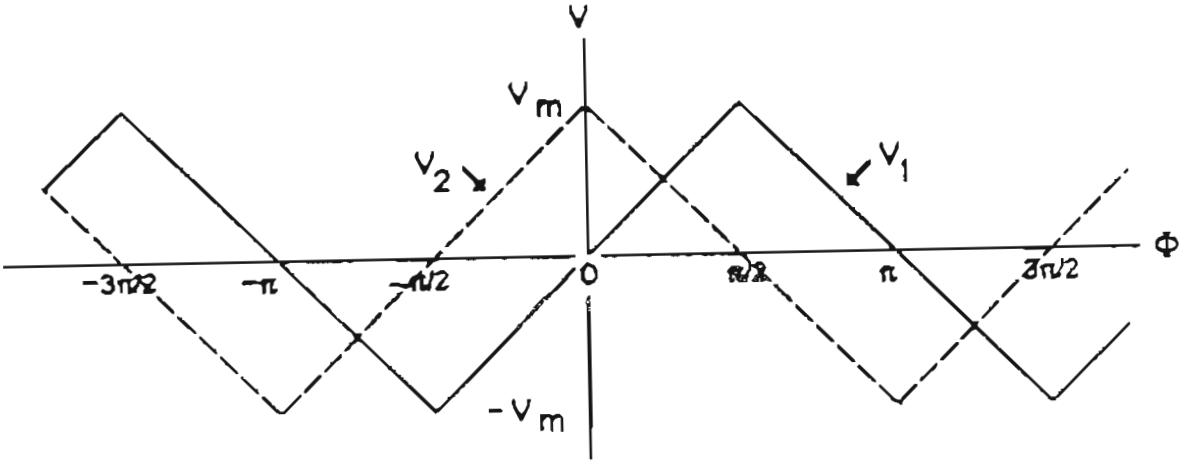

0–π

PHASE DETECTOR

RESPONSE

Figure 5.7 - 0-π Phase Detector Responses Shifted by π/2 Radians

if $V_2 < 0$ then

$$V_a = -V_1 - V_m$$

$$V_b = -V_1 + V_m \quad .$$

The wrapped phase data was then unwrapped using the same digital processing algorithm that was used for the two 0 to 2π detectors described by the flow chart given in figure 5.5.

The advantage to using the 0 - π detectors was that the discontinuities would be narrow as shown in figure 5.4 rather than wide as shown in figure 5.3. However, if the phase shift between the two detectors is not exactly 90 degrees, there will be a finite width to the transition zone of the equivalent 0 - 2π detectors and unwrapping problems similar to those with the other phase detectors will occur.

5.3 Frequency Dividers

If the maximum number of phase unwrappings that are required is known, then the 100 kHz beterodyne frequency can be reduced by a set amount using frequency dividers, and the unwrapping problem can be avoided. The phase will be divided at the same ratio, and unwrappings will not be necessary as long as the unwrapped phase never exceeds the division ratio times 2π radians. Disadvantages of this method are that the resolution of the phase measurement is also reduced by the division ratio, a good estimate of the maximum phase change is required prior to the experiment, and very large phase errors will occur when the signal is temporarily obscured by noise. Without the frequency dividers, the noise produced only a temporary

loss of data and no permanent phase errors were added.

Phase data was taken using frequency dividers with division ratios from 4 to 256. Examples of data taken at division ratios of 32 and 128 are shown in figure 5.8a and b respectively. Phase errors due to noise occurred at random and resembled magnified unwrapping errors equivalent to several multiples of 2π. In addition, with the divide by 32 circuit, the phase occasionally exceeded the 32 times 2π phase detector limit causing additional errors.

The origin of the phase errors is described in what follows. Considering a bistable multivibrator used to divide the frequency and the phase by a factor of two, one complete period of the input represents a half period of the output. If one cycle is missed at the input, a 180 degree phase shift is artificially added to the data. The error will occur each time one detector suffers a loss of signal for an odd number of cycles of the input and the other for an even number of cycles. Frequency division by amounts other than two causes the same problem and an unknown number of phase errors, which appear as step changes in phase, are accumulated in the unwrapped data. The errors can represent extremely large phase values especially when large division ratios are used.

The problem was corrected by using a more complicated frequency divider that employed a phase locked loop with a frequency multiplier in the loop. The controlled oscillator in the loop was multiplied in frequency and locked in phase with the incoming signal frequency. The controlled frequency was used as the frequency divided output and was synchronous with the input as long as the loop was locked. Schematics of the frequency divider

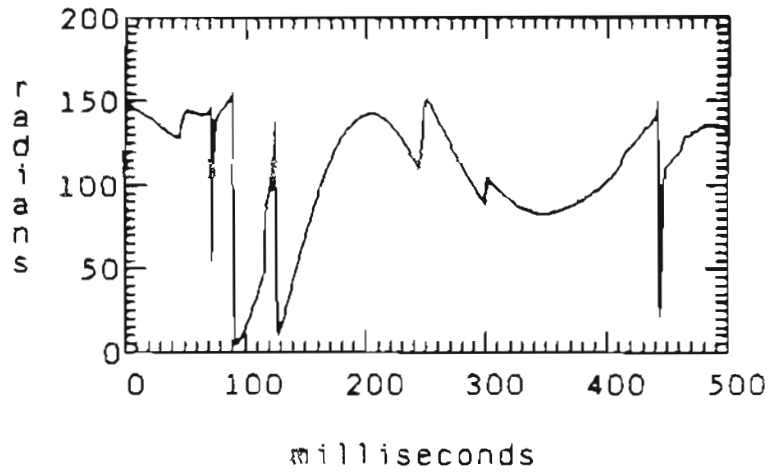

(a) 32

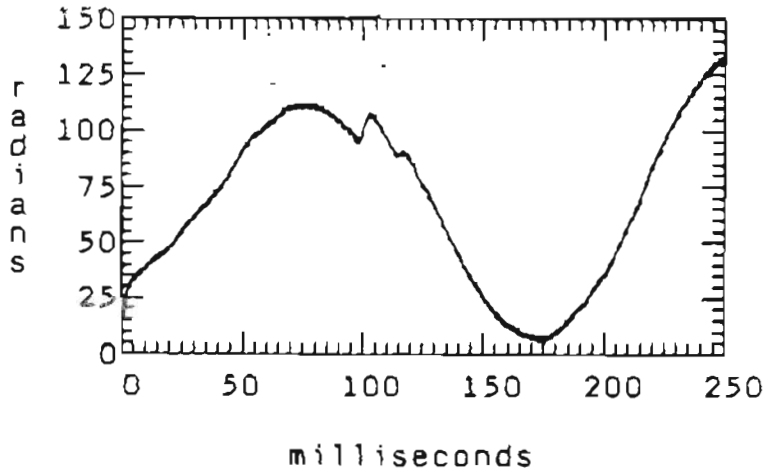

(b) 128

Figure 5.8 - Phase Data with Division Ratios of 32 and 128

with the phase locked loop are provided in Appendix D.

5.4 Frequency Detectors

Phase data was also obtained by recording the received frequency and numerically integrating the data to obtain phase. Phase unwrapping was not needed since frequency data is continuous within the dynamic range of a frequency detector. The frequency detector must be extremely linear, have very little drift, and have good sensitivity so that a resolvable output for very small frequency changes is provided. A detector that meets these requirements (figure 5.9) consists of a monostable multivibrator with a pulse duration time slightly less than the repetition period of the heterodyne signal. The average of the multivibrator pulses is directly proportional to the instantaneous frequency value. The output was digitized and recorded on the magnetic tape. The integration of the frequency data can be done before or after the data is recorded. Because large phase angles were accumulated by the optical signals, it was only practical to integrate the data after it was recorded. Simple rectangular or trapezoidal integration algorithms were used.

The only significant problems encountered with this detector were a very slow drift in the output due to pulse duration time variability and matching the response curves when two detectors were needed for phase difference measurements. These problems were not serious when measuring the frequency at one point since only one detector was used and very slow frequency changes were not measured due to the limited recording times. However, measuring the phase difference between two receivers was not possible using frequency detectors because the two detectors could not be matched

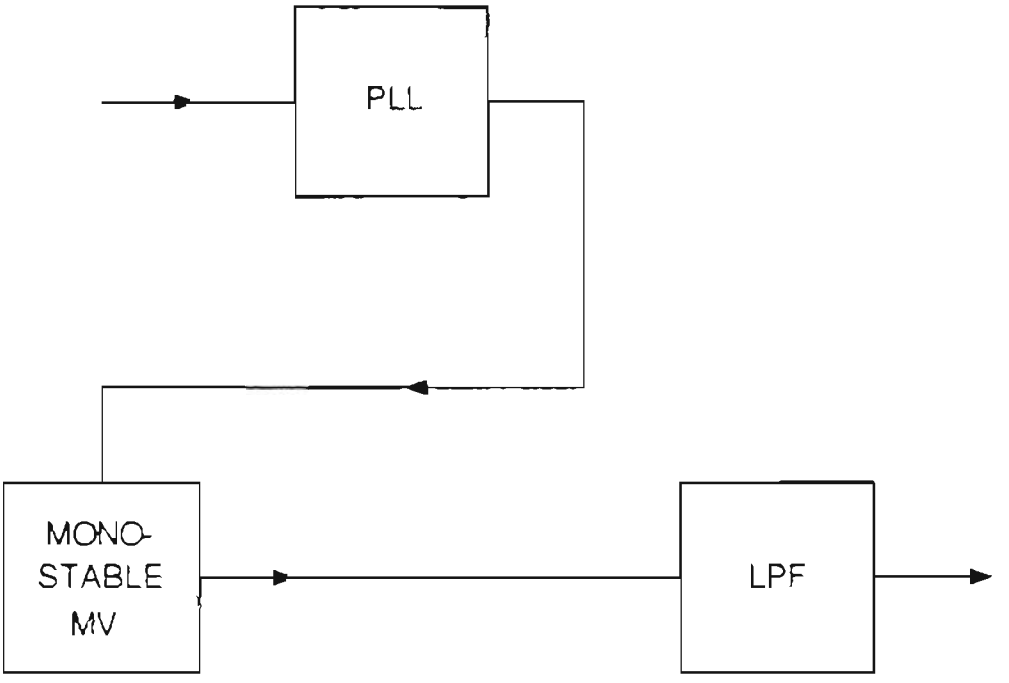

Figure 5.9 - Frequency Detector

well enough. Any differences in their response represented a frequency error. When the frequency data from each detector was subtracted and integrated, the desired phase difference information in the data was totally obscured by the integrated frequency detector errors. Unless a technique is developed for measuring the frequency difference directly, or the frequency detectors can be more closely matched, the frequency method is not suited for phase difference measurements.

One-point frequency and phase data were taken at the same time in order to compare the unwrapped phase produced by each. Figure 5.10 shows the integrated frequency and the unwrapped phase versus time. The differences between them is most likely due to the inability of the phase unwrapping algorithm to correctly unwrap the occasional rapid and large phase changes between sample points.

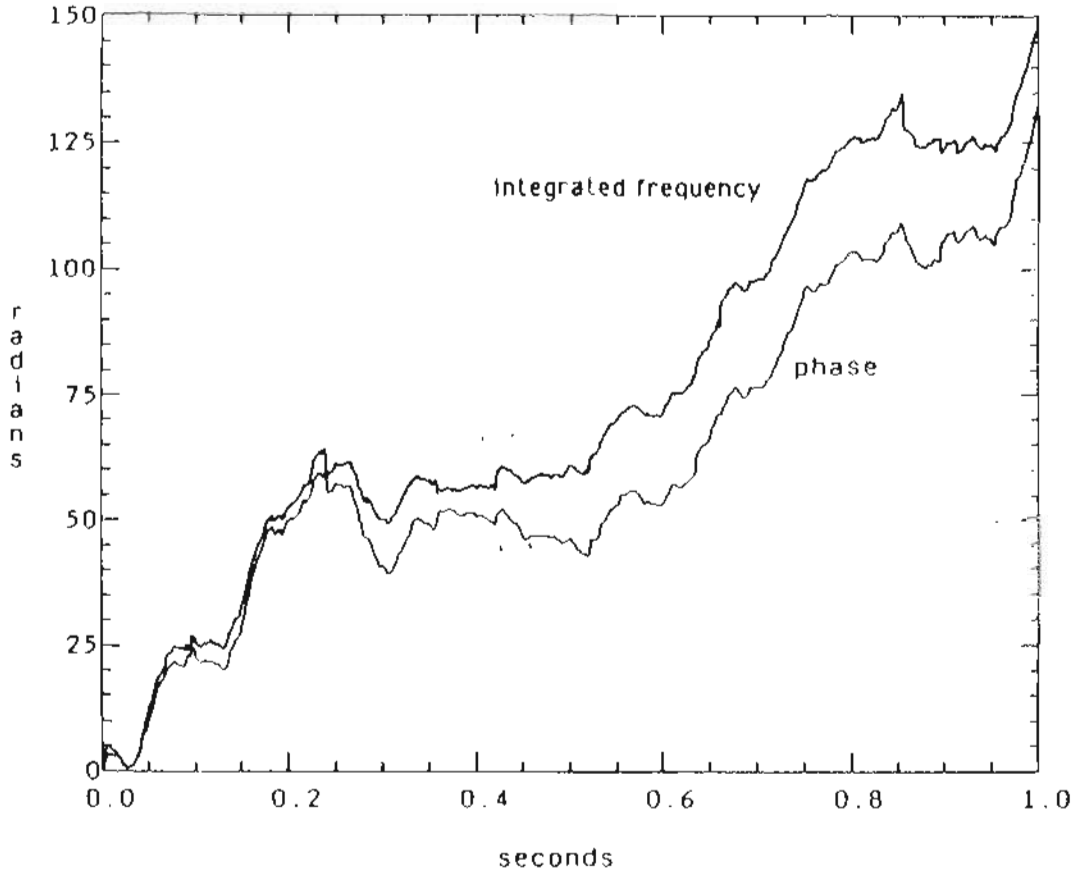

Figure 5.10 - Integrated Frequency Data Compared to Unwrapped Phase Data

CHAPTER 6

EXPERIMENTAL RESULTS

In this chapter, the results of phase and frequency measurements using an optical heterodyne system in the open atmosphere with sandblasted aluminum targets will be reported. The tests were performed at an atmospheric field site near St. Paul, Oregon using the single laser system. The two laser system was operated only at the OGI facility and did not provide phase or frequency data.

Data taken at the St. Paul facility are compared with the models for unwrapped phase and frequency given in chapters 2 and 3. The data indicate how measurements of the unwrapped phase difference at receiver points with an effective spacing of 8.6 millimeters can be used to distinguish between targets of different roughness at a range of 1000 meters. The data also indicate that the unwrapped phase and phase difference received from the remote target can predict turbulence levels in the atmosphere.

Unwrapped phase rather than the wrapped phase was used exclusively and was obtained from either frequency or wrapped phase data as explained in chapter 5. Unwrapped phase was needed because the small speckle phase variations caused by microscopic target roughness were obscured by phase variations greater than 2π that were produced by target motion and macroscopic target surface irregularities. Phase variations due to turbulence were sometimes greater than 2π and could not be measured with the wrapped phase. The speckle phase variations and the phase variations due to

turbulence could be extracted from the unwrapped phase using a combination of high pass and low pass filtering.

In the first section, the problem of separating the effects of speckle and turbulence in the phase data will be explained and the need for data filtering will be justified. Next, parameters of the experiment that predict the variance of the measured phase will be summarized.

Following that, the standard deviation of unwrapped phase difference versus the r.m.s. target surface roughness will be reported from the results of Peacock[33]. Histograms of the unwrapped phase data will be shown to resemble Gaussian functions after the data is filtered to extract speckle phase variations. These results will be supplemented by showing the dependence of unwrapped phase deviations on errors that resulted from unwrapping the phase data and on the cut-off frequency that is used to filter the data. Comparisons will be made to phase deviation predictions given in chapter 2.

Next, the standard deviation of the unwrapped phase obtained from frequency data and filtered to extract the turbulence phase variations measured at one receiver point will be compared to calibrated atmospheric turbulence levels and the predictions of chapter 2. Histograms of unwrapped phase filtered to extract turbulence variations will also show a close resemblance to a Gaussian function. Filtered unwrapped phase difference data will also be compared to measured turbulence levels.

6.1 Data Filtering

Most of the results to follow depend on selecting an acceptable method for filtering the phase or frequency data. The data are affected by both

macro-scopic and microscopic target features, temperature variations and on the target motion. Microscopic target surface variations cause speckle and occur on a scale of about the same order of magnitude as the laser wavelength. Microscopic surface variations were produced by sandblasting or flame spraying the aluminum targets to make them diffuse. Macroscopic target variations vary on a scale much larger than the laser wavelength and were caused by non-uniform target thickness and surface curvature in the targets. Phase changes due to microscopic effects extend to relatively high frequencies, however, the macro-scopic features produced only low frequency phase changes. Two other effects, target motion and slow variations in the refractive index of the atmosphere caused by changes in the air temperature, produced phase variations only at low frequencies. Target motion was due to an inability to fasten the target tight enough to prevent the wind from deflecting the target.

Figure 6.1 shows macro-scopic effects in the unwrapped phase data. Unwrapped phase data is shown before and after the target was supported by tightly cinched wires. Phase oscillations due to wind activity exciting the natural damped oscillation of the target can be seen in each trace. The tightening of the target had two major effects on the oscillations. The first effect was to reduce the amplitude of the oscillations from more than 32 cycles (200 radians) peak to peak to less than 8 cycles (50 radians) peak to peak. The second effect was to increase the frequency of oscillations from about 5 Hz to 20 Hz.

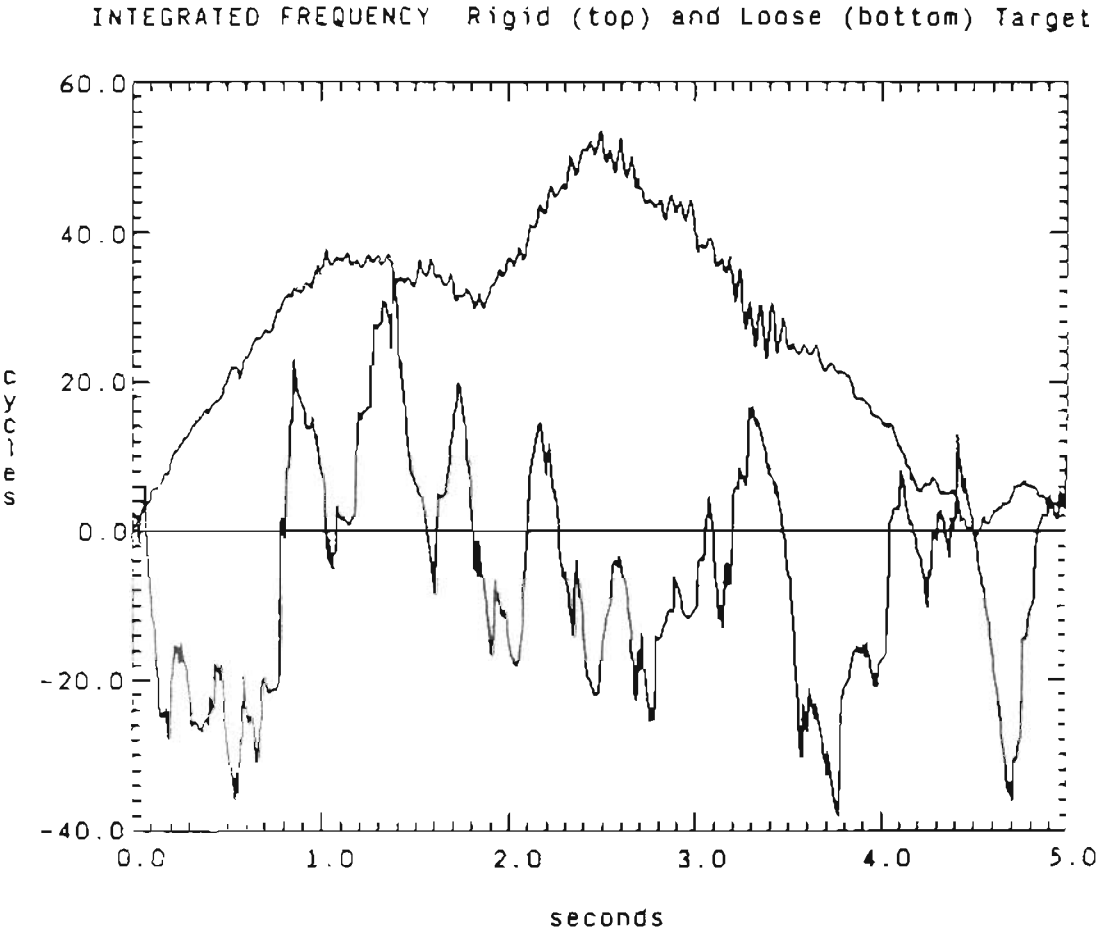

Figure 6.1 - Unwrapped Phase Data Showing Effects of Target Motion

The very low frequency phase changes are due to macro-scopic target features and also on refractive index changes in the atmosphere caused by temperature gradients. The phase change over a path length of 2000 meters, representing the two way optical path, was calculated to be 1120 radians per degree centigrade. Therefore a temperature change of only 0.1° represents a phase change of 100 radians.

Two different methods were used to filter out the effects of the oscillations and the macro-scopic target characteristics in the data. In one method, a digital Fourier transform (DFT) of the data points was generated. Data points of the spectrum were altered according to the filter characteristic desired. Then an inverse DFT was generated to obtain the filtered data.

When data lengths were longer than 2500 points it was difficult to perform a DFT. For these cases a running point average was subtracted from the data to produce a high pass filter characteristic that had a more gradual roll off than with the DFT method.

A major problem in filtering the data was the choice of appropriate cut-off frequencies. To help select the cut-off frequencies, the frequency bands covered by the speckle and turbulence data were estimated. Both speckle and turbulence data theoretically extend to d.c.

Figure 6.2 shows typical spectra of the one-point unwrapped phase and two-point phase difference. The majority of the phase information is at low frequencies. This is especially true of the one-point data. The normalized power spectrum for the phase of a point source propagating through a turbulent atmosphere assuming a Von Karman spectra of C_n^2 is given by[34],

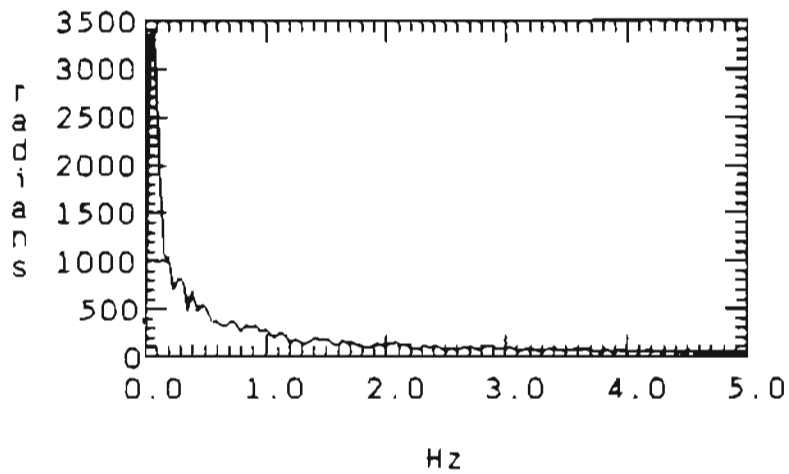

(a) Phase Data

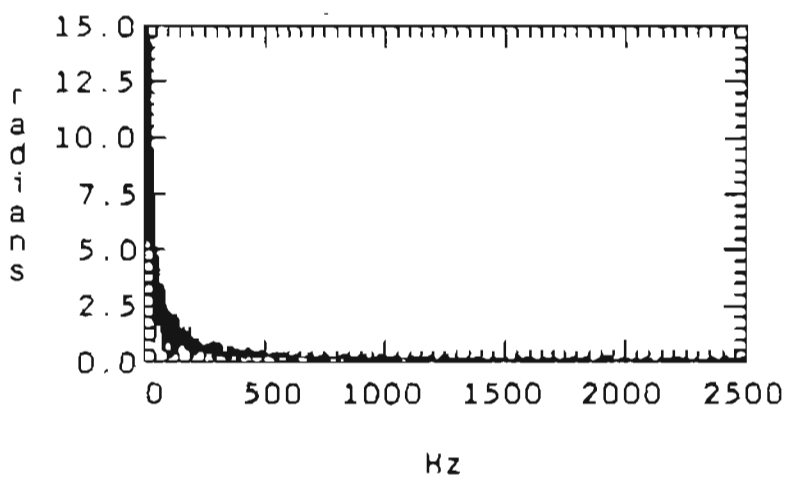

(b) Phase Difference Data

Figure 6.2 - Typical Spectra of Unwrapped Phase Data

$$\frac{<\phi^2(f)>}{<\phi^2>} = (5.56\text{x}10^{-2}) \left(\frac{V_T}{2\pi L_o} \right)^{5/3} \frac{1}{\left(f^2 + \left(\frac{V_T}{2\pi L_o} \right)^2 \right)^{4/3}} \qquad (6.1)$$

where V_T is the transverse wind speed, L_o is the outer scale of turbulence and f is the frequency. $\frac{V_T}{2\pi L_o}$ represents the high frequency cut-off. The laser height above the ground was about 1 meter and is an estimate of the outer scale. Therefore, the high frequency cut-off is less than 1 Hz for wind speeds up to 10 meters/sec. Consequently, the phase variations due to turbulence are concentrated at frequencies below the target motion frequency.

A low pass filter with a cut-off frequency set slightly below the target motion frequency was used to extract turbulence information from the phase data. A high pass filter was also needed to remove very low frequencies since a finite sample length prevented data from extending to d.c. The cut-off frequency was chosen to be approximately ten times the reciprocal of the maximum time of a data set. This gave a reasonable average of low frequency data within any set. Five pole filters producing 100 dB per decade attenuation characteristics were used to achieve good selectivity since the desired information was contained in a narrow band of frequencies.

Speckle frequencies cover a much wider band of frequencies extending to relatively high frequencies. The highest speckle frequency can be estimated by determining the minimum time for a change in the speckle pattern at the receiver. The minimum time depends on the rate of beam wander on the target and the target correlation length and can be estimated by dividing the correlation length by the transverse wind speed. The highest frequency will

be the reciprocal of this time. Typical limiting values for correlation length and a wind speed are 50μm and 5 meters/second respectively. However, when taking data for the purposes of measuring the speckle, the wind was usually less than 1 meter/second so data rates greater than 20 kHz were not expected.

The maximum available sampling rate was 7.15 kHz, and the highest recorded frequency was set accordingly to 4 kHz. Therefore, some high frequency speckle information was lost. The sampling rate was slightly less than the Nyquist rate of twice the highest frequency, so a small amount of aliasing is expected. To extract the speckle information, a 10 point running average was subtracted from the unwrapped phase difference data. This simulated a high pass filter with a cut-off frequency of about 114 Hz. The cut-off frequency had to be set well above the target motion frequency since the running point average filter was not very selective.

A sample of the unwrapped phase data before it was filtered is given in figure 6.3a. It is evident from the figure that it was impossible to eliminate all of the unwrapping errors. The target motion and macro-scopic target variations caused rapid and violent phase changes which made phase unwrapping very difficult. Unwrapping errors were attributed to an insufficient sampling rate and the inability to take simultaneous samples of both phase channels. Figure 6.3b shows the same data set after phase changes greater than π radians between adjacent samples were removed. Since the standard deviation of speckle phase was expected to be less than 1 radian, changes greater than π radians represent more than three standard

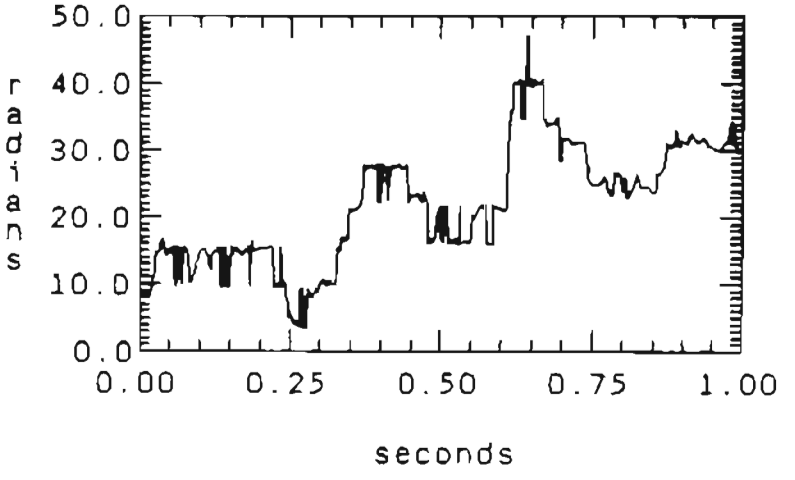

(a) before

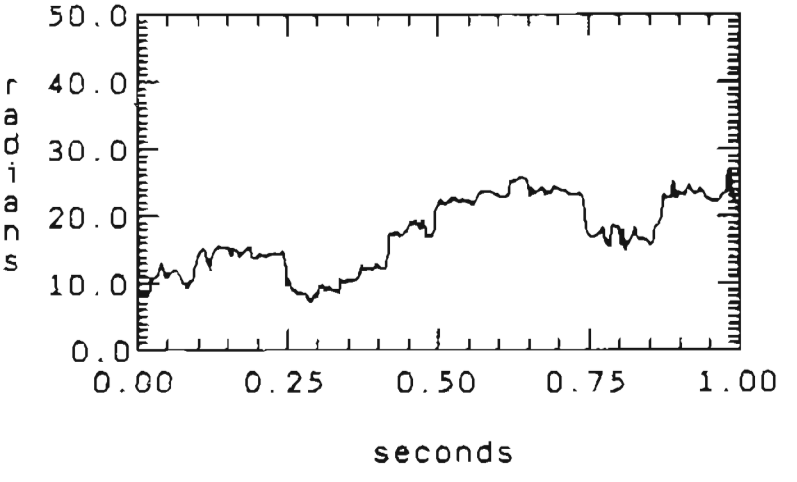

(b) after

Figure 6.3 - Unwrapped Phase Difference before and after changes $> \pi$ radians are removed

deviations from expected phase deviations. This did eliminate most unwrapping errors, however, more complicated algorithms for unwrapping the phase data or for correcting the unwrapping errors may be more effective in preventing unwrapping errors.

Slightly larger phase variances due to speckle and turbulence might be expected than is shown by the data due to the loss of information in the filtering process. On the other hand the inability to remove unwanted phase variations may in fact produce phase variances larger than expected. Consequently, some of the conclusions that can be drawn from the data are compromised by the uncertainty of the origin of the phase variations because of imperfect filtering. Nevertheless the indications are that the filtering was able to separate the various effects reasonably well.

6.2 Laser Beam Properties and Target Parameters

Figure 6.4 summarizes the laser beam propagation to the target. The target was situated 1 km from the laser source and receiver. A 3x and 10x beam expander were used to produce an overall laser beam expansion of 30x and a beam radius of 36 millimeters at the exit lens of the transmitter. The laser beam size was adjusted at the 10x beam expander to produce a maximum average signal level at the receiver. Maximum receiver level is achieved when the beam diameter on the target is a minimum[27]. Originally it was thought that adjustment of the beam expander could produce a waist of the laser beam at the target.

However, it was subsequently determined that it was impossible to produce a waist at the target under the conditions of the experiment. The

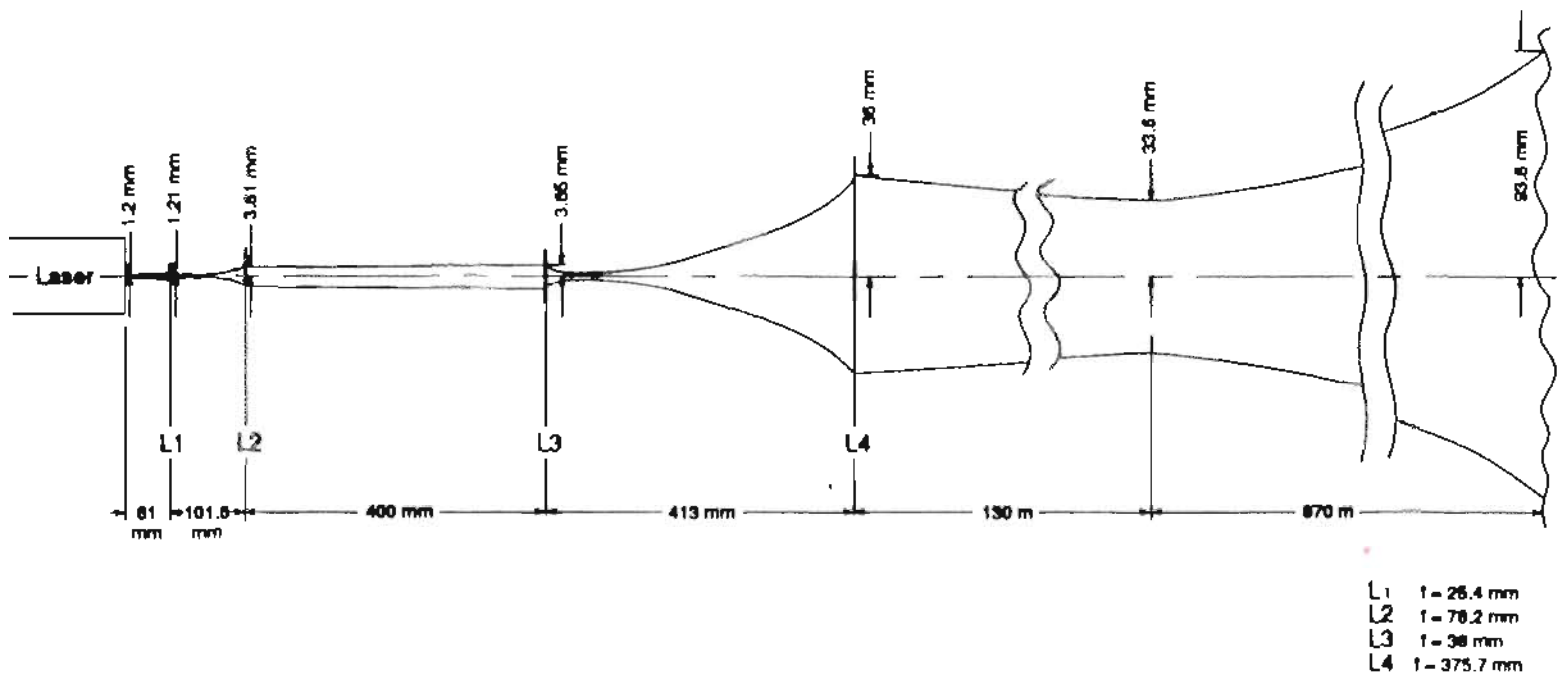

Figure 6.4 - Laser Beam Propagation to the Target

conditions that would be necessary to produce a minimum radius at the target were calculated. The minimum beam radius at the target was found to be 93.6 millimeters when the beam was focused at a distance of 130 meters from the beam expander.

Sandblasted aluminum targets of differing surface roughness were used to test the ability to distinguish surface roughness by phase difference measurements. 30,16 and 8 grit sandblasted aluminum targets were produced and measured for r.m.s. surface roughness and surface correlation length using a calibrated laboratory profilometer[33]. After taking some of the data, the 30 grit target was coated with a flame spray in order to produce a rougher surface than was possible by sandblasting. The rougher surface made it difficult to measure with the profilometer, and although the surface roughness was measured, the correlation length could not be measured. A fifth target, called a standard target, was permanently situated at the field site and could not be measured. It's surface roughness is estimated to be on the order of the 30 grit target roughness. Table 6.1 summarizes the results of the measurements made using the profilometer.

R.M.S. roughness varied from 4.8 μm for the 30 grit target to 39.5 μm for the flame-sprayed target. The phase standard deviations represented by the surface roughness measurements are computed using equation (2.6) from chapter 2 giving a phase deviation range of 3 to 24 radians at the laser wavelength of 10.6μm. Correlation lengths ranged from 42.9 μm to 96.4 μm for all of the targets except for the flame sprayed target which was not measured.

Table 6.1

from Peacock (33)

Target Type	R.M.S. Surface Height (μm)	Correlation Length (μm)
30 Grit	4.8	42.9
16 Grit	8.1	50.0
8 Grit	12.2	96.4
Flame Sprayed	39.5	———

6.3 Phase Difference Measurement of Speckle

Figure 6.5a shows a typical example of phase difference data before the phase is unwrapped and figure 6.5b shows a histogram of the data. Large transitions across the boundaries of the phase detector occur frequently. The histogram shows two distinct peaks where the phase makes the transitions. These transitions are due to macro-scopic target characteristics and to the wind causing the target to vibrate and produce large phase changes. These large phase transitions dominate the wrapped phase data and microscopic target characteristics of the data are hardly noticeable. Consequently, wrapped phase distributions are not very revealing of target characteristics and are useless in distinguishing between targets of different roughness.

On the other hand if the phase is unwrapped and appropriately filtered, the histograms are approximately Gaussian and the variance depends on the roughness of the target. In figure 6.6a, unwrapped and filtered phase difference data is shown for the standard target. In figure 6.6b, a histogram of the data in figure 6.6a is shown along with a Gaussian curve with a standard deviation of 0.02 radians. In the figures, a running point average was subtracted from the unwrapped phase data to implement the high pass filtering necessary to extract the speckle phase variations from the macro-scopic effects.

Variance of Phase Difference versus Target Roughness.

Peacock[33] has shown that differences in surface roughness of sandblasted aluminum targets can be distinguished from the high pass filtered unwrapped phase difference measured remotely at a distance of 1000 meters. Figure 6.7

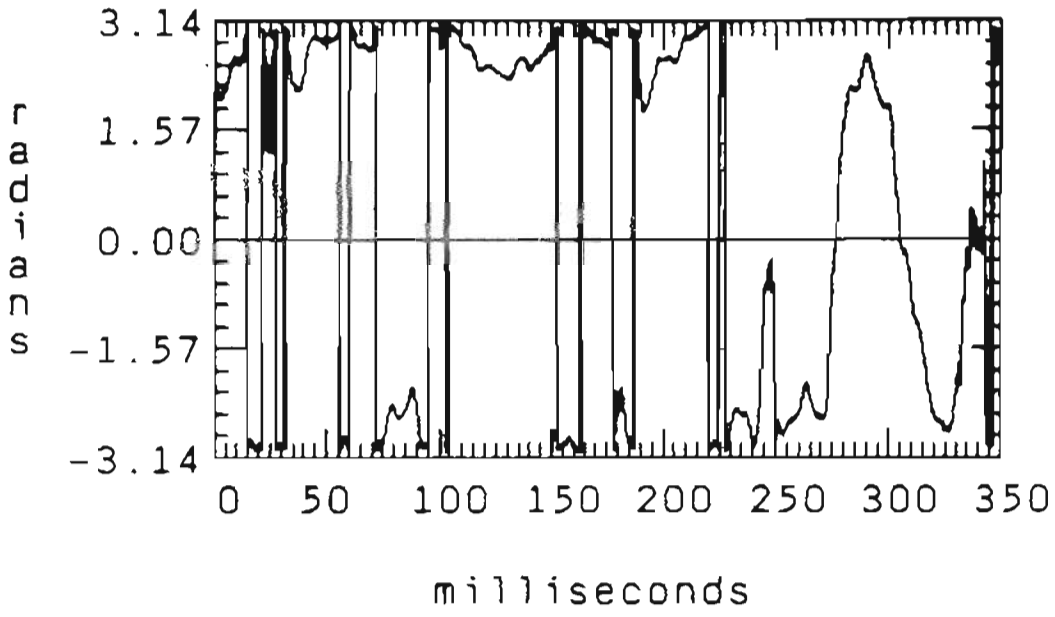

Figure 6.5 (a) - Wrapped Phase Data

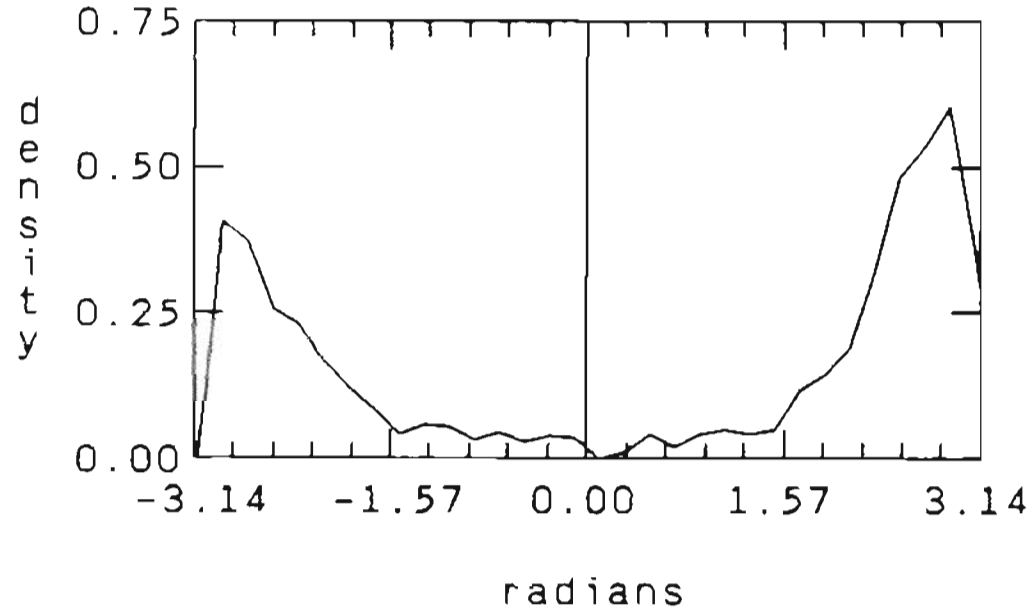

Figure 6.5 (b) - Histogram of Wrapped Phase Data

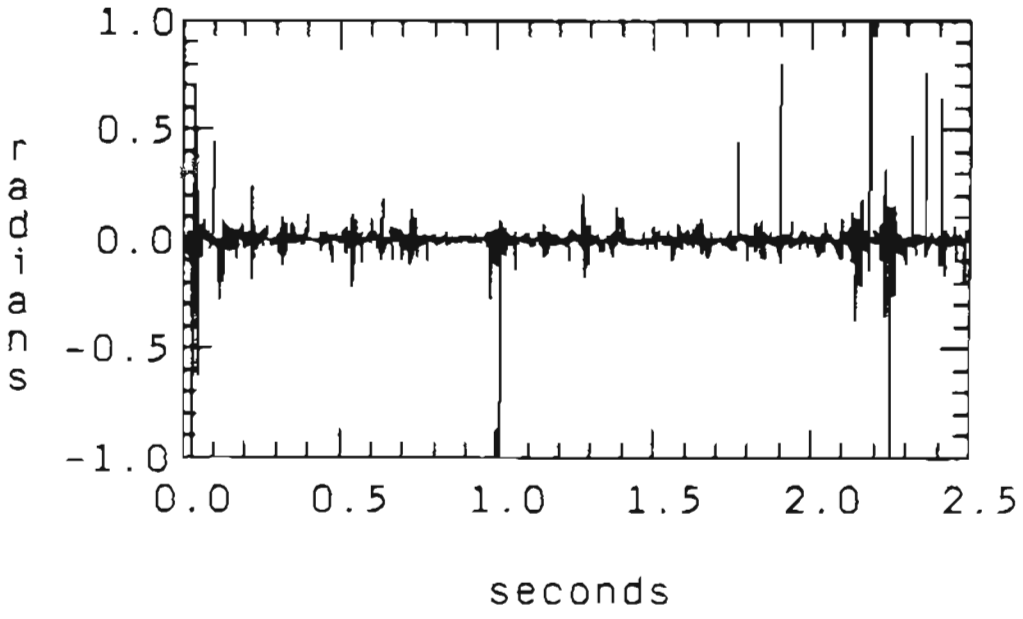

Figure 6.6 (a) - Filtered Unwrapped Phase Data

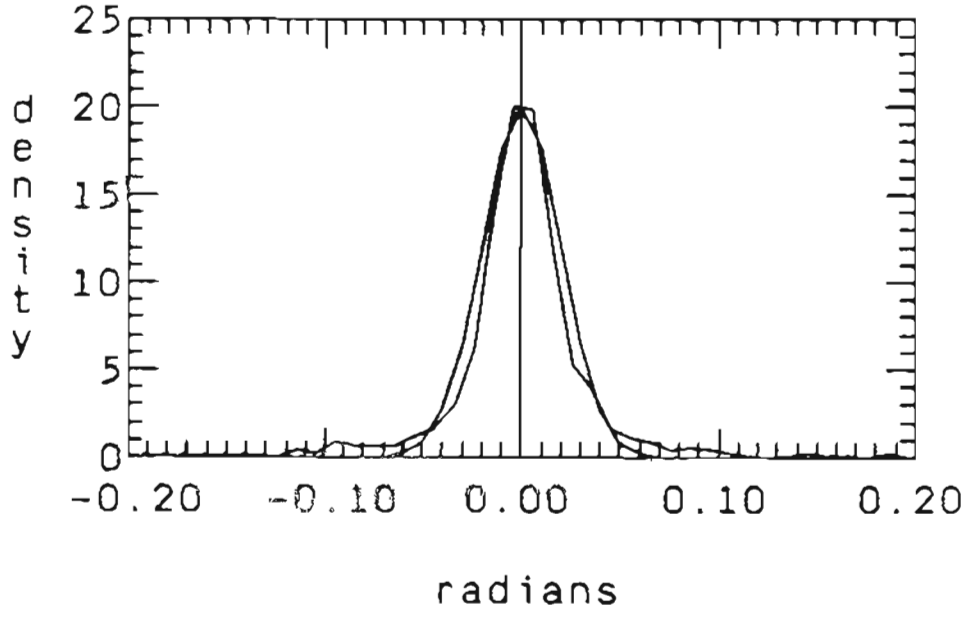

Figure 6.6 (b) - Histogram of (a) compared to Gaussian function

summarizes his results. The highest recorded frequency was 4 kHz. Each set of data contained 25,000 data points for a data set length of 3.5 seconds. A 10 point running average of the unwrapped data was subtracted in order to produce a high pass filter characteristic of about 114 Hz cut-off. The data was taken on two different days. On the first day the 30,16 and 8 grit sand-blasted aluminum targets were used. Then the 30 grit target was converted to a flame sprayed target and data was taken on the 8 grit 16 grit and flame sprayed targets.

The phase variances plotted in figure 6.7 were obtained from Gaussian functions that represented the data. A histogram of the filtered data points was constructed, and because the histograms did not resemble a Gaussian curve for large phase values, values having a magnitude larger than 0.38 radians were removed from the histograms and a Gaussian curve was selected that produced the minimum average deviation from the histogram. It is the Gaussian curve's standard deviation that is plotted in the figure. It should be pointed out that in producing the results of figure 6.7, unwrapping errors like the ones shown in figure 6.3a were not removed from the filtered unwrapped phase data. Reference 33 has details of these methods.

Using the data recorded on the second day of tests, the standard deviation of the filtered unwrapped phase data after the unwrapping errors were removed as shown in figure 6.3b, produced standard deviations slightly higher than in figure 6.7. The filtered data was used directly without constructing histograms truncated to fit Gaussian curves but was high pass filtered in the same way. This suggests that the truncation of the histograms

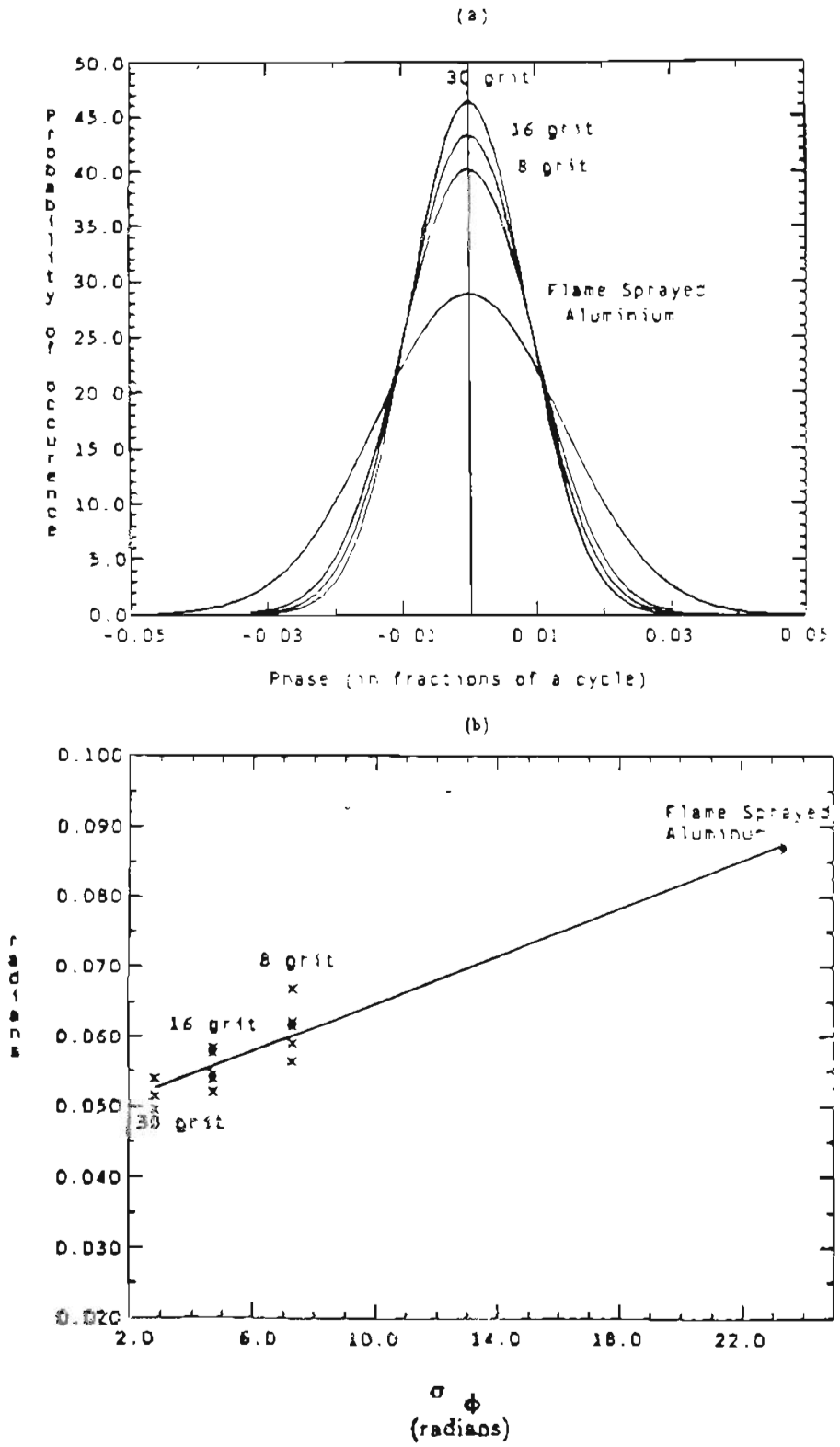

Figure 6.7 - (a) Histograms of Measured Unwrapped Phase Difference Data
(b) Measured Standard Deviation vs. σ_Φ from Peacock (33)

leading to figure 6.7 had a similar effect as the removal of unwrapping errors and lends more credibility to the data in figure 6.7.

In order to emphasize the need for proper filtering of the data, standard deviations of the unwrapped phase before being filtered is shown in figure 6.8 as a function of target phase deviation. Extremely large phase deviations are experienced which for the most part are due to the target motion and the phase unwrapping errors that result from these large phase changes. In one set of data where the wind speed was virtually zero, the phase deviation was the smallest, even though the target surface was the roughest.

6.4 Comparison of Speckle Phase Measurements and Theory

It was difficult to predict the expected phase difference variations for the conditions of the atmospheric field site. The relationships given in chapter 2 that predict speckle phase and phase difference apply to special cases that do not accurately fit the experimental conditions.

The phase extent for the conditional probability density ellipse of the complex fields at one point given the complex field at a second point predicts the phase difference standard deviation when the phase extent is small. In this case the phase extent is approximately equal to the standard deviation of phase differences and is valid when the observation point is in the far-field of the diffuse target. With a laser beam waist radius of 33.4 mm, the Rayleigh range is 300 m, and for a target range of 1000m, the receiver is in the far-field.

Unfortunately, the theory applies only to the case where the laser waist appears at the target, producing a wave with no curvature on the target.

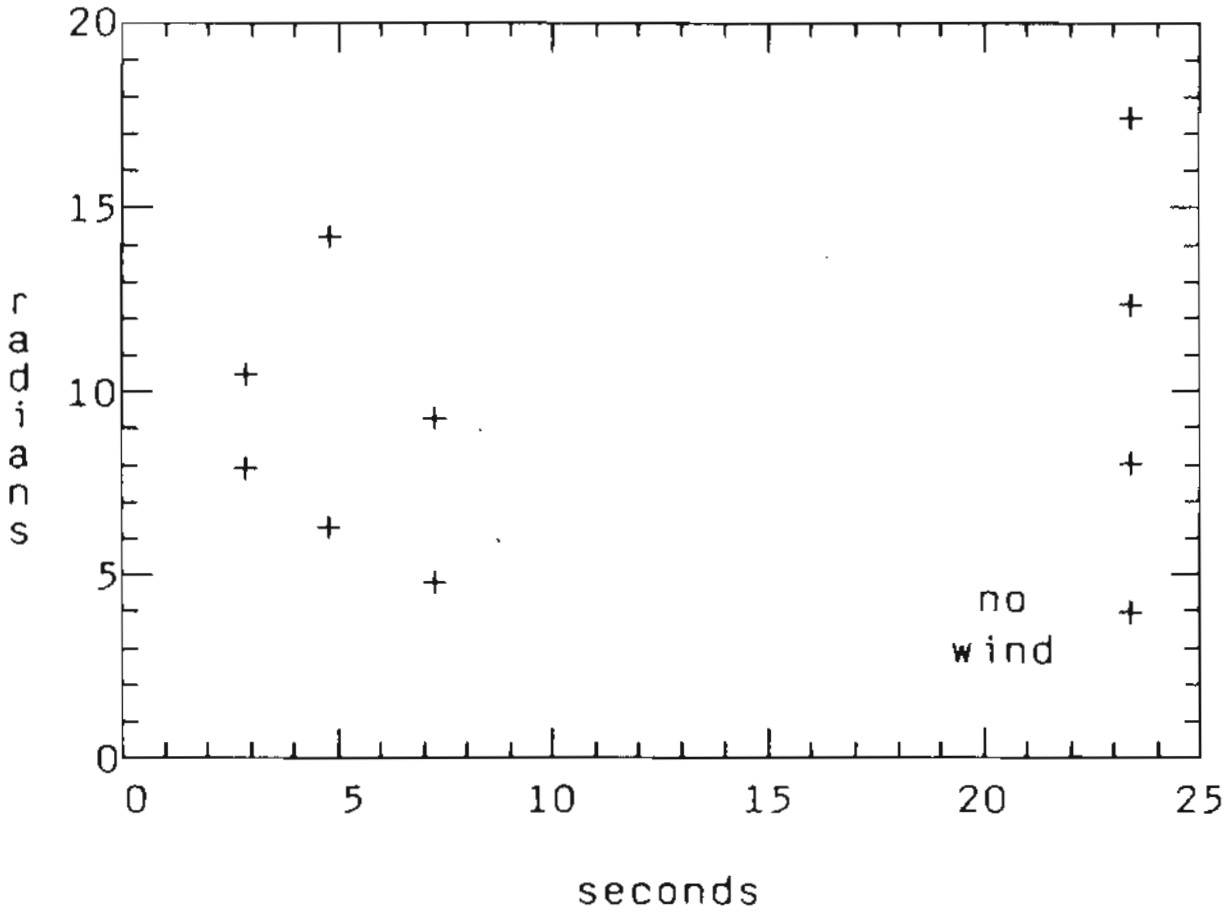

Figure 6.8 - Unfiltered Unwrapped Phase Deviation vs. σ_ϕ

The laser waist was calculated to be 870 meters in front of the target so that the beam would be diverging at a half-angle of about 0.1 milliradian with a radius of curvature of about 975 meters by the time it reaches the target. In the theoretical formulation, the waist radius along with the target surface correlation length determines the effective number of scatterers on the target. If the laser waist radius is assumed to be at the target, the number of scatterers would be incorrectly calculated in the formulation.

However, the correlation coefficient of the real components of the complex fields at the two receiver points (γ_r) and the corresponding correlation coefficient of the imaginary components (γ_i) do not depend on the number of target scatterers and only depend on the receiver separation, the off-axis distance of the receiver and the standard deviation of target phases.

When γ_r and γ_i are both equal to one, the fields are completely correlated and the phase extent is zero. This indicates zero variance of phase difference. When the correlation coefficients are both zero, the fields are uncorrelated and the phase difference variance is the same as the phase variance at either point. In chapter 2 it was shown that for small phase variances, the correlation coefficient of phase differences is approximately equal to $\sqrt{\gamma_i}$.

The correlation coefficients are plotted in figure 6.9 versus the standard deviation of target phase using a receiver separation of 8.6 millimeters, a laser waist radius of 33.6 millimeters and a total path length of 1870 meters equal to the distance from the laser waist to the target plus the distance from the target to the receiver. The correlation coefficients are shown for the on-

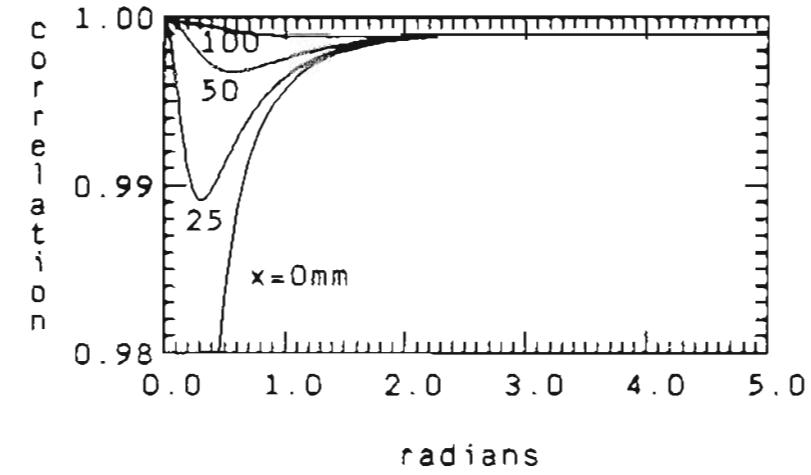

(a) γ_r

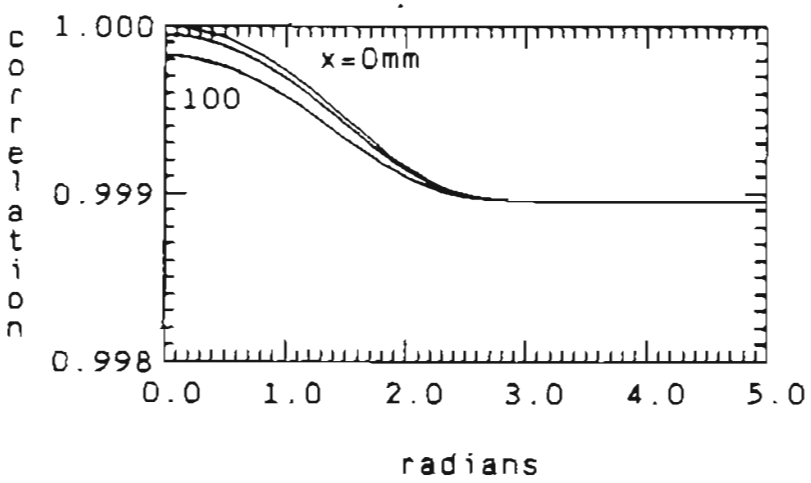

(b) γ_i

Figure 6.9 - γ vs. σ_ϕ ; Δx=8.6mm, w_o=33.6mm, L=1870m, x1=0, 25, 50, 100 mm

axis case and also for cases where the receiver is off the optical axis of the laser. The figure shows a high degree of correlation between both the real and the imaginary fields for all but very small target phase deviations. When the receiver is slightly off-axis the correlation coefficients are about the same value and approximately one for all target phase deviations. Consequently, the phase difference standard deviations are expected to be much smaller than the phase deviations at either point.

The expected phase deviation at either receiver point was predicted assuming the receiver was in the far-field of the target. In this case the single point standard deviation of phase is $\sigma_\phi/\sqrt{N}$, where N is the number of scatterers and σ_ϕ is the standard deviation of target phase. Using a beam radius of 93.6 millimeters on the target and a target correlation distance of 100 μm, the expected single point phase standard deviation is $\sigma_\phi/936$ or 25 milliradians for the flame sprayed target. The single point standard deviation of the speckle phase was measured from integrated frequency data recorded with the flame sprayed target. The data was filtered using a 5 pole high pass filter with a cut-off frequency of 200 Hz to remove the large phase oscillations of the target motion and other low frequency effects not associated with speckle. The speckle phase deviation was measured in 8 sets of data with and average value of 56.9 milliradians. The standard deviation of the measurement was 46.3 milliradians. When the largest and smallest measurements were eliminated, the average and standard deviations were 48.6 milliradians and 24.4 milliradians respectively.

The other special case that predicts the expected phase difference stan-

dard deviations assumes that the one point speckle phase is fully developed so that the complex field at each receiver point is circularly Gaussian. In this case the phase difference variations should have no dependence on the target phase deviations which we know not to be the case. In the far-field, the one point fields are not circularly Gaussian, so this formulation does not apply.

It is concluded that some change in the model is needed to predict the phase difference variations from the experiment. However, the high frequency unwrapped phase difference deviations are clearly dependent on the target phase deviations and the target surface roughness.

6.5 Measurements of Turbulence Phase

The unwrapped phase data should be able to predict the atmospheric turbulence levels. Unfortunately, the macrostructure of the target and the target motion interfere. The microsurface roughness is not a problem for measuring turbulence since these irregularities produce high frequency effects. These macro-surface irregularities in the surface profile produce much lower frequencies and along with the effects of target motion, interfere with the turbulence phase measurement.

Nevertheless, various filtering methods were used that appeared to extract turbulence information from the phase and frequency data. Figure 6.10 shows the relationship between the standard deviation of integrated frequency as a function of the measured turbulence levels. Target motion and macro-scopic target effects were attenuated using a low pass filter and a high pass filter was used to average out the low frequency data. Five pole filters with an attenuation of 100 dB per decade were used for both the high pass

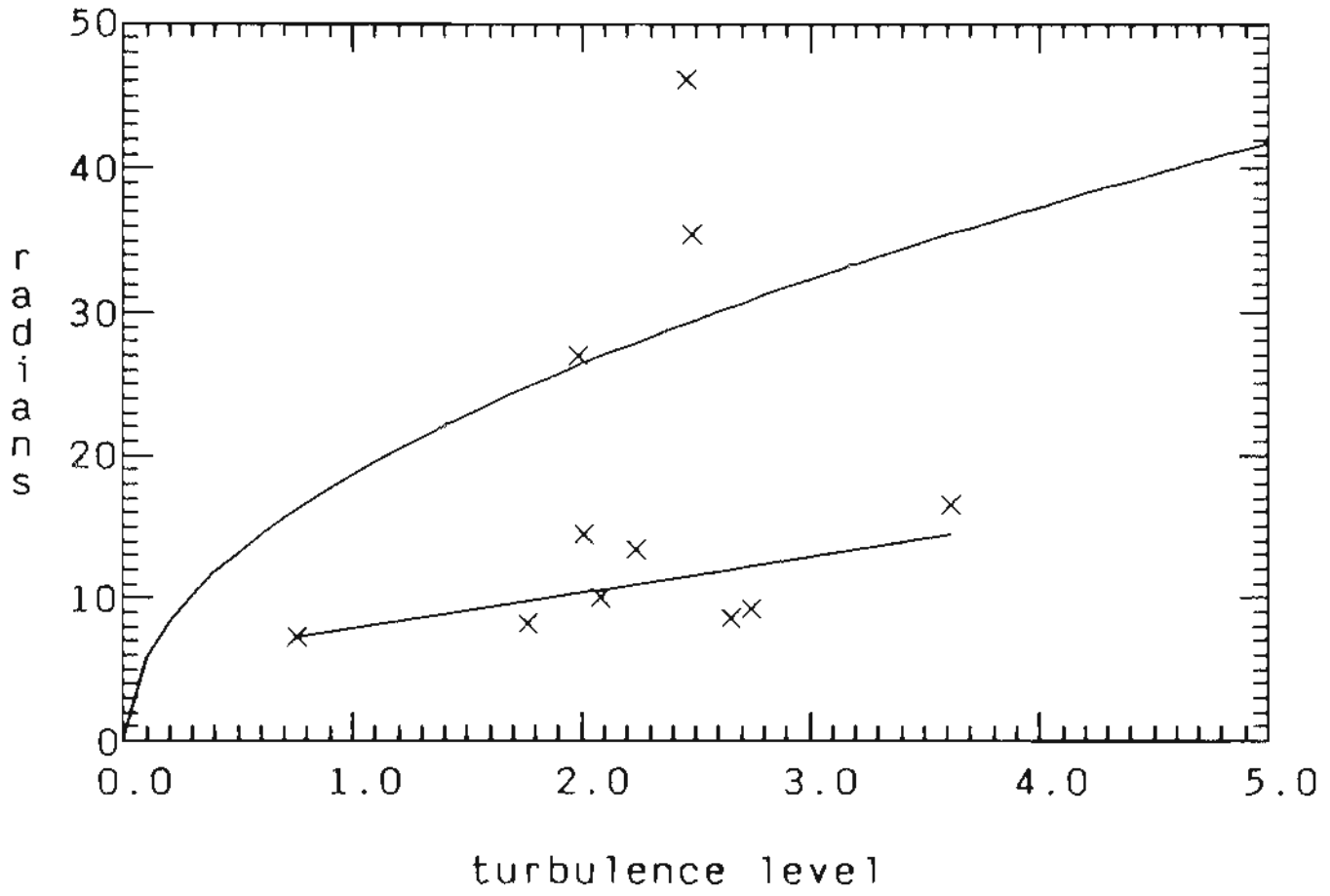

Figure 6.10 - Measured Standard Deviation of Filtered Integrated Frequency Data vs. C_n^2

and low pass filter. The 3 dB cut-off frequencies were 0.5 Hz and 5 Hz. Each data set represents 30 seconds of data and 2500 data points. Figure 6.11 shows a typical histogram of the filtered unwrapped phase showing a close resemblance to a Gaussian curve with a standard deviation of 10 radians also shown in the figure.

The data in figure 6.10 show reasonably good agreement with theory. The square root of equation (2.23) is plotted along with the data assuming an L_o value of 1 meter. A factor of 2 is included in the equation to account for the two way path. Three out of the eleven sets used to construct figure 6.10 had extremely large phase variances well above the norm of the other sets. A linear regression of the other eight points is shown in the figure. Extremely large phase jumps which can not be explained by normal atmospheric effects were experienced in the three sets that were excluded. They are possibly the result of some unusual laser activity such as a loss of coherence due to mode shifting in the laser.

Two point unwrapped phase measurements should also show a dependence on turbulence levels. Phase difference measurements[9,14,33,34] have already been shown to agree with the theoretical predictions of (2.41), however, in these instances phase differences were measured over a one way path rather than with reflections from a remote diffuse target.

Figure 6.12 shows the standard deviation of unwrapped phase difference as a function of measured turbulence level compared to the curve predicted by the square root of equation (2.41). 5-pole low and high pass filters were also used to remove unwanted effects in the data. Since the sample lengths

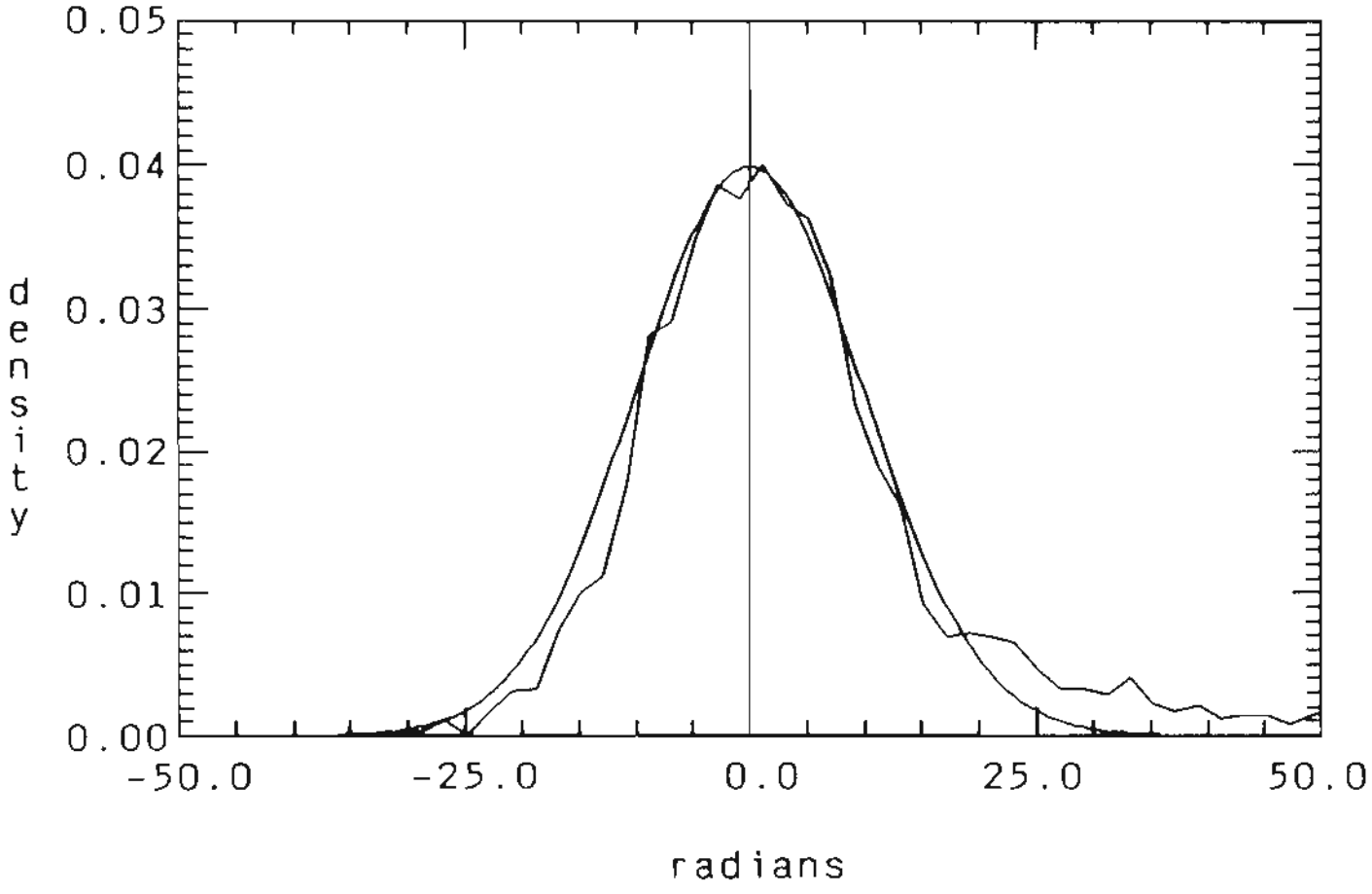

Figure 6.11 - Histogram of Filtered Integrated Frequency and Gaussian Function

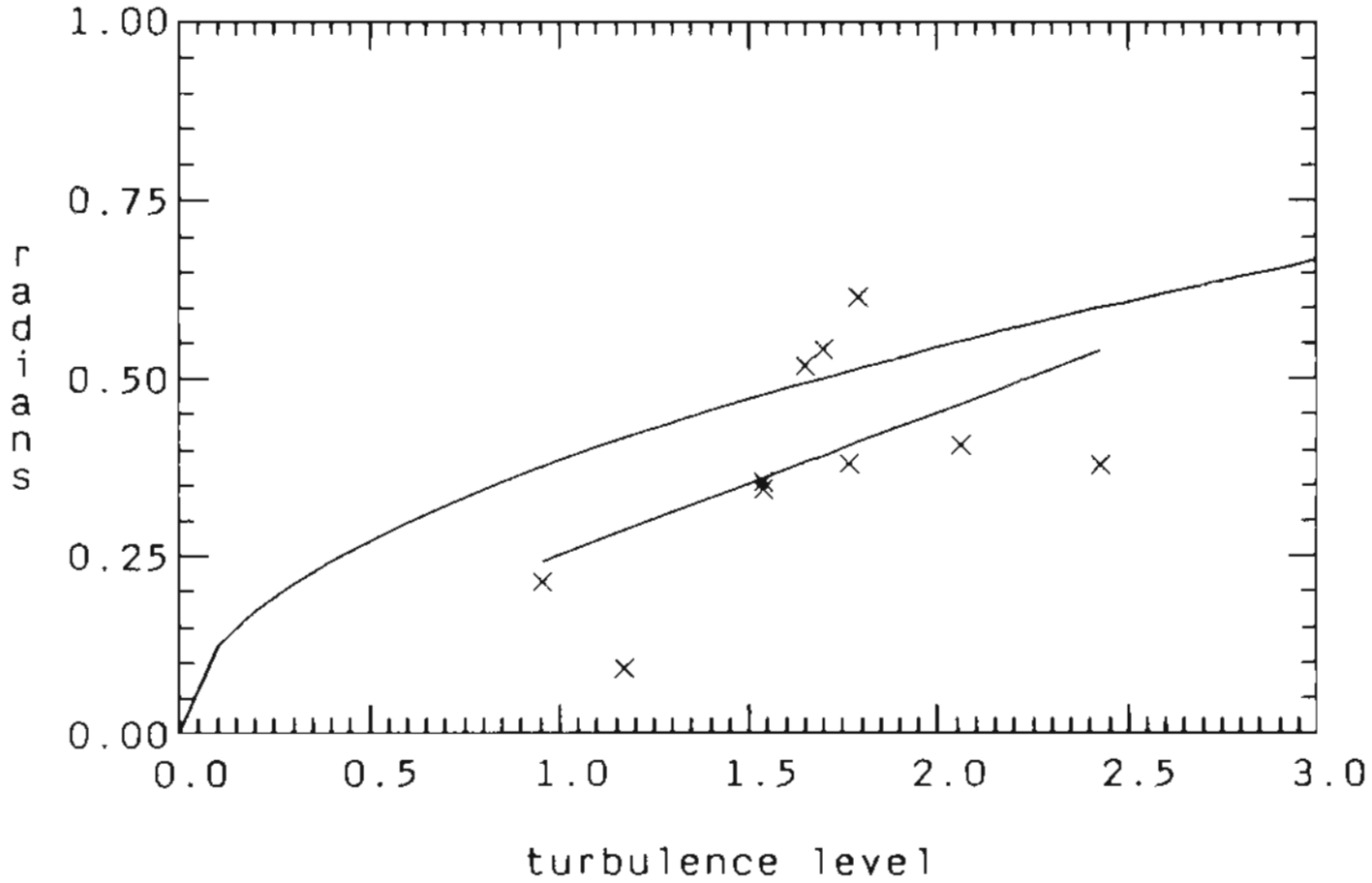

Figure 6.12 - Measured Standard Deviation of Filtered Phase Difference Data vs. C_n^2

for the unwrapped phase data were only 4.2 seconds, the high pass cut-off frequency was raised to 2 Hz.

6.6 Applications of Unwrapped Phase Measurement

Figure 6.1 dramatically shows the effects that the motion of the target had on the received unwrapped phase and figure 6.7 indicates how surface roughness can be determined from the unwrapped phase. It seems obvious that measurements of unwrapped phase will be useful in determining certain features of a remote target and its motion. Information about target motion and vibration can be obtained directly from the unwrapped phase or from the power spectra of unwrapped phase or frequency[35,36]. It may also be possible to determine the wind activity from the unwrapped phase since the wind can produce the target motion. It should be emphasized again that the frequency or unwrapped phase is necessary for this. The wrapped phase contains virtually no information about the target or the atmosphere unless the total phase deviations from all sources combined is less than about 1 radian.

It seems very likely that the measurement of unwrapped phase will be useful in determining vibration frequencies and eccentricity of rotating shafts or machinery from a remote location. The phase of a laser is extremely sensitive to minute propagation path changes and has already been used to measure optical surface characteristics in a laboratory environment[37–40] and in the atmosphere[35].

REFERENCES

1. J.W. Goodman,"Statistical Properties of Laser Speckle Patterns", in Laser Speckle and Related Phenomena, J.C. Dainty, ed., Springer-Verlag, (1975)

2. E. Jakeman, W.T. Welford, "Speckle Statistics in Imaging Systems", Optics Communications, 21, 72-79, (1977)

3. J. Ohtsubo, T. Asakura, "Statistical Properties of Laser Speckle Produced in the Diffraction Field", App. Opt., 16, 1742-1753, (1977)

4. S. Donati and G. Martini, "Speckle-Pattern Intensity and Phase: Second-Order Conditional Statistics", J. Opt. Soc. Am., 69, 1690-1694 (1979)

5. J. Uozumi and T. Asakura, "First-Order Intensity and Phase Statistics of Gaussian Speckle Produced in the Diffraction Region", App. Opt., 20, 1454-1466 (1981)

6. N. Takai, H. Kadono and T. Asakura, "Statistical Properties of the Speckle Phase in Image and Diffraction Fields", Opt. Engr., 25, 627-635 (1986)

7. Q. Wang, "Second-Order Conditional Statistics of Phase for Partially Developed Speckle Field in the Far Field", J.Opt.Soc.Am., 8, 105-111 (1991)

8. V.T. Tatarski, "Wave Propagation in a Turbulent Medium", translated by R.S. Silverman, McGraw Hill (1961)

9. S.F. Clifford, G.M.B. Bouricius, G.R. Ochs, M.H. Ackley, "Phase Variations in Atmospherical Optical Propagation", J.Opt.Soc.Am., 61, 1279-1284 (1971)

10. A. Ishimaru, "Temporal Frequency Spectra of Multifrequency Waves in a Turbulent Atmosphere", IEEE Trans. Antennas Propag. AP-20, 10-19 (1972)

11. A. Ishimaru, "The Beam Wave Case and Remote Sensing", in Laser Beam Propagation in the Atmosphere, J.W. Strohbehn, ed., Springer-Verlag, (1978)

12. S.F. Clifford, "The Classical Theory of Wave Propagation in a Turbulent Medium", in Laser Beam Propagation in the Atmosphere, J.W. Strohbehn, ed., Springer-Verlag, (1978)

13. J.W. Strohbehn, "Modern Theories in the Propagation of Optical Waves in a Turbulent Medium", in Laser Beam Propagation in the Atmosphere, J.W. Strohbehn, ed., Springer-Verlag, (1978)

14. K. Schatzel, "K-Distributed Phase Differences in Turbulent Random Phase Screens", J.Opt.Soc.Am., 73, 269-276 (1983)

15. R. L. Phillips, L. C. Andrews, "The Significance of the Class of K-Distributions", SPIE Vol. 926, Optical Infrared and Millimeter Wave Propagation Engineering, 2-7 (1988)

16. L. C. Andrews, R.L. Phillips, "Phase Models for Weak Fluctuations", SPIE Vol. 926, Optical Infrared and Millimeter Wave Propagation Engineering, 8-12 (1988)

17. V.S. Rao Gudimetla and J. F Holmes, "Probability Density Function of the Intensity for a Laser-Generated Speckle Field After Propagation Through the Turbulent Atmosphere", J.Opt.Soc.Am., 72, 1213-1218 (1982)

18. V.S. Rao Gudimetla, J. F. Holmes and R.A. Elliott, "Two-Point

Joint-Density Function of the Intensity for a Laser-Generated Speckle Field After Propagation Through the Turbulent Atmosphere", J.Opt.Soc.Am.,A, 7, 1008-1014 (1990)

19. P. Beckmann, A. Spizzichino, "The Scattering of Electromagnetic Waves from Rough Surfaces", Pergamon/Macmillan, (1963)

20. J. Uozumi and T. Asakura, "First-Order Probability Density Function of the Laser Speckle Phase", Opt. and Quan. Elec., 12, 477-494 (1980)

21. D. Middleton, "Introduction to Statistical Communication Theory", McGraw Hill, (1960)

22. W. Feller, "An Introduction to Probability Theory and Its Applications", 2nd Ed., Wiley, (1971)

23. R. Barakat, "Weak-Scatterer Generalization of the K-Density Function. II. Probability Density of Total Phase", J.Opt.Soc.Am. A, 4, 1213-1219 (1987)

24. H. Stewart, R. Hopfield, "Atmospheric Effects", in Applied Optics and Optical Engineering, Kingslake, ed., Academic Press, New York (1965)

25. S. Flatte', Personal communication with J.F. Holmes, 1 October 1986

26. W. Fante, "Progress in Optics", E. Wolf ed., vol. 22 , 343-398, Amsterdam, North-Holland (1961)

27. F. Amzajerdian, "Remote Sensing of Atmospheric Winds by Utilizing Speckle-Turbulence Interaction and Optical Heterodyne Detection", Ph.D. Thesis, Oregon Graduate Center, June 1988

28. J. F. Holmes, F. Amzajerdian, J.M. Hunt, "Improved Optical Local-Oscillator Isolation Using Multiple Acousto-Optic Modulators and Frequency Diversity", Opt. Lett., 12, 637-639 (1987)

29. D. Draper, J.F. Holmes, J.M. Hunt and J. Peacock, "Simple Two-Laser Optical Heterodyne System with Large Transmitter- Local Oscillator Isolation", App. Opt., 28, 4048-4050 (1989)

30. W. R. Leeb, H. K. Philipp, A. L. Scholtz and E. Bonek, "Frequency Synchronization and Phase Locking of CO_2 Lasers", Appl. Phys. Lett., 41 No.7, 592-594 (1982)

31. J. Tribolet, "A New Phase Unwrapping Algorithm", IEEE Trans. on Acoustics, Speech and Signal Processing ASSP-25 170-177 (1977)

32. D. C. Ghiglia, G. A. Mastin and L. A. Romero, "Cellular-Automata Method for Phase Unwrapping", J. Opt. Soc. Am. A, 4, 267-280 (1987)

33. J. S. Peacock, "Optical Remote Sensing of Surface Roughness", Master of Science Thesis, Oregon Graduate Center, May, 1989

34. V. P. Lukin and V. V. Pokasov, "Optical Wave Phase Fluctuations", App. Opt., 20, 121-135 (1981)

35. I. E. Balkarei, B. L. Davydov, V. M. Epikhin, K. S. Kozlov, L. L. Palitsev and Yu. D. Samorodov, "Remote Detection of Small Vibrations of Objects Across the Atmosphere with the Aid of a CO_2 Laser Heterodyne System", Sov. J. Quantum Electron., 19, 964-967 (1989)

36. W. Kranz, "Target Classification by Vibration Sensing", Proc. SPIE-Int. Soc. Opt. Eng., 972, 383-387 (1988)

37. G. E. Sommargren, "Optical Heterodyne Profilometry", App. Opt., 20, 610-618 (1981)

38. R. A. Smythe, "Heterodyne Profiler Moves from R&D to the Marketplace", Laser Focus/Electro-Optics, 92-95 (July, 1987)

39. J. M. Bennett, "Comparison of Techniques for Measuring the Roughness of Optical Surfaces", Optical Engineering, 24, 380-387 (1985)

40. H. Kadono, N. Takai and T. Asakura, "Experimental Study of the Laser Speckle Phase in the Image Field", Optica Acta, 1223-1234 (1987)

APPENDIX A

AMPLITUDE STATISTICS

In this appendix, the amplitude and intensity probability density functions for the speckle and turbulence models of chapters 2 and 3 will be presented. Most of the intensity distributions were taken directly from the literature, and and in several cases they were converted to the corresponding amplitude probability density functions. For the two point functions and also for the case of speckle combined with turbulence, only fully developed speckle is considered.

One Point Probability Density Function of Speckle Amplitude

Totally Diffuse Target

The one point amplitude and intensity statistics of speckle in a vacuum are based on the joint Gaussian probability density function of (2.5). Using the change of variables defined by $I = A^2 = X^2 + Y^2$ and $\theta = \tan^{-1}(Y/X)$, Uozumi and Asakura[5] give the probability density function of intensity to be,

$$p(I) = \frac{1}{4\pi\sigma_r\sigma_i}\int_0^{2\pi} e^{(f)}d\theta \tag{A1}$$

where

$$f = -\left[\left(\frac{\cos^2\theta}{2\sigma_x^{\,2}} + \frac{\sin^2\theta}{2\sigma_y^{\,2}}\right)I - \left(\frac{\langle X\rangle}{\sigma_x^{\,2}}\cos\theta + \frac{\langle Y\rangle}{\sigma_y^{\,2}}\sin\theta\right)I^{1/2} + \frac{\langle X\rangle^2}{2\sigma_x^{\,2}} + \frac{\langle Y\rangle^2}{2\sigma_y^{\,2}}\right]$$

which reduces[2] to,

$$p(I)=\frac{1}{2\sigma_x\sigma_y}\exp\left(-\frac{1}{4}\left(\left(\frac{1}{\sigma_r^2}+\frac{1}{\sigma_i^2}\right)I+\frac{1}{2}\left(\frac{<X>^2}{\sigma_r^2}+\frac{<Y>^2}{\sigma_y^2}\right)\right)\right)$$

$$x\left(I_0(s_1)I_0(s_2)+2\sum_{n=1}^{\infty}I_n(s_1)I_n(s_2)\cos(2n\Omega)\right) \qquad (A2)$$

where

$$s_1=-\frac{1}{4}\left(\frac{1}{\sigma_x^2}-\frac{1}{\sigma_y^2}\right)I$$

$$s_2=-\sqrt{I}\left(\frac{<X>^2}{\sigma_x^4}+\frac{<Y>^2}{\sigma_y^4}\right)^{1/2}$$

$$\tan\Omega=\sigma_x^2<Y>/\sigma_y^2<X>$$

and

$I_n(s)$ is a modified Bessel function of order n

At the on axis point in the far field of diffraction,

$$<U>=<X>=z^{-1}\exp(-\sigma^2_\phi/2)$$

$$<V>=<Y>=0$$

$$\sigma_r^2=\sigma_x^2=\frac{\exp(-2\sigma^2_\phi)S_-}{4Nz^2}$$

$$\sigma_i^2=\sigma_y^2=\frac{\exp(-2\sigma^2_\phi)S_+}{4Nz^2}$$

where

$$S_-=\sum_{n=1}^{\infty}\frac{\sigma_\phi^{4n}}{(2n)(2n)!}$$

$$S_+=\sum_{n=1}^{\infty}\frac{\sigma_\phi^{2(2n+1)}}{(2n+1)(2n+1)!}$$

In this case, (A1) and (A2) reduce[3] to,

$$p(I)=\frac{1}{2\sigma_r\sigma_i}\exp\left(-\frac{1}{4}\left(\left(\frac{1}{\sigma_r^2}+\frac{1}{\sigma_i^2}\right)I+\frac{2}{\sigma_r^2}I_S\right)\right)$$

$$x\left[I_0(s_1)I_0(s_2)+2\sum_{n=1}^{\infty}I_n(s_1)I_n(s_2)\right] \tag{A3}$$

where

$$s_1=\frac{1}{4}\left(\frac{1}{\sigma_r^2}-\frac{1}{\sigma_i^2}\right)I$$

$$s_2=\frac{\sqrt{I_S I}}{\sigma_r^2}$$

$I_S=<U>^2$ is the mean field squared or the mean intensity

σ_r is the variance of the real component and

σ_i is the variance of the imaginary component of the field

Using the change of variable, $I=A^2$ in (A3) and multiplying by $dI/dA=2A$, the probability density function for amplitude becomes,

$$p(A)=\frac{A}{\sigma_r\sigma_i}\exp\left[-\frac{1}{4}\left[\left(\frac{1}{\sigma_r^2}+\frac{1}{\sigma_i^2}\right)A^2+\frac{2}{\sigma_r^2}I_S\right]\right]$$
$$x\left[I_0(s_1)I_0(s_2)+2\sum_{n=1}^{\infty}I_n(s_1)I_n(s_2)\right] \tag{A4}$$

and

$$s_1=\frac{1}{4}\left(\frac{1}{\sigma_r^2}-\frac{1}{\sigma_i^2}\right)A^2$$

$$s_2=A\frac{\sqrt{I_S}}{\sigma_r^2}$$

Fully Developed Speckle

For the fully developed speckle case, $<U>=0$, $\sigma_r=\sigma_i=\sigma$. Consequently, $s_1=s_2=0$ and (A4) reduces to,

$$p(A)=\frac{2A}{\sigma^2}\exp\left[-\frac{A^2}{\sigma^2}\right] \tag{A5}$$

Equation (A5) is the Rayleigh distribution. The corresponding density function of intensities is given by the negative exponential distribution,

$$p(I)=\frac{1}{<I>}\exp\left(\frac{-I}{<I>}\right) \tag{A6}$$

where $<I>$ is the mean value of intensity $= \sigma^2$.

Partially Diffuse Target

For the case of a partially diffuse target, with circular Gaussian statistics for the random portion, the probability density function of amplitudes is described by the Rice-Nakagami distribution[1,21]

$$p(A)=\frac{2A}{\sigma^2}\exp\left(-\frac{A^2+B^2}{\sigma^2}\right)I_0\left(2A\frac{B}{\sigma^2}\right) \tag{A7}$$

where

I_0 is a modified Bessel function of zero order.

B is the constant mean value of the complex field amplitude

$$\sigma^2=\sigma_r^2+\sigma_i^2=2\sigma_r{}^2=2\sigma_i{}^2$$

is the combined variance of the real and imaginary components of the random part of the field.

The beam ratio parameter is defined by,

$$r=I_s/<I_D>=B^2/\sigma^2 \tag{2.14a}$$

where I_s is the intensity of the coherent component, and $<I_D>$ is the mean intensity of the random part.

As σ becomes very large relative to B, circular Gaussian statistics are approached and the amplitude distribution reduces to the Rayleigh

distribution given by (A5) and the intensity distribution becomes the negative exponential distribution of (A6).

Alternately as σ approaches zero, the distribution approaches a delta function occurring at the amplitude B. This situation corresponds to a perfectly smooth target.

Interestingly, (A4) also reduces to the Rice-Nakagami distribution of (A7) with a beam ratio parameter of $I_s/2\sigma_r^2$ when σ_r and σ_i are equal and $I_s = <U>^2$ is not equal to zero. However, it can be seen from equations (2.3c) and (2.3d) that when the target is totally diffuse with σ_Φ large relative to π, the speckle phases have an even distribution, σ_r and σ_i are equal and I_s equals zero. This is the fully developed speckle case and the amplitude is described by the Rayleigh distribution of (A5). Therefore, the totally diffuse target will never produce the Rice-Nakagami distribution for amplitudes if the target surface has an even distribution of target surface heights except for the special case of a Rayleigh distribution produced by fully developed speckle.

One Point Probability Density Function of Turbulence Amplitude

Single Scattering

For the case of single scattering, the probability density of amplitudes is well described by[13] the Rice-Nakagami distribution of (A7), where the beam ratio parameter is defined by (2.14a).

Multiple Scattering

For multiple scattering, assuming a single propagating path, since the probability density function for $\chi = \ln A$ is Gaussian, the distribution for the logarithm of the amplitude will also be Gaussian and[13],

$$P(\chi)=\frac{1}{\sigma_\chi\sqrt{2\pi}}\exp\left[-\frac{(\chi-<\chi>)^2}{2\sigma_\chi^2}\right] \tag{A8}$$

or

$$P(\ln A)=\frac{1}{\sigma_{\ln A}\sqrt{2\pi}}\exp\left[-\frac{(\ln A-<\ln A>)^2}{2\sigma_{\ln A}^2}\right] \tag{A9}$$

By a change of variable and multiplying by $d\ln A/dA$, the probability density function for the amplitude is found to be,

$$P(A)=\frac{1}{A\sigma_{\ln A}\sqrt{2\pi}}\exp\left[-\frac{(\ln A-<\ln A>)^2}{2\sigma_{\ln A}^2}\right] \tag{A10}$$

The intensity distribution will also be lognormal[13] and can be obtained using the variable substitution $I=A^2$ in (A10) or $\ln I = 2 \ln A$ in (A9). Using the latter substitution in (A9) and multiplying by $d\ln A/d\ln I = 1/2$ gives,

$$\begin{aligned} P(\ln I)&=\frac{1}{2\sigma_{\ln A}\sqrt{2\pi}}\exp\left[-\frac{(\frac{\ln I}{2}-<\ln A>)^2}{2\sigma_{\ln A}^2}\right] \\ &=\frac{1}{2\sigma_{\ln A}\sqrt{2\pi}}\exp\left[-\frac{(\ln I-2<\ln A>)^2}{8\sigma_{\ln A}^2}\right] \end{aligned} \tag{A11}$$

Multiplying (A11) by $d\ln I/dI = 1/I$ or alternately using the substitution $I = A^2$ in (A10) and multiplying by $dA/dI = \frac{1}{2A}$ and using the substitution $I=A^2$ gives,

$$p(I)=\frac{1}{2I\sigma_{\ln A}\sqrt{2\pi}}\exp\left[-\frac{(\frac{\ln I}{2}-<\ln A>)^2}{2\sigma_{\ln A}^2}\right]$$

$$= \frac{1}{2I\sigma_{\ln A}\sqrt{2\pi}} \exp\left[-\frac{(\ln I - 2<\ln A>)^2}{8\sigma^2_{\ln A}}\right] \tag{A12}$$

Defining $\sigma_{\ln I} = 2\sigma_{\ln A}$ and using $<\ln I> = 2<\ln A>$, (A11) and (A12) can be rewritten as,

$$P(\ln I) = \frac{1}{\sigma_{\ln I}\sqrt{2\pi}} \exp\left[-\frac{(\ln I - <\ln I>)^2}{2\sigma^2_{\ln I}}\right] \tag{A13}$$

and

$$p(I) = \frac{1}{I\sigma_{\ln I}\sqrt{2\pi}} \exp\left[-\frac{(\ln I - <\ln I>)^2}{2\sigma^2_{\ln I}}\right] \tag{A14}$$

where $\sigma_{\ln I}$ is the standard deviation of the logarithm of I and $<\ln I>$ is the mean value of the logarithm of I.

The log amplitude variance is given by[8,11,13] as,

$$\sigma^2_\chi = \sigma^2_{\ln A} = 0.124 C_n^2 k^{7/6} L^{11/6} \tag{A15}$$

for a spherical wave. For a plane wave, σ^2_χ is given by (A15) with the constant 0.124 replaced by 0.307, and for the beam wave case, the constant varies between these values depending on the propagation distance.

Multiple Paths to Receiver

For multiple paths adding together at the receiver location, the complex field will be,

$$E = B + \sum_{j=1}^{N} U_j + iV_j \tag{A16}$$

where B is the unscattered portion of the field which is assumed to be real. Each U_j and V_j will have a distribution described by the lognormal distribution, and the resultant amplitude and intensity distributions are expected to also be lognormal.

Two Point Amplitude Statistics

Two Point Amplitude Statistics for Fully Developed Speckle

Two point statistics of speckle amplitude and intensity have been found for the case of fully developed speckle in a vacuum. The joint probability density function of intensities is given by[1],

$$p_I(I_1,I_2)=\frac{\exp\left(-\frac{I_1+I_2}{<I>(1-|\mu|^2)}\right)}{<I>^2(1-|\mu|^2)}I_0\left(\frac{2|\mu|\sqrt{I_1I_2}}{<I>(1-|\mu|^2)}\right) \qquad \text{(A17)}$$

where μ is the mutual coherence factor defined by (2.28a). The magnitude of $|\mu|$ can be written as,

$$|\mu|=\frac{\Gamma}{\sqrt{<I_1><I_2>}}$$

and Γ is the mutual coherence function defined by,

$$\Gamma=<E_1,E_2^*>$$

E_1 and E_2 are the complex field values at points 1 and 2 respectively.

$<>$ denotes the ensemble average and * the complex conjugate.

Using the change of variables, $I_1=A_1^2$ and $I_2=A_2^2$ the corresponding two point density function for amplitudes becomes,

$$p_A(A_1,A_2)=4A_1A_2\frac{\exp\left(-\frac{A_1^2+A_2^2}{<I>(1-|\mu|^2)}\right)}{<I>^2(1-|\mu|^2)}I_0\left(\frac{2|\mu|A_1A_2}{<I>(1-|\mu|^2)}\right) \qquad \text{(A18)}$$

Under the limiting conditions where the complex coherence factor $|\mu|$ is either zero or one, the equation reduces to expected results. For instance if $|\mu|$ is zero, there is no correlation between the two intensities and the intensities are independent. For this case the density functions reduce to,

$$p_I(I_1,I_2)=p_I(I_1)p_I(I_2)=\frac{\exp\left[-\frac{I_1}{<I>}\right]\exp\left[-\frac{I_2}{<I>}\right]}{<I>^2} \tag{A19}$$

and

$$p_A(A_1,A_2)=p_A(A_1)p_A(A_2)=$$
$$\frac{2A_1}{\sigma_1^2}\exp\left[-\frac{A_1^2}{\sigma_1^2}\right]\frac{2A_2}{\sigma_2^2}\exp\left[-\frac{A_2^2}{\sigma_2^2}\right] \tag{A20}$$

On the other hand if $|\mu|$ is one, there is perfect correlation between the two intensities and the density functions become,

$$p_I(I_1,I_2)=p_I(I_1)\delta(I_2-I_1) \tag{A21}$$

and

$$p_A(A_1,A_2)=p_A(A_1)\delta(A_2-A_1) \tag{A22}$$

Two Point Amplitude Statistics of Turbulence

The joint probability density function for the intensities at the two receiver points for a point source propagating in turbulence is given by[18],

$$P(I_1,I_2)=\frac{4(I_1I_2)^{\frac{M-1}{2}}M^{M+1}}{\Gamma(M)\rho_a^{\frac{M-1}{2}}(1-\rho_a)(<I_1><I_2>)^{\frac{M+1}{2}}} \tag{A23}$$

With the change of variable $A=\sqrt{I}$,

$$P(A_1,A_2)=\frac{16A_1A_2(A_1A_2)^{2M-2}M^{M+1}}{\Gamma(M)\rho_a^{\frac{M-1}{2}}(1-\rho_a)(<I_1><I_2>)^{\frac{M+1}{2}}} \tag{A24}$$

where $M=<x>^2/\sigma_x^2$ and $<x>=$ the mean value and $\sigma_x^2=$ the variance of intensity and ρ_a is the complex coherence factor for a point source propagating in turbulence.

For a plane wave propagating in turbulence Γ is shown by to be[13],

$$\Gamma=I_o\exp(-1.47C_n^2k^2L\Delta x^{5/3})[1-0.805(\Delta x/L_o)^{1/3}] \tag{A25}$$

when

$$\sqrt{\lambda L}<<\Delta x$$

Δ_x is the separation distance between the two receivers and L is the length of the path.

Amplitude Statistics for Fully Developed Speckle in Turbulence

The probability density function of intensity for fully developed speckle propagating in turbulence has been determined by Holmes and Gudimetla[17] to be,

$$P_I(I)=2\left(\frac{M}{<x>}\right)\frac{I^{\frac{M-1}{2}}}{\Gamma(M)}K_{M-1}\left(2\left(\frac{M}{<x>}I\right)^{1/2}\right) \tag{A26}$$

Substituting $I = A^2$ for I in (2) and multiplying by dI/dA gives,

$$P_A(A)=P_I(A^2)(2A) \tag{A27}$$

and

$$P_A(A)=2\left(\frac{M}{<x>}\right)\frac{A^{M-1}}{\Gamma(M)}K_{M-1}\left(2\left(\frac{M}{<x>}A^2\right)^{1/2}\right)2A$$

which equals

$$P_A(A)=4\left(\frac{M}{<x>}\right)\frac{A^M}{\Gamma(M)}K_{M-1}\left(2A\left(\frac{M}{<x>}\right)^{1/2}\right) \tag{A28}$$

or

$$P_A(A)=4\left(\frac{<x>}{\sigma_x^2}\right)\frac{A^M}{\Gamma(M)}K_{M-1}\left(2A\left(\frac{<x>}{\sigma_x^2}\right)^{1/2}\right) \tag{A29}$$

M has been replaced by $<x>/\sigma_x^2$ in selected places.

The Two Point Probability Density Function of Amplitude for Fully Developed Speckle in Turbulence

The two point density of amplitudes can also be obtained from the equivalent density function for intensities using the same variable change. The joint density function of intensities for fully developed speckle at two points has been determined by Holmes, Gudimetla, and Elliot[18] to be,

$$P_{a,s}(I_1,I_2)=\frac{4(I_1I_2)^{\frac{M-1}{2}}M^{M+1}}{\Gamma(M)\rho_a^{\frac{M-1}{2}}(1-\rho_a)(1-\rho_s)^M\left(<I_1><I_2>\right)^{\frac{M+1}{2}}} \qquad \text{(A30)}$$

$$\times\sum_{N=0}^{\infty}\sum_{S=0}^{\infty}\frac{(I_1I_2)^{\frac{S+N}{2}}M^{S+N}\rho_s^S\rho_a^N}{\Gamma(N+1)\Gamma(N+M)\Gamma^2(S+1)(1-\rho_a)^{S+N}(1-\rho_s)^{S+N}\left(<I_1><I_2>\right)^{\frac{S+N}{2}}}$$

$$\times K_{S-M-N+1}\left(2\left(\frac{MI_1}{<I_1>(1-\rho_a)(1-\rho_s)}\right)^{1/2}\right)K_{S-M-N+1}\left(2\left(\frac{MI_2}{<I_2>(1-\rho_a)(1-\rho_s)}\right)^{1/2}\right)$$

where M and ρ_a have the same meaning as before, ρ_s is the complex coherence factor for speckle in a vacuum and K is a Bessel function. Substituting A for I in (A30) and multiplying by the Jacobian $|J|=|dI_{ij}/dA_{ij}|$ gives,

$$P_{A_1,A_2}(A_1,A_2)=P_{a,s}(A_1^2A_2^2)(4A_1A_2)$$

$$=\frac{16A_1A_2(A_1^2A_2^2)^{\frac{M-1}{2}}M^{M+1}}{\Gamma(M)\rho_a^{\frac{M-1}{2}}(1-\rho_a)(1-\rho_s)^M\left(<A_1^2><A_2^2>\right)^{\frac{M+1}{2}}}$$

$$\times\sum_{N=0}^{\infty}\sum_{S=0}^{\infty}\frac{(A_1^2A_2^2)^{\frac{S+N}{2}}M^{S+N}\rho_s^S\rho_a^N}{\Gamma(N+1)\Gamma(N+M)\Gamma^2(S+1)(1-\rho_a)^{S+N}(1-\rho_s)^{S+N}\left(<A_1^2><A_2^2>\right)^{\frac{S+N}{2}}}$$

$$\times K_{S-M-N+1}\left(2\left(\frac{MA_1^2}{<A_1^2>(1-\rho_a)(1-\rho_s)}\right)^{1/2}\right)K_{S-M-N+1}\left(2\left(\frac{MA_2^2}{<A_2^2>(1-\rho_a)(1-\rho_s)}\right)^{1/2}\right)$$

and (A31)

$$P_{A_1,A_2}(A_1,A_2)=\frac{16A_1^M A_2^M M^{M+1}}{\Gamma(M)\rho_a^{\frac{M-1}{2}}(1-\rho_a)(1-\rho_s)^M\left(<A_1^2><A_2^2>\right)^{\frac{M+1}{2}}}$$

$$\times\sum_{N=0}^{\infty}\sum_{S=0}^{\infty}\frac{(A_1A_2)^{S+N}M^{S+N}\rho_s^S\rho_a^N}{\Gamma(N+1)\Gamma(N+M)\Gamma^2(S+1)(1-\rho_a)^{S+N}(1-\rho_s)^{S+N}\left(<A_1^2><A_2^2>\right)^{\frac{S+N}{2}}}$$

$$\times K_{S-M-N+1}\left(2A_1\left(\frac{M}{<A_1^2>(1-\rho_a)(1-\rho_s)}\right)^{1/2}\right)K_{S-M-N+1}\left(2A_2\left(\frac{M}{<A_2^2>(1-\rho_a)(1-\rho_s)}\right)^{1/2}\right)$$

APPENDIX B

DERIVATION OF THE WEAK SCATTERER VARIANCE

Uozumi and Asakura[20] have shown that the probability density function for wrapped speckle phase in the far diffraction field on the axis normal to a diffuse target assumed to have a Gaussian distribution of discrete scatterers is given by

$$P_\theta(\theta)=\frac{\eta}{2\pi\tau}\left[1+\zeta\sqrt{\pi}\exp(\zeta^2)[1+\mathrm{erf}(\zeta)]\right]\exp\left[-\frac{<U>^2}{2\sigma_r^2}\right] \qquad \text{(B1)}$$

where

$$-\pi<\theta<\pi$$

$$\tau=\cos^2\theta+\eta^2\sin^2\theta$$

$$\zeta=\frac{<U>\cos\theta}{\sigma_r\sqrt{2\tau}}$$

$$\eta=\sigma_r/\sigma_i$$

$$<U>=N\exp(-\sigma_\phi^2/2)$$

$$\sigma_r^2=(N/2)[1+\exp(-2\sigma_\phi^2)-2\exp(-\sigma_\phi^2)]$$

$$\sigma_i^2=(N/2)[1-\exp(-2\sigma_\phi^2)]$$

N = number of scattered fields at the receiver

σ_ϕ = standard deviation of target scatterers

$<U>$ and σ_r are the mean and standard deviation of the real part of the complex field representing the speckle and σ_i is the standard deviation of the imaginary part. The mean value of the imaginary part and the correlation coefficient between the real and imaginary fields are both zero under the stated conditions.

Using the series approximation $e^x = 1+x+x^2/2+x^3/3!+x^4/4!+\ldots\ldots$,

$$\eta^2=(\sigma_\phi^2/2)\left\{\frac{1-\sigma_\phi^2+7\sigma_\phi^4/12-\sigma_\phi^6/4+\cdots}{1-\sigma_\phi^2+2\sigma_\phi^4/3-\sigma_\phi^6/3+\cdots}\right\}$$

$$\frac{<U>^2}{2\sigma_r^2}=\frac{N}{\sigma_\phi^4}\left\{\frac{(1-\sigma_\phi^2/2+\sigma_\phi^4/8-\sigma_\phi^6/48+\ldots)^2}{1-\sigma_\phi^2+7\sigma_\phi^4/12-\sigma_\phi^6/4+\cdots}\right\}$$

$$\zeta=\frac{\sqrt{N/\tau}}{\sigma_\phi^2}\left\{\frac{1-\sigma_\phi^2/2+\sigma_\phi^4/8-\sigma_\phi^6/48+\cdots}{\sqrt{1-\sigma_\phi^2+7\sigma_\phi^4/12-\sigma_\phi^6/4+\cdots}}\right\}\cos\theta$$

For values of $\sigma_\phi << 1$,

$$\zeta=\frac{\sqrt{N/\tau}}{\sigma_\phi^2}\cos\theta$$

$$\eta^2=\sigma_\phi^2/2$$

$$\frac{<U>^2}{2\sigma_r^2}=\frac{N}{\sigma_\phi^4}$$

$$\tau=\cos^2\theta+\frac{\sigma_\phi^2}{2}\sin^2\theta$$

As long as $\sigma_\phi^2 << \sqrt{N}$, zeta will be large compared to one, so the first term in (B1) can be ignored and erf(ζ) can be approximated by one. In that case

$$P_\theta(\theta)=\frac{\cos(\theta)\sqrt{N/2\pi}}{\sigma_\phi\tau^{3/2}}\exp\left\{\frac{N(\frac{\cos^2\theta}{\tau}-1)}{\sigma_\phi^4}\right\}$$

$$=\frac{\cos(\theta)\sqrt{N/2\pi}}{\sigma_\phi|\cos^2\theta+(\sigma_\phi^2/2)\sin^2\theta]^{3/2}}\exp\left\{\frac{-N}{2\sigma_\phi^2}\left\{\frac{\sin^2\theta}{\cos^2\theta+(\sigma_\phi^2/2)\sin^2\theta}\right\}\right\}$$

and with $\sigma_\Phi << 1$, $\tau = \cos^2\theta$ so that

$$P_\theta(\theta) = \frac{\sqrt{N/2\pi}}{\sigma_\Phi \cos^2\theta} \exp\left(\frac{-N}{2\sigma_\Phi^2}\tan^2\theta\right)$$

Using the small angle approximations for tan θ and cos θ and the fact that the numerator converges to zero faster than the denominator as θ approaches $\pi/2$, when $\sigma_\Phi^2 << N$, the function becomes vanishingly small for values of θ $> 3\sigma_\Phi/\sqrt{N}$ and the function can therefore be approximated by the Gaussian function,

$$P_\theta(\theta) = \frac{1}{\sigma_s\sqrt{2\pi}} \exp\left(\frac{-\theta^2}{2\sigma_s^2}\right)$$

where

$$\sigma_s = \sigma_\Phi/\sqrt{N}$$

In the other extreme when $\sigma_\Phi >> 1$ and $\sigma_\Phi^2 >> N$, $\eta = 1$, $\tau = 1$ and, ζ and $<U>$ are both nearly zero. Therefore,

$$P_\theta(\theta) = 1/2\pi \qquad -\pi < \theta < \pi$$

APPENDIX C

Computer Processing Codes

Fortran 77

1. Program for reading the TK50 mag tape

```
c
      program tk50program
c
c     ************************************************************
c     Originated by Li-Bo Sun
c     Edited by Todd Clonlnger, Doug Draper and John Peacock
c     Last Modified: Sept 1991
c     ************************************************************
c
c
c     THIS VERSION WRITES WRAPPED PHASE, UNWRAPPED PHASE OR
c     INTEGRATED FREQUENCY DATA TO THE DISK. INCLUDES INSITU DATA
c     ACCOMODATES UP TO THREE CHANNELS OF DATA
c
c     NOTE that nr is used for number of records in main program
c          but as a data interval in some subroutines
c
c               PROGRAM SUMMARY
c  MAIN  ------  program control
c        SUBROUTINE (sk) --- skip ahead
c        SUBROUTINE (rw) --- rewind
c        SUBROUTINE (db) --- display a block of data
c        SUBROUTINE (tp) --- copy or process data from tape
c              SUBROUTINE (tph) --- process phase data
c              SUBROUTINE (tf) --- process frequency data
c
c
      integer tlu,tcsr,bn,fn,rn
      common issn, bn,kk
      logical eoff,errf,eotf
      character op*2
      character devname*15
      character*50000 B

      write(*,*)
      write(*,*) '  This program copies data from a TK50 tape to ',
     C'a file in your'
      write(*,*) 'directory that can be graphed.'
1011  write(*,*)
      write(*,1)

    1 format(
     -10x'*************************************************'/,
     -10x'*                COMMAND LIST                   *'/,
     -10x'*                                               *'/,
     -10x'*     sk:  skip nr records                      *'/,
     -10x'*     rw:  rewind tape                          *'/,
     -10x'*     db:  display a header or block of data    *'/,
     -10x'*     td:  copy or process data from tape       *'/,
     -10x'*     en:  exit program                         *'/,
     -10x'*************************************************')

2000  continue
      tlu=2
      issn=10000
*      # of ch/line in the text
      kk=72
*      device name
      devname='/dev/nrmt0'
*      bn is the record size in bytes
      bn=2048
      write(*,1500) devname,bn,kk
```

```
1500  format(x,'The device name is  ',a15,',the buffer size is ',i5
     1,',',i4,'ch/line')
      ito=topen (tlu,devname,.false.)
      print*,'ito=',ito
      ist=tstate (tlu,fn,rn,errf,eoff,eotf,tcsr)
      print*,'tlu=',tlu,'tcsr=',tcsr
      print*,'errf=',errf,'eoff=',eoff,'eotf=',eotf
1000  continue
      print*,'Input op(rw,sk,db,td,en),nr,(format a2,i4)'
      read(5,33,err=1000) op,nr
   33 format(a2,i4)
      if (nr.eq.0) nr = 1
      write(*,*)
      if (op.eq.'db') call db (tlu,B)
      if (op.eq.'rw') call rw (tlu)
      if (op.eq.'sk') call sk (tlu,B,nr)
      if (op.eq.'td') call td (tlu,B,nr)
      if (op.eq.'?') go to 1011
      if (op.ne.'en') go to 1000

      ics=tclose(tlu)
  828 write(*,*)
      write(*,*)
      write(*,*)'Program Terminated! '
      write(*,*)
      stop
      end

c     ********************************************************

      subroutine sk (tlu,B,nr)
      integer bn,fn,rn
      common issn, bn,kk
      character B*(*)
      integer tlu,tcsr
      logical eoff,errf,eotf
      do 134 i=1,nr
      ird=tread(tlu,B(1:bn))
      ist=tstate (tlu,fn,rn,errf,eoff,eotf,tcsr)
      issn=issn+1
c     print*,'block number is',rn,'fn=',fn,',errf=',errf,',eoff=',eoff
      if (errf) go to 144
   134 continue
      print*,'block number is',rn,'fn=',fn,',errf=',errf,',eoff=',eoff
      go to 145
   144 continue
      itc=tclose(tlu)
      print*,'itc=',itc
      ist=tstate (tlu,fn,rn,errf,eoff,eotf,tcsr)
      print*,'tlu=',tlu,'tcsr=',tcsr
      print*,'errf=',errf,'eoff=',eoff,'eotf=',eotf
      ito=topen (tlu,devname,.false.)
      print*,'ito=',ito
      ist=tstate (tlu,fn,rn,errf,eoff,eotf,tcsr)
      print*,'tlu=',tlu,'tcsr=',tcsr
      print*,'errf=',errf,'eoff=',eoff,'eotf=',eotf
   145 continue
      return
      end

c     ********************************************************

      subroutine rw (tlu)
      integer tlu,tcsr,fn,rn
      common issn, bn,kk
      logical eoff,errf,eotf
```

```
      irw=trewin (tlu)
      print*,'irw=',irw
      ist=tstate (tlu,fn,rn,errf,eoff,eotf,tcsr)
      issn=0
      print*,'errf=',errf,'issn=',issn
      print*,'you are at the beginning of the tape,issn=',issn,' rn=',rn
      return
      end

c     ********************************************************

      subroutine db (tlu,B)
      integer tlu,tcsr,bn,fn,rn,i,j,n,inul
      common issn, bn,kk
      logical eoff,errf,eotf
      character B*(*)
      character cnul*1,cti*2
      equivalence (cnul,inul)
      equivalence (cti,ifc)

      inul=0
      do 67 kp=1,50000
      B(kp:kp)=cnul
   67 continue

      print*,'This option displays a header block'
      print*,'or 1 block of data from the tape.'

      ird=tread(2,B(1:bn))
      issn=issn+1
      write(*,2002) (B(j:j+1),j=1,16,2)
      write(*,2002) (B(16+j:j+17),j=1,16,2)
      write(*,2002) (B(32+j:j+33),j=1,16,2)
      n=48
      cti=B(1:2)
      if (ifc.ne.0) go to 20
   16 do 17 i=1,17
       write(*,2004) (B(n+j:n+j+1),j=1,16,2)
       n = n + 16
   17 continue
   18 go to 22
   20 do 21 i=1,17
       write(*,2002) (B(n+j:n+j+1),j=1,16,2)
       n = n + 16
   21 continue
   22 continue
 2002 format(x,8i6)
 2004 format(x,32a2)
      ist=tstate (tlu,fn,rn,errf,eoff,eotf,tcsr)
      print*,'record address is ',rn,', errf=',errf,',eoff=',eoff
      return
      end

c     ********************************************************
      subroutine td (tlu,B,nr)
20    dimension h(175000)
      integer tlu,tcsr,bn,fn,rn,dcnum,inul,ifc
      integer dcnum1,dcnum2,h
      real dt,t
      common issn, bn,kk
      logical eoff,errf,eotf
      character B*(*),ofilnam*15,ofilnam1*15,ofilnam2*15
      character ofilnam3*15,op*3
      character cti*2, cnul*1
      equivalence (cti,ifc)
      equivalence (cnul,inul)
```

```
      inul=0
      do 67 kp=1,50000
      B(kp:kp)=cnul
   67 continue

 1201 format(a15)
      t = 0.0
      i=1
      ird=tread(2,B(1:bn))
      issn=issn+1
      cti=B(1:2)
      if (ifc.eq.0) go to 19
      idata=0
      do 11 j=17,32,2
       cti=B(j:j+1)
       idata=idata+ifc
11    continue
      jdata=0
      do 9 j=33,48,2
       cti=B(j:j+1)
       jdata=jdata+ifc
 9    continue
       wind = float((idata/8-2048)*25.6/2047)
       sigma = float((jdata/8-2048)*5.1175/2047)

*      get sampling interval (usec)
      cti=B(5:6)
*      convert to millisec
      dt=ifc/1000.0
      print*,'The sample time (dt) in ms is'
      write(6,*) dt
        print*,' the maximum number of data points'
        print*,' that can be filtered is 2500 due to limitations'
        print*,' of the nag library routine for fft'
        print*
      print*,'number of channels =?'
      read(5,*) ichan
      print*,'data interval per channel (msec)=?'
      print*,'    '
      print*,'interval must be a multiple of the number'
      print*,'of channels times the sample time'
      read(5,*) samtim
      print*,'maximum time(sec)=?'
      read(5,*) tmax
      nr=samtim/dt
      mr=tmax*1000/dt
      go to 5
18    ird=tread(2,B(1:bn))
      issn=issn+1
      cti=B(1:2)
      if (ifc.eq.0.and.ichan.eq.3) i=i-1
      if (ifc.eq.0) go to 19
5     do 17 j=49,2048,2
      cti=B(j:j+1)
      h(i)=ifc
      i=i+1
17    continue
19    if (i.lt.mr) go to 18

      print*,'Type tf if you want to integrate frequency data'
      print*,'Type tph if you want to unwrap phase data'
      print*,'Type tc if you want to copy data to a file'
      read(5,*) op
      if (op.eq.'tc') go to 333
      if (op.eq.'tf') call tf (h,mr,nr,dt,samtim,wind,sigma)
```

```
      if (op.eq.'tph') call tph (h,mr,nr,dt,samtim,wind,sigma)
      go to 400

333   print*,'This option copies data from tape to your directory'
 330  write(*,*)
 2003 format('Do you want to copy 1,2 or 3 channels? (1,2 or 3) '$)
      write(*,2003)
      read(*,*,err=330) dcnum
      if (dcnum.eq.1) go to 3000
      if (dcnum.eq.2) go to 4000

      print*,'Input filename for writing ch 1 (< 16 char.)'
      read(*,1201) ofilnam1
      print*,' Copying from tape to: ',ofilnam1
      open (9,file=ofilnam1,status='unknown')
      rewind 9

      print*,'Input filename for writing ch 2 (< 16 char.)'
      read(*,1201) ofilnam2
      print*,' Copying from tape to: ',ofilnam2
      open (8,file=ofilnam2,status='unknown')
      rewind 8

      print*,'Input filename for writing ch 3 (< 16 char.)'
      read(*,1201) ofilnam3
      print*,' Copying from tape to: ',ofilnam3
      open (7,file=ofilnam3,status='unknown')
      rewind 7

      do 15 j=1,mr,nr
       write(9,2002) t,h(j)
       write(8,2002) t+dt,h(j+1)
       write(7,2002) t+dt*2.0;h(j-2)
       t=t+dt*nr
15    continue
      go to 200


3000  continue
 2001 format('Which data channel do you want to copy? (1,2 or 3) '$)
      write(*,2001)
      read(*,*,err=3000) dcnum
      if ((dcnum.ne.1).and.(dcnum.ne.2).and.dcnum.ne.3) go to 3000

      print*,'Input filename for writing (< 16 char.)'
      read(*,1201) ofilnam
      print*,' Copying from tape to: ',ofilnam
      open (9,file=ofilnam,status='unknown')
      rewind 9

13    do 14 j=1,mr,nr
       write(9,2002) t,h(j+dcnum-1)
       t=t+dt*nr
14    continue
      go to 200

4000  continue
 2004 format('Which two channels do you want to copy?  '$)
      print *, 'Enter each channel separated by a space'
      write(*,2004)
      read(*,*,err=3000) dcnum1,dcnum2
      if ((dcnum1.ne.1).and.(dcnum1.ne.2).and.dcnum1.ne.3) go to 4000
      if ((dcnum2.ne.1).and.(dcnum2.ne.2).and.dcnum2.ne.3) go to 4000
      print*,'Input filename for writing',dcnum1,'< 16 char.'
      read(*,1201) ofilnam1
      print*,' Copying from tape to: ',ofilnam1
```

```
      open (9,file=ofilnam1,status='unknown')
      rewind 9

      print*,'Input filename for writing',dcnum2,'< 16 char.'
      read(*,1201) ofilnam2
      print*,' Copying from tape to: ',ofilnam2
      open (8,file=ofilnam2,status='unknown')
      rewind 8

      do 16 j=1,mr,nr
       write(9,2002) t+dt*(dcnum1-1),h(j+dcnum1-1)
       write(8,2002) t+dt*(dcnum2-1),h(j+dcnum2-1)
       t=t+dt*nr
16    continue

200   continue
2002  format(x,f8.2,i6)
      ist=tstate (tlu,fn,rn,errf,eoff,eotf,tcsr)
      print*,'block number is ',rn,', errf=',errf,',eoff=',eoff
      close (7)
      close (8)
      close (9)
400   continue

      return
      end
c
c*****************************************************************

      subroutine tph (h,mr,nr,dt,samtim,wind,sigma)
c       This subroutine takes a phase vs time signal generated by the
c       phase detector (new 7/88) and unwraps the 2 volt signal to
c       a 4v signal.
c
c       Writen by John Peacock 8-2-88 and Doug Draper
c
        dimension phi1(50000),phi2(50000),h(50000)
        dimension x(50000),,t(50000)
        integer ch1,ch2,phi1,phi2,h,dcnum1,dcnum2
        real t,x,pi
        character ofilnam*15
20      format (a15)
        pi=3.1415927

c
c       This part of the program uses the two channels of phase data
c       that vary between 0 to 2.5 volts (or 0 to pi) and are 90
c       degrees out of phase. The data is then converted to
c       produce two channels of phase data that range from 0 to 2pi
c       (or 0 to 5 volts) and are 180 degrees (pi) out of phase.

4000  continue
 2004 format('Which two channels do you want to process?  '$)
      print *, 'Enter each channel(1,2 or 3) separated by a space'
      write(*,2004)
      read(*,*,err=4000) dcnum1,dcnum2
      if ((dcnum1.ne.1).and.(dcnum1.ne.2).and.dcnum1.ne.3) go to 4000
      if ((dcnum2.ne.1).and.(dcnum2.ne.2).and.dcnum2.ne.3) go to 4000

2002  format(x,f8.2,i6)

        do 30 i=1,mr,nr
       ch1=h(i+dcnum1-1)
       ch2=h(i+dcnum2-1)

c       convention is each channel goes between 0 to 2.5 volts or
```

```
c       digitally 2048 to 3072. However the detector may not be
c       completely acurate so the values may go over or under by
c       a little bit.
              if (ch2 .le. 2560) then
                 phi1(i)= ch1+1024
                 if (phi1(i) .gt. 4096) phi1(i)=4096
              else
                 phi1(i)= -ch1+1024+4096
                 if (phi1(i) .lt. 2048) phi1(i)=2048
              end if

              if (ch2 .gt. 2560) then
                 phi2(i)= -ch1+4096+2048
                 if (phi2(i) .gt. 4096) phi2(i)=4096
              else
                 phi2(i)= ch1
                 if (phi2(i) .lt. 2048) phi2(i)=2048
              end if
30      continue

c       This part of the program unwraps the data into intervals
c       greater than two pi.

        c=0
        n=0
        tx=0
        do 200 i=1,mr,nr
          if (phi1(i).gt.3584) go to 170
          if (phi1(i).lt.2560) go to 180
          if (phi2(i).gt.3584) go to 160
          if (phi2(i).lt.2560) go to 163
          if (c.eq.1) go to 165
          h(i)=phi1(i)
          go to 190
160       if (c.eq.1) go to 162
          go to 168
162       n=n+1
          go to 168
163       if (c.eq.1) go to 167
          go to 168
165       h(i)=phi2(i)
          go to 190
167       n=n-1
168       h(i)=phi1(i)
          c=0
          go to 190
170       if (c.eq.1) go to 175
          n=n+1
175       h(i)=phi2(i)
          c=1
          go to 190
180       if (c.eq.1) go to 175
          n=n-1
          go to 175
190       h(i)=h(i)+n*1024
100       continue

          index=(i-1+nr)/nr

*                convert phase data to radians
*                and re-index array
          x(index)=float((h(i)-2048))/2048.0*2*pi
                tx=tx+tsmtim
                t(index)=tx

200     continue
```

```
        print*, 'Type 2 if you want unwrapped phase data'
        print*, 'Type 0 if you do not'
        read (*,*) iphase
          if (iphase.ne.2) go to 1000
        print*, 'Enter the number of data points to skip'
        print*, 'in phase data file. Type 1 if none skipped.'
        read (5,*) iskip
        print*, 'Total unwrapped output filename (< 16 char.)'
        read (*,20) ofilnam
        open (9,file=ofilnam,status='unknown')
*               write corrected data in file
*                express phase in radians
          write(9,*) ofilnam,wind,sigma
        do 201 i=1,mr/nr,iskip
          write(9,600) t(i),x(i)
201     continue
600     format(1x,f8.2,2x,f15.4)

        close(1)
        close(2)
        close(9)
1000    continue
      return
      end

c  ***************************************************************
      subroutine tf (h,mr,nr,dt,samtim,wind,sigma)

c     This subroutine integrates frequency data and provides
c     integrated data and statistics of integrated data.

        real x(50000)
        integer h(50000),iskip
        integer i,m,l,dcnum,npts,mr,nr,j,k,ifreq
        real ave,s,t,factor,dt,samtim,pi
        character filename*15
10     format(a15)
60     format(1x,f8.2,2x,f15.4)
        parameter(pi=3.1415927)

 330  write(*,*)
        print*, 'Type 2 if you want to copy integrated frequency data'
        print*, 'Type 0 if you do not'
        read (*,*) ifreq

3000  continue
 2001 format('Which data channel do you want to process? (1,2 or 3) 'S)
      write(*,2001)
      read(*,*,err=3000) dcnum
      if ((dcnum.ne.1).and.(dcnum.ne.2).and.dcnum.ne.3) go to 3000

          if (ifreq.ne.2) go to 4000
      print*,'Input filename for writing (< 16 char.)'
      read(*,10) filename
      print*,' Copying from tape to: ',filename
      open (9,file=filename,status='unknown')
      print*,'Input V/kHz sensitivity of frequency detector'
      read*, factor
        print*, 'Enter the number of data points to skip'
        print*, 'in frequency data file. Type 1 if none skipped.'
        read (5,*) iskip
      rewind 9
          write(9,*) filename,wind,sigma
4000  continue
```

```
        print*, 'factor=', factor
        factor=5000/factor/2048
        print*, 'factor=', factor
        npts=mr/nr
        s=0
        t=dt
        m=0
        l=0
        do 100 j=1,mr,nr
        m=h(j+dcnum-1)+m
100     continue
        ave=m/npts
        do 200 k=1,mr,nr
        l=l+1
        s=h(k+dcnum-1)-ave+s
        x(l)=s*samtim*2*pi*factor/1000
200     continue
           if (ifreq.ne.2) go to 1000
        do 400 i=1,npts,iskip
        write(9,60) t,x(i)
        t=t+samtim*iskip
400     continue
1000   continue

        return
        end

c  ***************************************************************

*********************  end of program  ***********************
```

Computer Processing Codes

Fortran 77

2. Program for filtering the phase or frequency

```
c     ************************************************************
           program  filter

        real y(2500)
        double precision x(2500),s(2500),z(2500)
        real t,pi,hz,hz2
        integer n,i,j,k,npts,Pnps,Pnpsd2
        real dfreq,highfactor,lowfactor,polenum
        integer i,j,k
        integer ifail
        parameter(pi=3.1415927)

       open(3,file='filtered.data',status='new')

******          sampling time (ms)
      samtim=12
      npts=2500
******          tmax= 30 sec
        Pnps=npts
        Pnpsd2 = Pnps/2
       dfreq = 1/(samtim*1.0e-3*Pnps)

********************  read data file  ****************************


        do 25 i=1,npts
          read (1,*,end=26) t,y(i)
25      continue
26      continue

********************  phase filtering  ***************************

******          high pass cut-off frequency
             hz=0.5
******          low pass cut-off frequency
             hz2=5.0

********************  n pole fltr.  ******************************

          polenum=5.0
          n=polenum
       highfactor=sqrt(2-2**(1/polenum))
          hz=hz/highfactor
       lowfactor=sqrt(2**(1/polenum)-1)
          hz2=hz2/lowfactor


*****  getting FFT  *****

       do 35 i=1,npts
            x(i)=y(i)
  35    continue

          ifail =0
       write(2,*) 'ifail=',ifail
          call c06faf(x,k,s,ifail)
       print*, 'ifail=',ifail

*******  n pole filtering  *****

          do 7500 l=1,n
```

```
*******  high pass filtering  *****
            a=hz
            a=2*pi*a
          x(1)=0
          z(1)=0
          do 1503 j=2, Pnpsd2
             denom=a**2+(2*pi*(j-1)*dfreq)**2
             z(j)=(2*pi*(j-1)*dfreq)**2/denom
1503      continue
          do 2001 j=Pnps,Pnpsd2+1,-1
             denom=a**2+(2*pi*(Pnps-j+1)*dfreq)**2
             z(j)=(2*pi*(Pnps-j+1)*dfreq)*a/denom
2001      continue

          do 1504 j=2, Pnpsd2
             x(j)=x(j)*z(j)-x(Pnps+2-j)*z(Pnps+2-j)
1504      continue
          do 2002 j=Pnps,Pnpsd2+1,-1
             x(j)=x(j)*z(Pnps+2-j)+x(Pnps+2-j)*z(j)
2002      continue

*******  low pass filtering  *****

            a=hz2
            a=2*pi*a
          do 1507 j=2, Pnpsd2
             denom=a**2+(2*pi*(j-1)*dfreq)**2
             z(j)=a**2/denom
1507      continue
          do 2004 j=Pnps,Pnpsd2+1,-1
             denom=a**2+(2*pi*(Pnps-j+1)*dfreq)**2
             z(j)=(-2*pi*(Pnps-j+1)*dfreq)*a/denom
2004      continue

          do 1508 j=2, Pnpsd2
             x(j)=x(j)*z(j)-x(Pnps+2-j)*z(Pnps+2-j)
1508      continue
          do 2006 j=Pnps,Pnpsd2+1,-1
             x(j)=x(j)*z(Pnps+2-j)+x(Pnps+2-j)*z(j)
2006      continue

7500      continue

*****  getting inverse FFT  *****

             ifail =0
             call c06gbf(x,k,ifail)
           write(*,*) 'ifail=',ifail
             call c06fbf(x,k,z,ifail)
           write(*,*) 'ifail=',ifail

          do 35 i=1,npts
             write(3,*) samtim*i,x(i)
  35     continue

             close (3)

           end
********************  end of program  **********************
```

APPENDIX D

Schematics of Phase Detectors

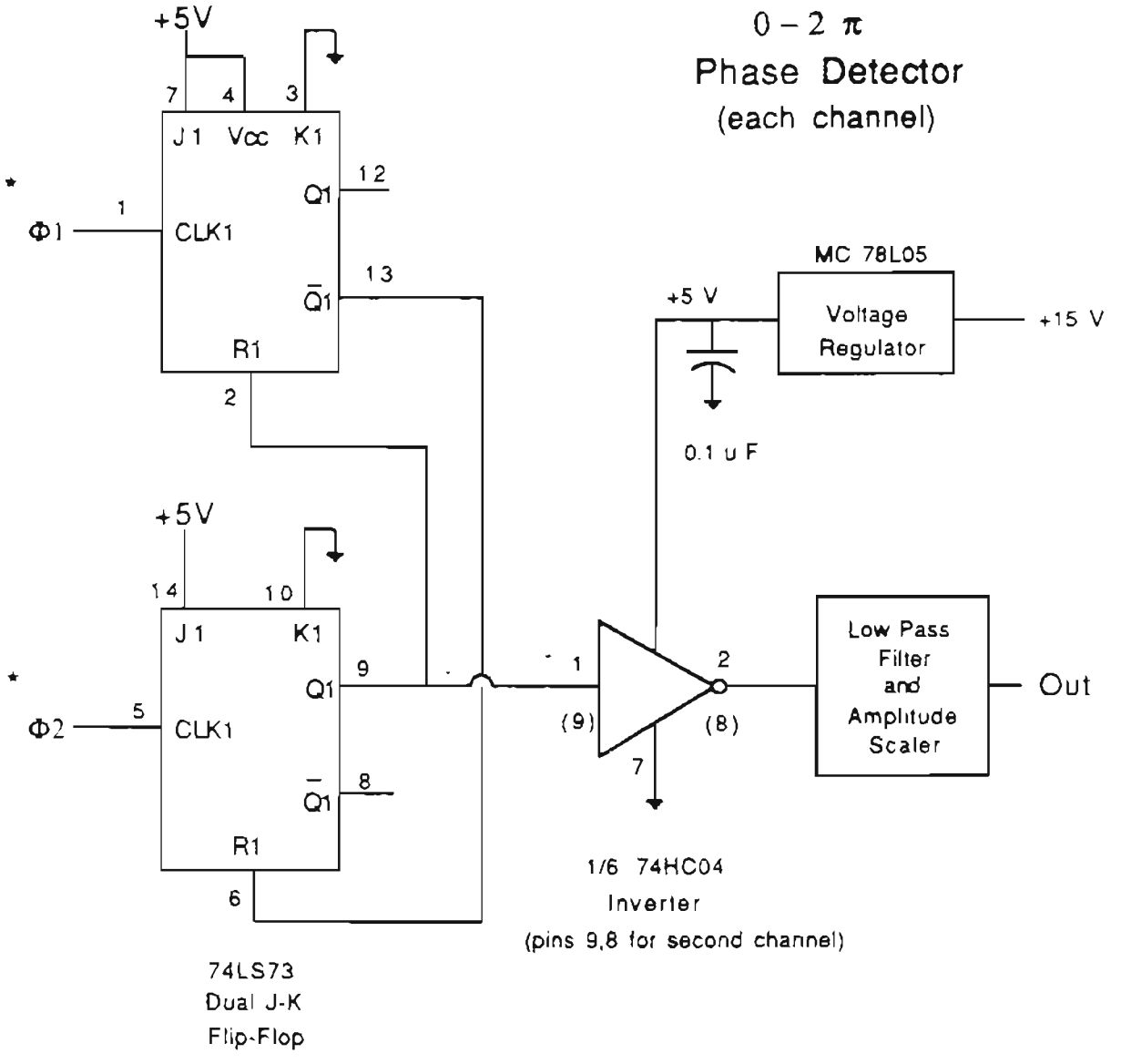

* Φ1, Φ2 *from divider circuit output*

0 – π
Phase Detector
(each channel)

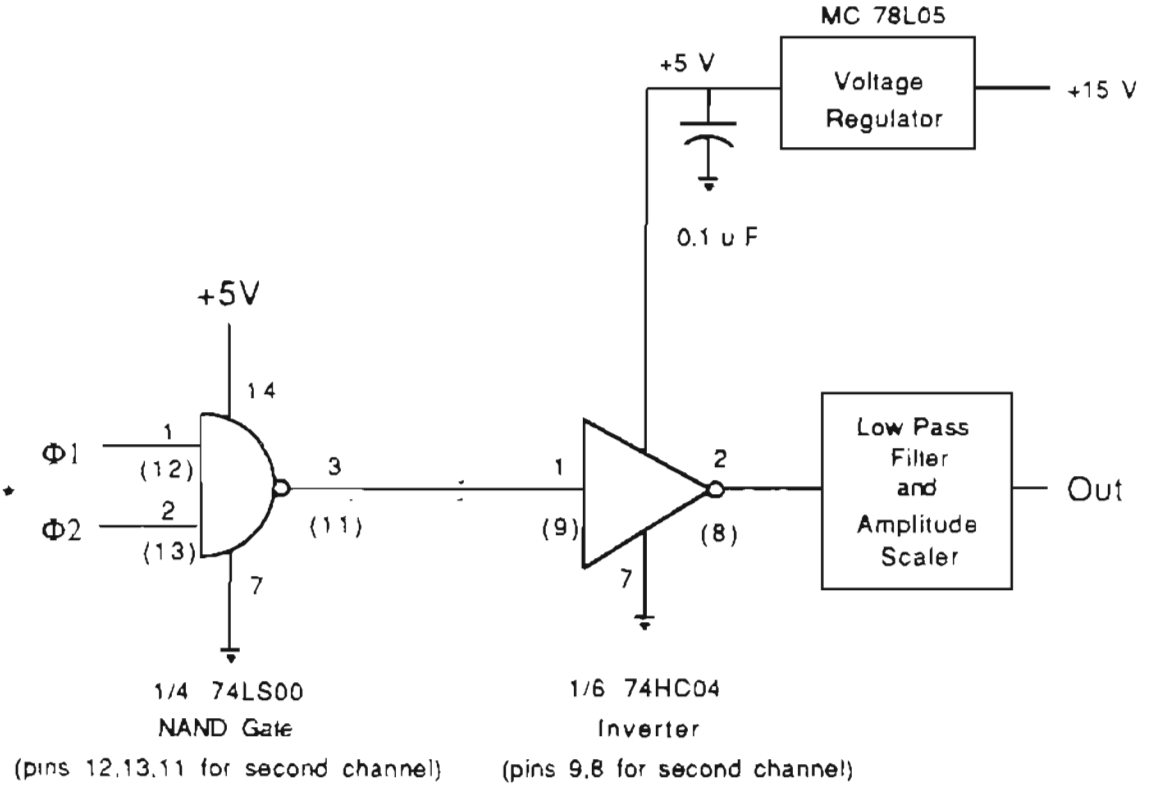

* Φ1, Φ2 from divider circuit output

SIGNAL CONDITIONER

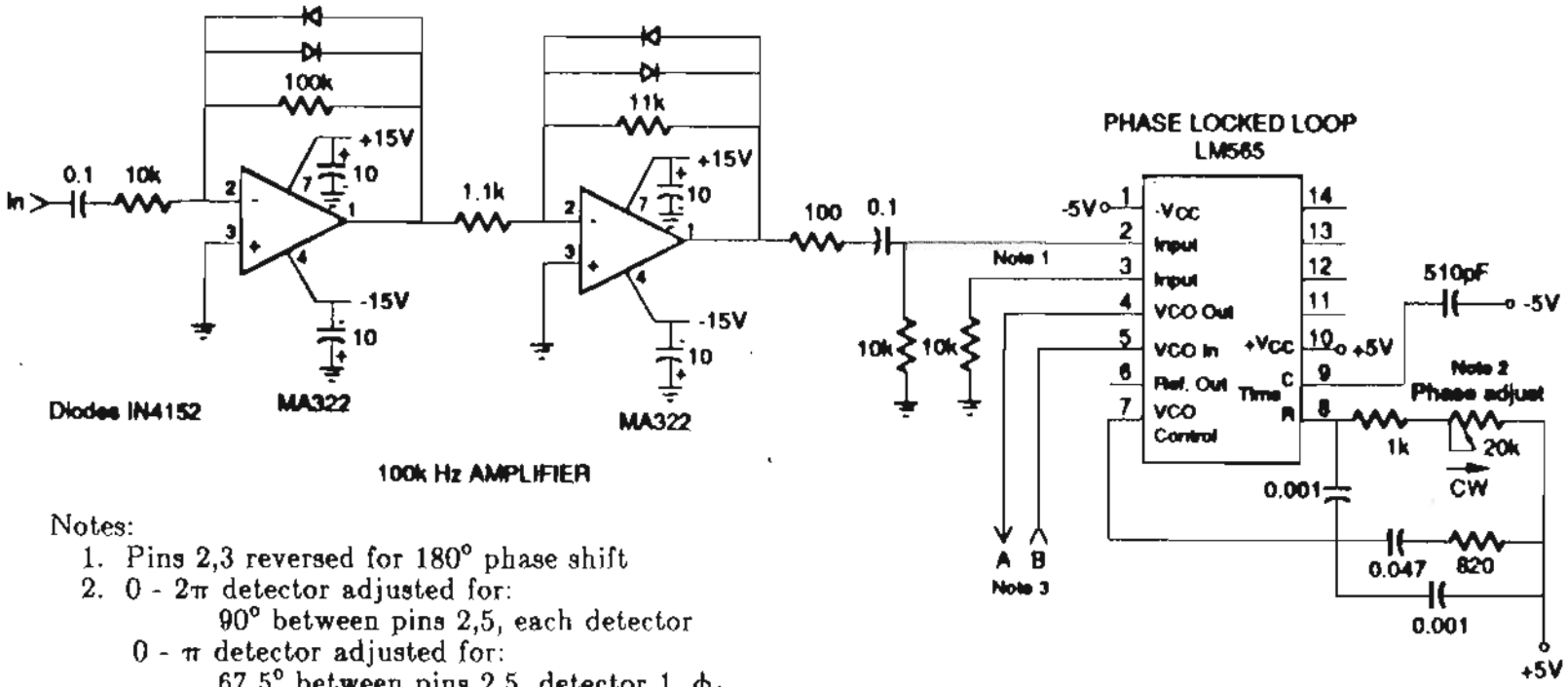

Notes:

1. Pins 2,3 reversed for 180° phase shift
2. 0 - 2π detector adjusted for:
   90° between pins 2,5, each detector
   0 - π detector adjusted for:
   67.5° between pins 2,5, detector 1, ϕ_1
   112.5° between pins 2,5, detector 1, ϕ_2
   112.5° between pins 2,5, detector 2, ϕ_1
   67.5° between pins 2,5, detector 2, ϕ_2
3. To divider circuit

DIVIDER CIRCUIT

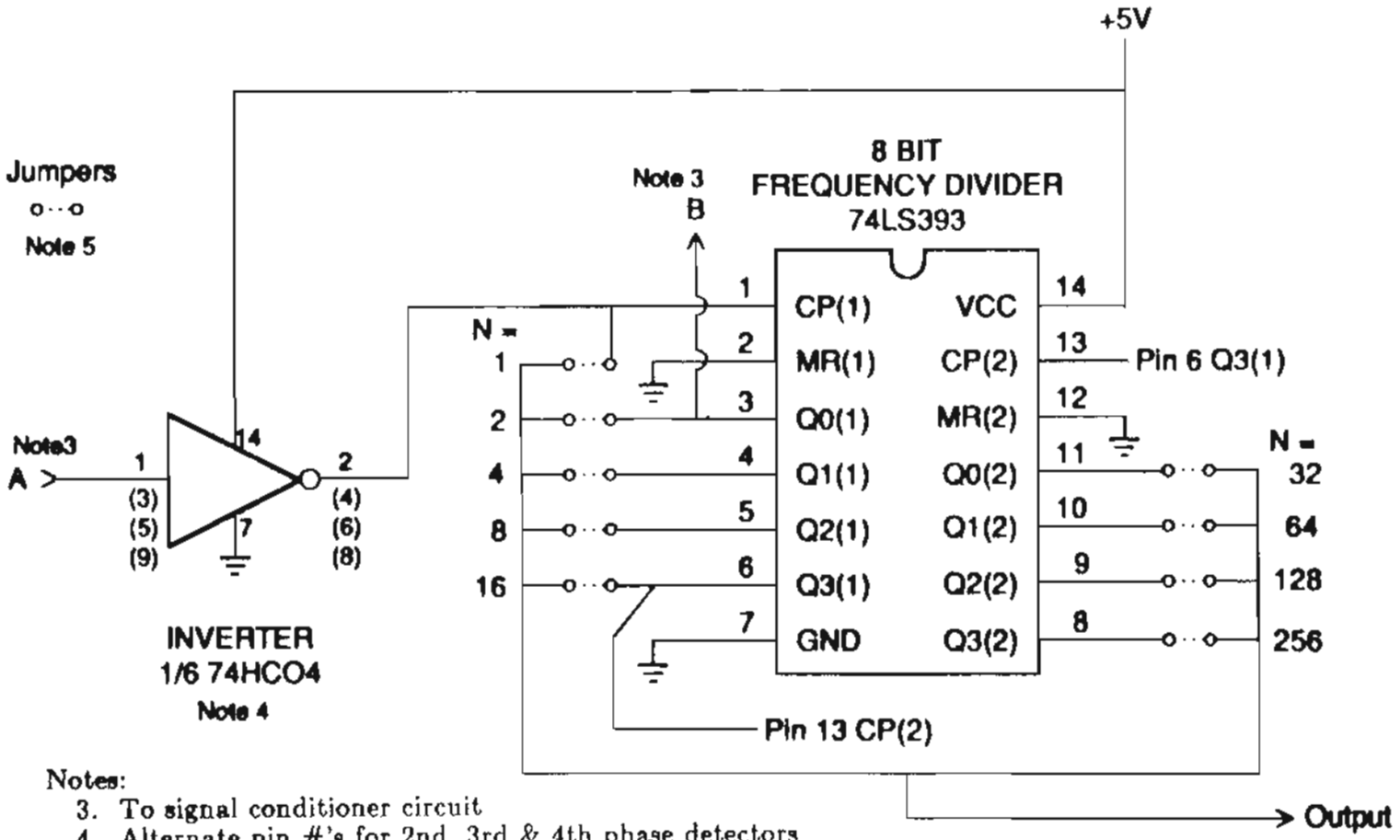

Notes:

3. To signal conditioner circuit
4. Alternate pin #'s for 2nd, 3rd & 4th phase detectors
5. N=1 for 200 kHz output
   N=2 for 100 kHz output
   N=4 for 50 kHz output
   ....

LOW PASS FILTER
and
AMPLITUDE SCALER

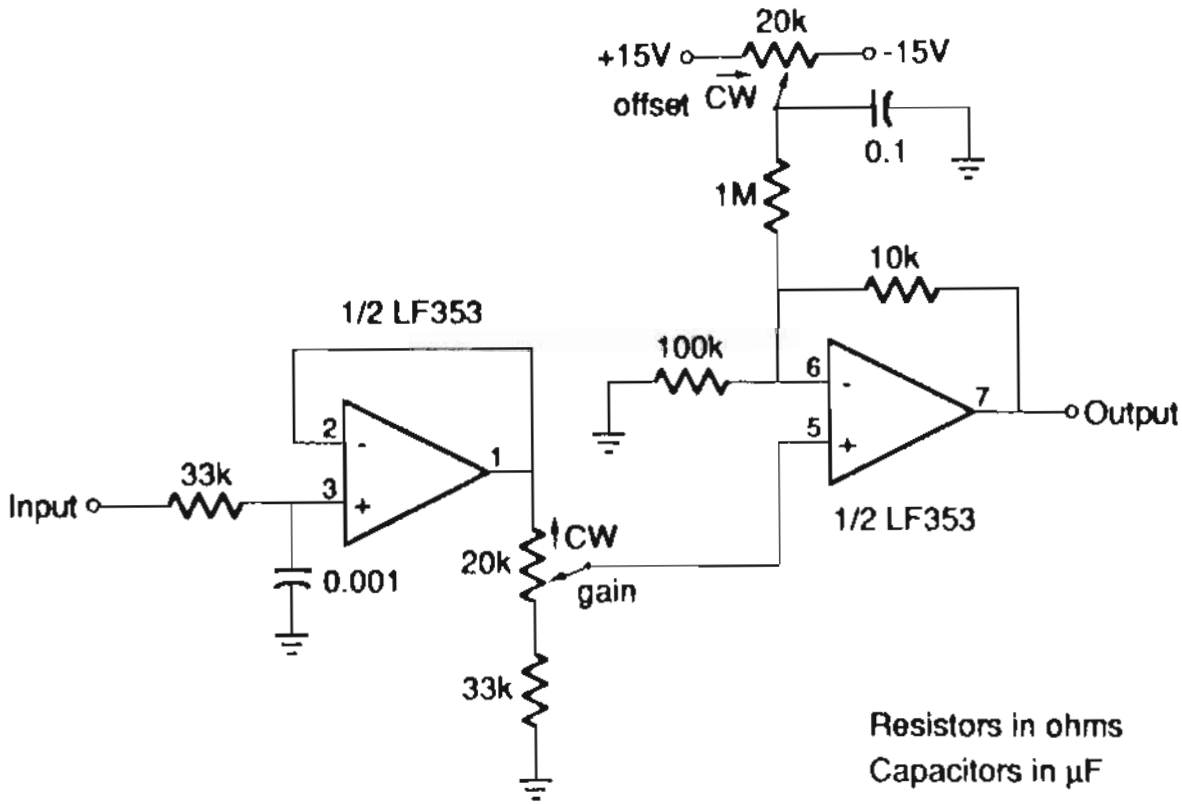

Voltage Regulators for Phase Detector

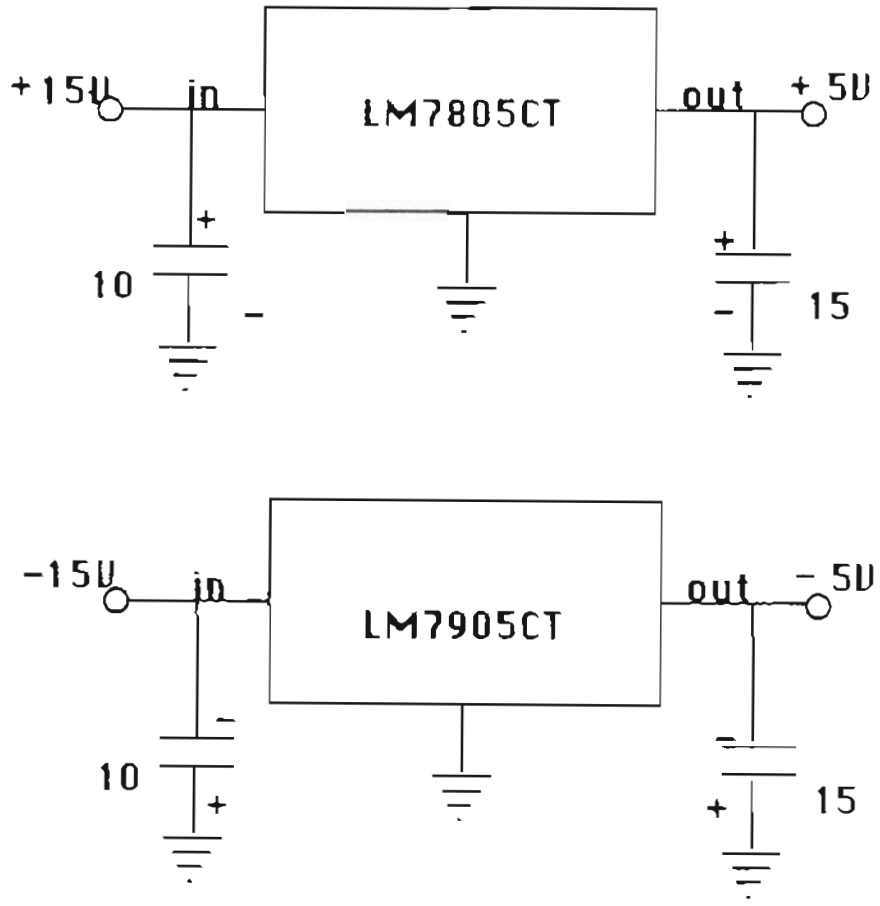

capacitors in μF

APPENDIX E

Schematic of Frequency Detectors

DUAL FREQUENCY DETECTORS

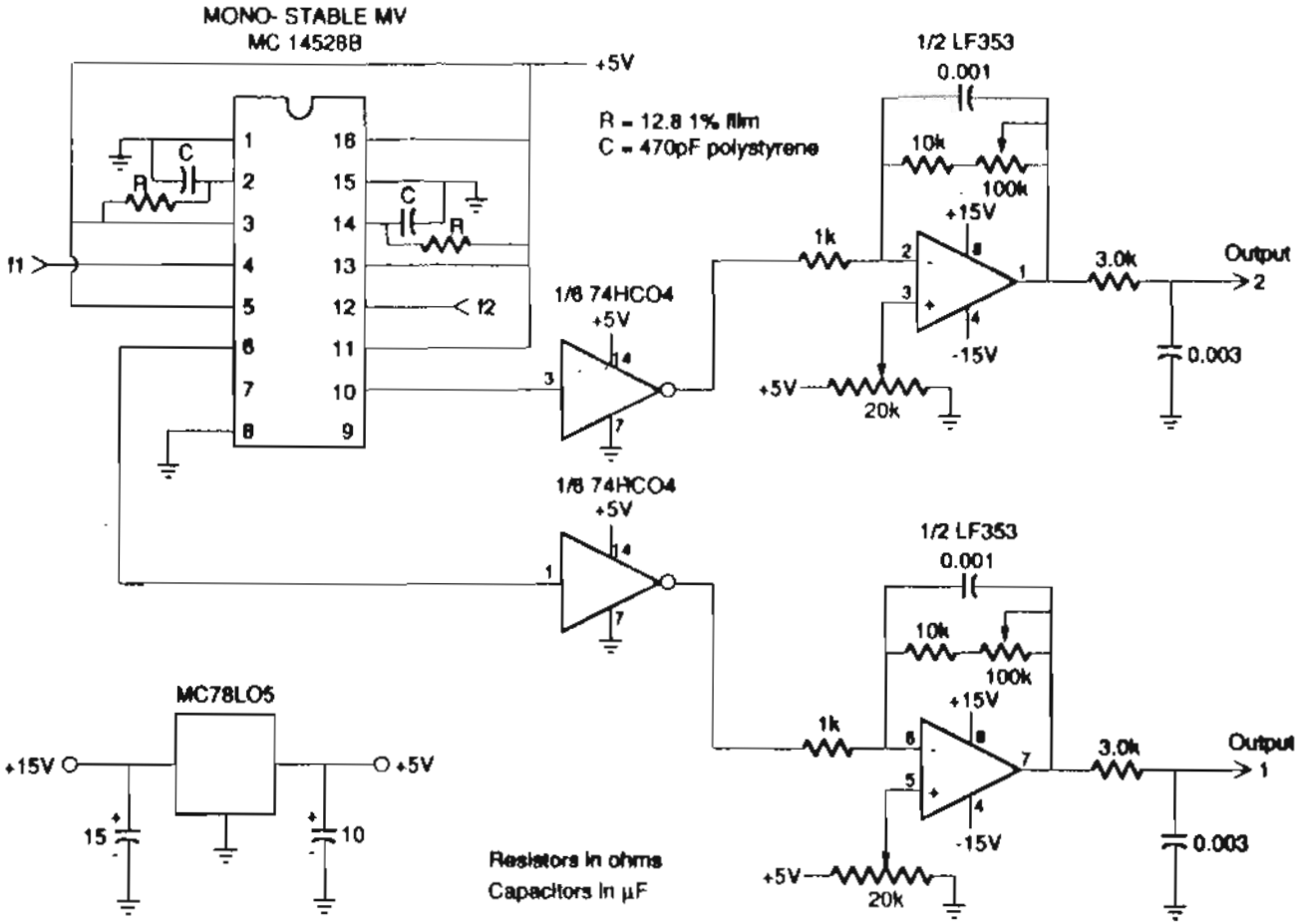

VITA

Douglas Draper was born on March 9, 1939 in St. Louis, Missouri. He attended primary schools there, and at the age of twelve he moved with his family to Monrovia, California, a suburb of Los Angeles. He graduated from Monrovia High School and enrolled at the University of Arizona in Tucson, Arizona where he graduated with a Bachelor of Science in Electrical Engineering in January of 1961. During the summers he worked for the Jet Propulsion Laboratory as a wind tunnel technician and an electronic technician.

Upon graduation he worked for four years as a systems engineer at Aerojet-General Corporation in Azusa, California in various aspects of a torpedo development program. Then he moved to Dobbs Ferry, New York to work for Hudson Laboratories of Columbia University as a senior electrical engineer supporting underwater acoustic research projects in the atlantic ocean.

In 1967 he took a position with AC Electronics Corporation in Goleta, California where he was a project engineer for the development of a piezoelectric accelerometer array and was also involved in field testing of torpedo hardware at the Naval Research Laboratory near Washington, D.C.

In 1970 he studied at The Pennsylvania State University on a National Science Foundation Grant to train teachers for the community college. He received an MEng degree from Penn State and for the last twenty years he has been teaching electrical engineering and electronic engineering technology at Portland Community College in Portland, Oregon.

In 1990 he visited the state of Kerala in southern India on a Fulbright grant. There he wrote a text on fiber optics for polytechnic colleges in Kerala.

He is married and has two daughters. He met his wife in Dobbs Ferry, N.Y. and both of their daughters were born in Portland, Oregon. His hobbies include tennis, skiing, and hiking.

His publications include,

An Unwrapped Phase Distribution Model for Speckle/Turbulence, Applied Optics 1992

Simple Two-Laser Optical Heterodyne System with Large Transmitter-Local Oscillator Isolation, Applied Optics, 1989

Laser Welding of Wax Patterns for Investment Casting, Proceedings of the American Foundarymen Association, 1988